SCIENTIFIC RATIONALE AND REQUIREMENTS FOR A GLOBAL SEISMIC NETWORK ON MARS

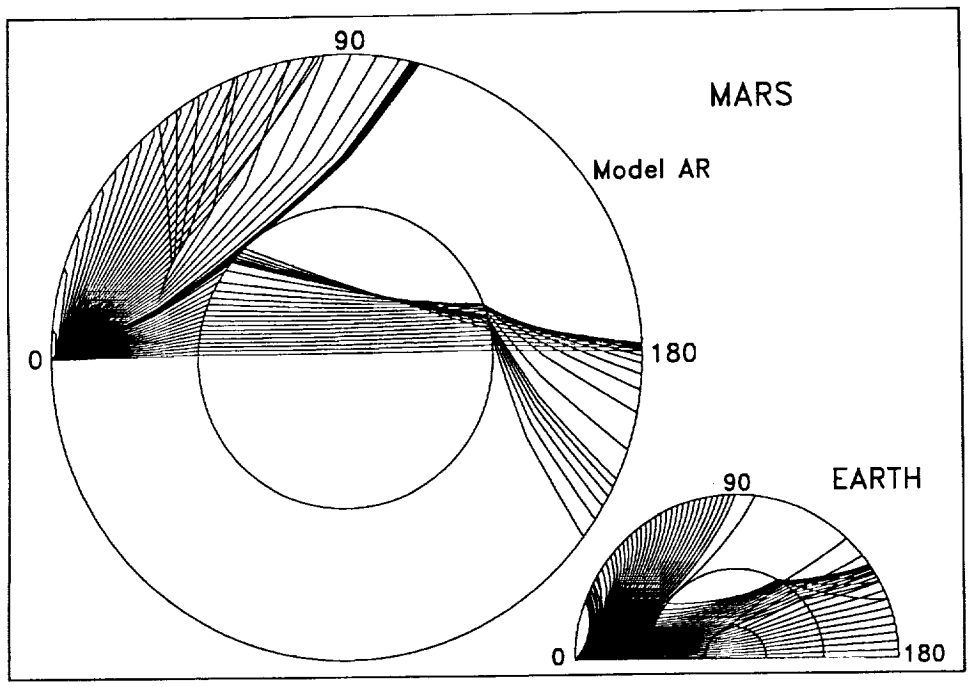

LPI Technical Report Number 91-02
LUNAR AND PLANETARY INSTITUTE 3303 NASA ROAD 1 HOUSTON TX 77058-4399
LPI/TR--91-02

SCIENTIFIC RATIONALE AND REQUIREMENTS FOR A GLOBAL SEISMIC NETWORK ON MARS

Sean C. Solomon, Don L. Anderson, W. Bruce Banerdt, Rhett G. Butler,
Paul M. Davis, Frederick K. Duennebier, Yosio Nakamura,
Emile A. Okal, and Roger J. Phillips

Report of a Workshop
Held at
Morro Bay, California
May 7-9, 1990

Lunar and Planetary Institute 3303 NASA Road 1 Houston TX 77058

LPI Technical Report Number 91-02
LPI/TR--91-02

Compiled in 1991 by the
LUNAR AND PLANETARY INSTITUTE

The Institute is operated by Universities Space Research Association under Contract NASW-4574 with the National Aeronautics and Space Administration.

This report may be cited as:
Solomon S. C. et al. (1991) *Scientific Rationale and Requirements for a Global Seismic Network on Mars.* LPI Tech. Rpt. 91-02, Lunar and Planetary Institute, Houston. 51 pp.

This report is distributed by:

ORDER DEPARTMENT
Lunar and Planetary Institute
3303 NASA Road 1
Houston TX 77058-4399

Mail order requestors will be invoiced for the cost of shipping and handling.

Cover: P and PKP ray paths inside Mars, assuming a surface-focus event. The take-off angles vary from 1° to 50° in 1° increments and from 16.5° to 17.5° in 0.1° increments. The smaller diagram is for the Earth.

Final Technical Report
for NASA Grant NAGW-1085

TECTONIC EVOLUTION OF MARS

May 1, 1989 to April 30, 1992

Southern Methodist University
3225 Daniel Avenue
Dallas, Texas 75275
for the
Department of Geological Sciences

Roger J. Phillips
Principal Investigator
Now at the
Department of Earth and Planetary Sciences
Washington University
One Brookings Drive
Campus Box 1169
St. Louis, MO 63130

Final Technical Report
for NASA Grant NAGW-1085

TECTONIC EVOLUTION OF MARS

This report is comprised of the following materials:

a) *LPI Technical Report Number 91-02*, "Scientific Rationale and Requirements for a Global Seismic Network on Mars"

b) Publication, "Permanent Uplift in Magmatic Systems With Application to the Tharsis Region of Mars," in the *Journal of Geophysical Research*, 1990

c) Abstract, "The Geophysical Signal of the Martian Global Dichotomy," in *EOS*, 1988

Contents

Executive Summary

Little is known of the internal structure or composition of Mars or the present rates and characteristics of tectonic activity and meteoroid impacts. The scientific tool best suited to address these issues is seismology. While a simple seismic experiment was included on the two Viking landers, one of the instruments did not operate and the experiment was severely limited by the location of the sensor high on the lander, the low sensitivity of the instrument, and the limited data rate allocated to seismic measurements. Thus, even after the Viking mission, our knowledge of the seismic characteristics of Mars remains poor.

The Mars Global Network Mission, now in the early stages of mission planning, offers an opportunity to deploy a global seismic network on Mars for the purposes of determining the internal structure and constitution of the planet and the characteristics of marsquakes and meteoroid impacts. At the request of the Mars Science Working Group, a workshop was held May 7–9, 1990, in Morro Bay, California, to define the scientific rationale and technical requirements for a global seismic network on Mars. This report is a summary of the findings and recommendations of that workshop.

The principal scientific objectives of a martian global seismic network are (1) to determine the nature and structure of the martian crust; (2) to determine the structure and state of the martian mantle; (3) to determine the radius and state of the martian core; (4) to determine the locations and mechanisms of marsquakes; (5) to determine the impact flux and characteristics of meteoroids in Mars-crossing orbits; and (6) to provide supporting information for meteorology.

From the experience of the Apollo seismic network, it is clear that when we design and conduct a seismic experiment on a new planet, (1) we must not assume that seismic signal characteristics are similar to those we see on Earth, (2) we must design an instrument with the highest possible bandwidth, dynamic range, and sensitivity, and (3) we must be alert to the possibility of unexpected seismic sources. The Viking seismic experiment, even though it was highly curtailed by mission priorities and by the inability to uncage the seismometer on the Viking 1 lander, provided valuable information for the planning of future missions to Mars. First, it established that the seismic background noise on Mars due to winds and atmospheric pressure fluctuations is very low. Seismometers more sensitive than the Viking instrument by a factor of at least 10^4 can operate on the planet without being affected by typical martian winds. Second, a much broader frequency response is required than was used for the Viking seismometer, opening up the possibility of detecting normal modes, surface waves, tidal loading, and Chandler wobble. Finally, a significant network of instruments will be necessary to study seismicity and to determine internal structure.

The principal natural seismic events on Mars are marsquakes and meteoroid impacts. While the rates of occurrence are not known for either type of event, theoretical considerations and experience from the Moon provide a basis for their estimation. Thermal stress associated with the global cooling of the martian lithosphere is expected to give rise to marsquakes at a rate of more than 10 events with seismic moment in excess of 10^{23} dyn cm per Earth year and more than 2 events with seismic moment in excess of 10^{24} dyn cm per Earth year; events in this size range are expected to produce records observable throughout a global network. Additional possible contributors to lithospheric strain rate (and thus to expected seismicity) on a regional to global scale include enhanced cooling beneath major volcanic provinces (e.g., Tharsis), seasonal variations in polar cap loading, and membrane stresses induced by tides and by long-term changes in planetary obliquity. Potential sources of marsquake activity on a more local scale include magma motion, landslides, variations in solar insolation, and freeze-thaw cycles. We conclude that internal seismic activity will occur on Mars at a rate more than adequate to address the principal scientific objectives.

Available data indicate that we can expect impacts of both cometary meteoroids and asteroidal fragments at rates, per unit area, on Mars similar to those detected on the Moon by the Apollo network, with the impact rates of asteroidal objects possibly somewhat higher on Mars if there is an abundance of meteoroids with Mars-crossing orbits. Most meteoroids of cometary origin are likely to be effectively consumed in the atmosphere because of their low density, friability, and high encounter velocity, while those of asteroidal origin in the mass range that yielded detectable seismic signals on the Moon are likely to impact the surface. Overall, given the greater surface area of Mars than the Moon, but also the likely higher seismic attenuation in the interior, the effect of the martian atmosphere, and the probable intervals of significant wind-generated ground noise, the teleseismically detectable seismicity rate from meteoroid impacts of asteroidal origin is likely to be somewhat less on Mars than on the Moon, and that due to cometary impacts is likely to be substantially less.

For each of the identified scientific objectives, certain classes of seismic observations are likely to provide the most straightforward means to achieve the objective. The need to make these key observations in turn affects station siting plans. With a global network, crustal structure is most readily addressed by measurement of the dispersion of 10–100-s

surface waves; such a measurement can be made with a small array of three stations, even for sources with poorly known locations and origin times. Mantle structure is most readily addressed by the inversion of the travel times of body waves vs. epicentral distance; in particular, major discontinuities at depth (e.g., the olivine–β phase boundary) should be detectable through pronounced triplications in the travel-time curve. The radius and state of the core will be inferable from the measurement of the travel times and amplitudes of core-reflected body waves at short distances (0–20°) and from the location of the core shadow zone and the arrival times of core phases at large distances (100° and beyond). It is thus important that some seismic stations be located at considerable distance from areas of potential seismic activity. The state and structure of the core strongly affect the periods of the gravest free oscillations of the planet, but these modes (with periods as great as 2000 s) are not excited except by very large seismic sources. The location and characterization of natural seismic sources is aided by having seismic stations near the source; such a consideration does not affect station siting for effectively random sources (e.g., meteoroid impacts), but does call for the placement of several stations near areas of more likely tectonic seismicity (e.g., Tharsis). The objective of providing information in support of meteorological experiments (e.g., on surface boundary layer parameters) suggests that seismic and meteorological stations be cosited where respective siting criteria permit.

There are technical trade-offs for seismic experiment performance between emplacement of the seismic sensor beneath the martian surface (i.e., using a penetrator) and placing the sensor package on the surface from a lander. The subsurface package has superior coupling to ground motion, is far less susceptible to surface temperature variations and wind stress, and should yield a higher signal-to-noise ratio. The current lack of availability of a long-term power source sufficiently rugged to withstand the decelerations of penetrator impacts, however, apparently precludes consideration at present of subsurface emplacement for stations in a long-term network. Surface stations should be adequate for the recording of seismic signals at periods shorter than 25–100 s, which covers the desired bandwidth except for the longest period surface waves, normal modes, and tidal and solid-body excitations (e.g., Chandler wobble). It will be essential, however, to site the seismic sensors as far as possible from the lander, which is likely to be the principal local source of seismic noise, particularly if the lander presents a large cross section to near-surface winds. The sensors should also be installed in streamlined enclosures.

Other desirable specifications for a seismic station on Mars are as follows: number of data channels – 3 components of ground motion; A/D sample rate – 1000 sps; A/D – 24 bit; stored data rate – 50 sps; total data rate – 100 Mbits/day; bit error rate – $<10^{-4}$; bandwidth – <0.04–20 Hz; sensitivity – 10^{-10} g; mass – 1.5 kg (sensors only); volume – 0.01 m^3; power – 2 W; onboard RAM – 4 Mbytes; calibration – once per day. The total data rate presumes a simple data compression scheme that reduces data volume by a factor of 3. More powerful schemes can increase this compression factor somewhat, but triggering algorithms are considered scientifically undesirable in the absence of information on the types of signals likely to characterize martian seismic events.

A station siting plan must strike a compromise among the various scientific objectives. There must be a mix of closely spaced stations to detect and locate nearby seismic events and to serve as arrays for measurements of phase velocity and propagation direction, and more globally dispersed stations to provide planetary coverage and to ensure the recording of core phases and other signals diagnostic of deep structure. The recommended plan consists of nested triads of stations. Small triads of stations should be located approximately 100 km apart as local arrays. Each of these small triads should consist of 3 three-component short-period instruments arranged in a triangle around a broadband observatory-class three-component sensor. Sets of these small triads should be emplaced in larger triangular patterns, approximately 3500 km on a side, one each in the eastern and western hemispheres of Mars. Tentative locations for large triangle vertices consistent with the various scientific objectives include (1) west of Ascraeus Mons, north of eastern Valles Marineris, and in the southern highlands and (2) in the Elysium province, in the Isidis Basin, and in the northern lowlands.

Introduction

Little is known of the internal structure or composition of Mars. Also poorly known are the present rates and characteristics of tectonic activity and meteoroid impacts. The scientific tool best suited to address these issues is seismology. While a simple seismic sensor was included on the two Viking landers, one of the instruments did not operate and the experiment was severely limited by the location of the sensor high on the lander, the low sensitivity of the instrument, and the limited data rate allocated to seismic measurements. Thus, even after the Viking mission, our knowledge of the seismic characteristics of Mars remains poor.

The Mars Global Network Mission, now in the early stages of mission planning, offers an opportunity to deploy a global seismic network on Mars for the purposes of determining the internal structure and constitution of the planet and the characteristics of marsquakes and meteoroid impacts. At the request of the Mars Science Working Group (MSWG), a workshop was convened to define the scientific rationale and technical requirements for a global seismic network on Mars. The workshop was held May 7–9, 1990, in Morro Bay, California, and was attended by 10 scientists with interest and expertise in seismology and martian geophysics. A list of participants and the agenda for the workshop are included at the end of this technical report. This report is a summary of the findings and recommendations of that workshop.

It is important at the outset to recognize that observational seismology is quite different from meteorology, geochemistry, or most other planetary surface sciences. The nature of seismic signals and noise on a newly visited planet are unknown, and it is impossible to determine in advance all the optimum parameters of a global seismic experiment. In this respect, a seismic network is much like an imaging experiment. While we don't usually think of a camera system as an experiment in this sense, the appropriate bandwidth, wavelengths, and dynamic range are also not known in advance. This lack of knowledge is generally accommodated by the enormous data rates and sophisticated processing that we have come to accept for imaging experiments. The lack of prior knowledge is a handicap only if weight, power, and data-rate constraints make it necessary to select narrowly defined experimental parameters *a priori*. Such a preselection is not done for imaging, and it should not and need not be done for seismology.

Following a brief overview of the mission concepts for a Mars Global Network Mission as of the time of the workshop, we present the principal scientific objectives to be achieved by a Mars seismic network. We review the lessons for extraterrestrial seismology gained from experience to date on the Moon and on Mars. An important unknown on Mars is the expected rate of seismicity, but theoretical expectations and extrapolation from lunar experience both support the view that seismicity rates, wave propagation characteristics, and signal-to-noise ratios are favorable to the collection of a scientifically rich dataset during the multiyear operation of a global seismic experiment. We discuss how particular types of seismic waves will provide the most useful information to address each of the scientific objectives, and this discussion provides the basis for a strategy for station siting. Finally, we define the necessary technical requirements for the seismic stations.

Mars Global Network Mission Concepts

The Mars Global Network Mission, as conceived at the time of the workshop, is to consist of about 20 landed stations globally distributed over the surface of Mars. These stations may be launched during a single Mars opportunity and deployed sequentially from orbit, or launched a few at a time over several opportunities (at approximately two-year intervals), with deployment occurring directly from hyperbolic approach. There may be restrictions on allowable landing sites on the basis of altitude (altitudes ranging from −2 to 6 km are currently considered acceptable) and latitude (solar power is not thought to be viable poleward of about 45°). An orbiting platform may be available for communication support.

The landers are envisioned as relatively simple systems, with a landed mass of about 75 kg and an electrical power system capable of supplying 5–15 W continuously. Deceleration techniques will be used to minimize impact loads. Complexity of both mechanisms and operations will be kept to a minimum, and the stations should be capable of conducting operations on the surface for up to 10 years.

The objectives of this mission have been chosen to take advantage of the unique opportunities presented by a global network of stations: the ability to make simultaneous measurements of a given phenomenon at widely spaced locations and the capability for sampling a large number of different geological settings. The primary objectives are scientific, and include global seismology, meteorology, and geochemical investigations. Other key objectives relate to future plans for the exploration of Mars, such as characterizing the upper atmosphere for optimizing aerocapture techniques and identifying potential sources of accessible water and other resources.

In order to formulate a useful set of requirements and goals for a seismic network experiment on Mars, it is helpful to have a framework against which to judge their feasibility. Mission planners and engineers have developed several scenarios for a Mars network mission that attempt to address the technical constraints and science goals as they are currently understood. These scenarios have incorporated various assumptions about a seismic experiment, and result in a number of limitations as to how such an experiment could be conducted. Table 1 contains a list of parameters we consider relevant to seismology, taken from recent JPL and Ames Research Center network mission studies. While realizing that these values are subject to rapid change and may well be obsolete before this report is published, we include them here as our point of reference as to what is currently considered technically acceptable. In many areas we will argue for substantially more capability than is reflected in Table 1.

TABLE 1. Initial planning constraints on a Mars global seismic experiment.

Number of Stations	10–20
Location Accuracy	
Control	50–200 km
Knowledge	<1 km
Distribution	Global
Lifetime	2–10 years
Relative Timing Accuracy	20 msec
Telemetry Rate (per station)	
Via Orbiting Relay	5 Mbit/day
Direct to Earth	<300 kbit/day
Command Capability	Little or none
Emplacement	On surface, <1 m from lander
Landing Loads	40–100 g
Mass	1.5 kg
Power	2 W

Scientific Objectives for a Global Seismic Network on Mars

The principal scientific objectives of a martian global seismic network are to (1) determine the nature and structure of the martian crust; (2) determine the structure and state of the martian mantle; (3) determine the radius and state of the martian core; (4) determine the locations and mechanisms of marsquakes; (5) determine the impact flux and characteristics of meteoroids in Mars-crossing orbits; and (6) provide supporting information for meteorology.

DETERMINATION OF THE NATURE AND STRUCTURE OF THE MARTIAN CRUST

Mars has a distinct low-density crust of variable thickness, as indicated by the partial to complete isostatic compensation of surface topography (*Phillips et al.*, 1973; *Phillips and Saunders*, 1975). The mean thickness of the crust, however, is poorly constrained. A minimum value for the average crustal thickness of 28 ± 4 km (depending on choice of crust-mantle density difference) was obtained by *Bills and Ferrari* (1978) by fitting a model crust of uniform density and variable thickness overlying a uniform mantle to topography and gravity expressed in spherical harmonics to degree and order 10; for this minimum mean thickness the crust is of zero thickness beneath the Hellas Basin. For a crustal thickness of 15 km at the site of the Viking 2 lander, a result inferred from the tentative identification of narrow-angle Moho-reflected phases in the single recorded seismogram of possible tectonic origin (*Anderson et al.*, 1977), *Bills and Ferrari* (1978) obtained a mean crustal thickness of 37 ± 3 km, a maximum thickness of 69 ± 8 km (beneath Tharsis), and a minimum thickness of 9 ± 1 km (beneath Hellas). In a contrasting work, *Sjogren and Wimberly* (1981) used topography and gravity data to infer that an isostatically compensated Hellas Basin has an Airy compensation depth of 130 ± 30 km. From the models of *Bills and Ferrari* (1978), this value would correspond to a globally averaged crustal thickness of about 150 km.

The mean thickness of the martian crust bears strongly on the history of differentiation of the planet, in that the crustal volume consists of some combination of material remaining from postaccretional differentiation of crust from mantle plus later intrusive and extrusive magmas generated by partial melting of the martian mantle. A crust 30 to 150 km in thickness constitutes 3% to 13% of the planetary volume, a substantial range of uncertainty. Seismology offers the only direct tool to measure crustal thickness, either by the travel times of body wave phases at near and regional distances or by the dispersive characteristics of surface waves.

There are expected to be pronounced lateral variations in crustal thickness that bear strongly on the deep structure and mode of formation of major geological features on Mars. For instance, the global crustal dichotomy, the approximately hemispherical division of the martian surface between the topographically lower and stratigraphically younger northern plains and the heavily cratered southern uplands, is thought to be compensated by an Airy isostatic mechanism on the basis of analysis of gravity anomalies across the dichotomy boundary (*Janle*, 1983), but this hypothesis needs to be confirmed by seismic measurement of crustal thickness in each of the northern and southern hemispheres. The deep structure of the Tharsis province, which has been a focus for martian tectonic and volcanic activity over much of the history of the planet, has been a topic of considerable controversy. Structural models vary from a mix of Airy and Pratt isostasy (*Sleep and Phillips*, 1979, 1985; *Banerdt et al.*, 1982) to large-scale flexural support of the excess volcanic and intrusive material by the finite elastic strength of the martian lithosphere (*Willemann and Turcotte*, 1982; *Banerdt et al.*, 1982); the distinct crustal structures predicted by these models can be readily distinguished with regional seismic data from the Tharsis area. In general, once the crustal structure is established seismologically in a few areas, extrapolation to the rest of Mars by means of gravity and topography data—both those now available and those expected to be provided by the Mars Observer mission—can be readily accomplished (e.g., *Thurber and Solomon*, 1978).

Significant reservoirs of H_2O and other volatiles are likely to be present within the martian crust, as permafrost and saturated layers of regolith and bedrock (e.g., *Carr*, 1987). The presence of ice and water at depth will significantly affect the seismic wave velocities and attenuation. While active seismic experiments offer the most promising approach to the exploration of buried volatile reservoirs, seismic phases recorded by passive stations at near or regional distances may nonetheless contain signatures of a layered crustal velocity structure indicative of ice-rich or water-rich layers.

DETERMINATION OF THE STATE AND STRUCTURE OF THE MARTIAN MANTLE

The only direct constraints on the internal structure of Mars are its mean density and its moment of inertia. The latter quantity is not precisely known, and, in the absence of a direct determination of the martian precessional constant, must rather be derived from the second degree zonal coefficient J_2 in the spherical harmonic expansion of the gravitational potential by means of one or more additional assumptions. The appropriate assumptions are matters of current debate (*Bills*, 1989a,b; *Kaula et al.*, 1989),

and it may be concluded only that the dimensionless moment of inertia I/MR^2 most likely lies between 0.350 and 0.365, but lower values cannot be completely excluded. In addition, the interior constitution of Mars is constrained by geochemical and cosmochemical considerations relating the bulk composition to that of various classes of meteorites (e.g., *Anderson*, 1972), in particular by the hypothesis that the SNC meteorites were derived from Mars (e.g., *McSween*, 1984; *Bogard et al.*, 1984; *Becker and Pepin*, 1984).

An early analysis of the plausible ranges in the density of mantle and core material and in the radius of the core was made by *Anderson* (1972), who concluded the mantle of Mars is richer in FeO than the Earth's mantle. This analysis was updated by *Goettel* (1981), under the then commonly held view that the dimensionless moment of inertia of Mars was $I/MR^2 = 0.365$ (*Reasenberg*, 1977; *Kaula*, 1979). The zero-pressure density of the mantle under this assumption is between 3400 and 3470 kg/m^3, confirming a magnesium number [molar Mg/(Mg+Fe)] somewhat lower than petrological estimates for the Earth's upper mantle (*Goettel*, 1981). A comparatively FeO-rich composition has also been inferred for the source region of the magmas from which the SNC meteorites were derived (e.g., *McSween*, 1985), a result that has been used as one of the arguments favoring Mars as the SNC parent body (*Wood and Ashwal*, 1981). If the dimensionless moment of inertia I/MR^2 is as low as 0.345, as *Bills* (1989a) estimated, however, then the zero-pressure mantle density must be very low (3200–3220 kg/m^3) (*Bills*, 1990), implying a high magnesium number and a difficulty with the identification of Mars as the source of SNC meteorites. While this controversy would be lessened by a precise measurement of the martian precessional constant, definitive determination of the magnesium number of the martian upper mantle must come from measurement of the mantle seismic velocity structure, either by an inversion of body wave travel times or by an inversion of normal mode eigenfrequencies.

Determination of the radial structure of the martian mantle, of course, provides significantly more information than the mantle magnesium number. Prominent discontinuities, or rapid variations in seismic velocity with depth, can be signatures of solid-solid phase changes or of chemical layering resulting from whole-planet differentiation. For instance, the olivine–β phase transition should occur at a depth greater than 1000 km (*BVSP*, 1981), with the precise depth a function of mantle temperatures and magnesium number. Within layers of constant composition and phase, the radial gradients of compressional (P) and shear (S) wave velocities provide measures of the mean thermal gradient and thus constrain the efficiency of convection as a mantle heat transport mechanism. The nature of any asthenosphere on Mars—important for models of mantle dynamics, thermal structure, interior volatile budgets, and magmatism—will be revealed by zones of low seismic velocity and high seismic attenuation.

Once the average radial structure of the martian mantle is reasonably well established, it may be possible to determine major lateral variations from that average structure. Such a possibility will depend on there being a fairly good global distribution of energetic seismic sources. Lateral variations in the seismic velocity structure of the lithospheric mantle could result from melting-induced compositional variations, perhaps most notably beneath major volcanic provinces such as Tharsis (*Finnerty et al.*, 1988; *Phillips et al.*, 1990). Lateral variations in the deeper mantle are likely to be the signature of patterns of mantle upwelling and downwelling convective flow (e.g., *Schubert et al.*, 1990).

DETERMINATION OF THE RADIUS AND STATE OF THE MARTIAN CORE

While the moment of inertia of Mars indicates that the planet has a distinct high-density core, neither the size of the core nor its density are well constrained. For $I/MR^2 = 0.365$, the core could vary in radius from 1300 to 1900 km, corresponding to zero-pressure density varying from 8900 (pure Fe) to 5800 (FeS) kg/m^3 and core mass varying from 13% to 26% of planetary mass (*Goettel*, 1981). For I/MR^2 less than this figure, the core radius is larger (and the mantle density less) for a given value of core density (e.g., *Bills*, 1990). From siderophile and chalcophile abundances in SNC meteorites, *Laul et al.* (1986) and *Treiman et al.* (1987) have inferred that the SNC parent body has a core constituting 20–35% of the parent body mass and containing 12–14 wt% sulfur. The sulfur content of the core strongly influences the timing and extent of freezing of the core from an initially totally molten state; inner core freezing is a major potential source of energy for driving a martian core dynamo (*Stevenson et al.*, 1983; *Schubert and Spohn*, 1990). In particular, a totally molten core at present constrains the sulfur content (or that of other light elements in the core) to be at least 15% (*Schubert and Spohn*, 1990).

Seismic observations, including travel times and amplitudes of body waves and eigenfrequencies of longer period normal modes, are capable of determining the radius of the martian core, the radius of any solid inner core, and the average radial seismic velocity structure of the core. The size and average seismic velocity of the core will constrain core composition and thus the bulk composition of the planet, in particular the ratio of metal plus sulfide to silicate. The relative fractions of liquid and solid core will strongly constrain the fraction of light elements in the core, the thermal history of the core, and the availability of inner core freezing as an energy source for generation of a planetary magnetic field.

DETERMINATION OF THE LOCATIONS AND MECHANISMS OF MARSQUAKES

The distribution and character of tectonic sources of seismic energy in a planet provide measures of the internal stress field and of the processes that have generated those stresses. Mars displays an abundance of tectonic features that must have formed by seismogenic faulting, and models for the present distribution of stresses within the martian lithosphere (e.g., *Banerdt et al.*, 1982; *Sleep and Phillips*, 1985) suggest that marsquakes should be generated wherever ongoing lithospheric processes (e.g., differential cooling, tidal or seasonal loading, fluid migration) induce further stresses that add constructively to the long-term stress field.

Experience on the Earth and Moon suggests that a suitably configured seismic network on Mars operational over a duration of several years will permit the determination of the principal regions of marsquake activity and should yield at least approximate source mechanisms indicative of the style of faulting. Such data will provide direct tests of current models for lithospheric stress on Mars. It can be anticipated that the most likely areas of seismicity are those that display geological evidence for relatively recent volcanic or tectonic activity, such as the Tharsis Montes, Olympus Mons, or Valles Marineris (e.g., *Lucchitta*, 1987; *Tanaka et al.*, 1988). Some densification of the seismic network in the most probable areas of seismic activity is warranted to ensure adequate resolution of marsquake hypocenters and source mechanisms.

DETERMINATION OF THE IMPACT FLUX AND CHARACTERISTICS OF METEOROIDS IN MARS-CROSSING ORBITS

Before the era of space missions, practically all the information about meteoroids, the small interplanetary objects in the inner solar system, came from observations of meteors and recovered meteorites. Various lunar and planetary missions have expanded this database to include crater statistics on most of the planets and satellites with solid surfaces, giving us information on the history and size distribution of impacts of relatively large meteoroids.

The Apollo lunar seismic experiment, in particular, yielded a unique dataset that allowed determination of the flux and orbital characteristics of several types of meteoroids crossing the orbit of the Earth-Moon system (e.g., *Oberst and Nakamura*, 1991). Most prominent among these objects are those originating from the break-up of long-period comets and asteroids. Many of those of cometary origin are associated with meteor showers observed on Earth. In contrast, a majority of those considered to be asteroidal fragments are observed as sporadic impacts. However, some of them form streams and swarms, indicating relatively recent break-up from their parent bodies, and some of them even appear to be related to known meteorites.

The true nature of these impacting objects is not clearly understood, and there are yet many open questions about their origin. Our present interpretation is limited by the fact that all our observations to date concerning the current population of these objects are restricted to those in Earth-crossing orbits. Similar observations on Mars will expand our knowledge to include those in Mars-crossing orbits. This will greatly advance our understanding of the nature and orbital properties of these objects, and thus will help us decipher their role in the recent evolution of the solar system. In particular, a determination of the relative impact fluxes on Mars and the Moon will provide a critical test of competing crater chronologies used for the dating of relatively young surfaces on Mars (e.g., *Hartmann*, 1977; *Neukum and Hiller*, 1981; *BVSP*, 1981).

SUPPORTING INFORMATION FOR METEOROLOGY

Seismic noise on Earth is generally of meteorological and oceanographic origin. Winds and waves couple into the ground and result in propagating seismic disturbances. On Mars this type of "noise" is actually a useful meteorological "signal" that is relevant to such boundary-layer parameters as surface friction velocity and surface roughness. Seismic instruments yield information about high-frequency wind parameters that are generally not measured by meteorological observations.

Ideally seismic and meteorological observatories on Mars should be combined. The electronics and processing requirements are similar and can be shared. Having the seismological and meteorological data corecorded helps in the analysis of both. The expertise of seismologists in time series processing can be used to advantage in designing the meteorological electronics, and the expertise of meteorologists can be used to advantage in helping to interpret the background "noise." Thermoelastic stresses due to propagating temperature gradients (sunrise, sunset, clouds, eclipses) and propagating weather fronts may also provide useful seismic sources for probing the shallow interior.

Lessons from Apollo and Viking

There have been two previous experiments in extraterrestrial seismology, the Apollo seismic network that operated on the lunar surface for the 8-year period 1969–1977 and the Viking seismology experiment that operated on the martian surface for a 19-month period. Both of these experiments yielded valuable lessons for the design and operation of future seismic networks on other planets.

THE APOLLO SEISMIC NETWORK

The Apollo lunar seismic network was established during the lunar landing missions in the period 1969–72 and operated until it was shut down in 1977. Despite the very limited number of stations, the network was highly successful in determining the seismicity and internal structure of the Moon (Fig. 1) and in documenting the nature of interplanetary objects in Earth-crossing orbits (e.g., *Nakamura et al.*, 1982). This success, however, did not come as a simple extension of what we knew about seismology on Earth. In fact, the majority of seismic events found on the Moon would not have been detected had we simply looked for normal earthquake-type signals with instruments of a sensitivity typical for terrestrial use.

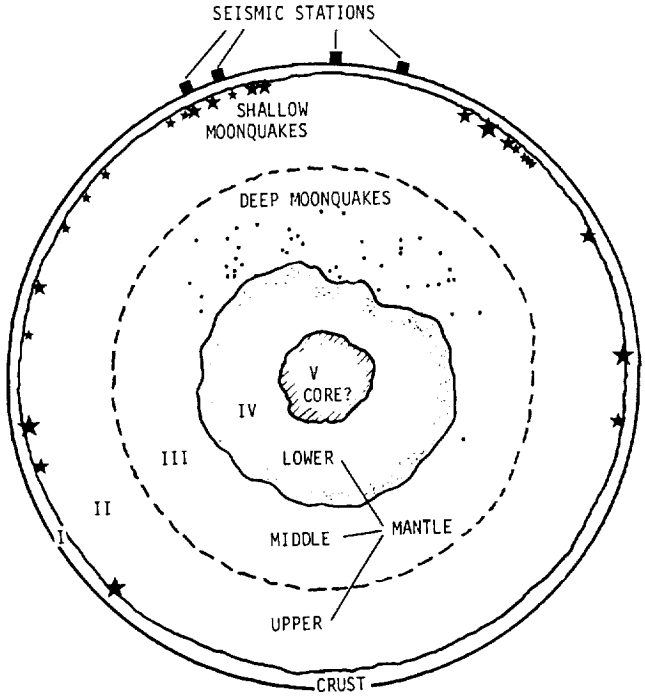

Fig. 1. Schematic diagram of the lunar interior inferred from the Apollo seismic data. The information depicted was derived from records obtained over an eight-year period by a four-station network. From *Nakamura et al.* (1982).

The tidally triggered deep moonquakes, which constituted the majority of the detected events, occurred at depths significantly greater than those of any earthquakes. Rare but energetic shallow moonquakes, tectonic in origin, had a much higher frequency content than normal earthquakes of comparable magnitudes. All seismic signals, with long and nearly incoherent codas, were much more prolonged in signal duration than their counterparts on Earth (Fig. 2). More than 99% of the detected signals would have been too small to be detectable had we deployed instruments of sensitivity comparable to those used on Earth. That we were able to detect these events and use them quite profitably was because the instruments used on the Moon had sufficiently high sensitivity, at least two orders of magnitude higher than any on Earth, and because we collected continuous data without assuming *a priori* any characteristics of seismic signals or hypocentral locations for seismic sources.

From this experience, it is clear that when we design and conduct a seismic experiment on a new planet such as Mars, we must (1) not assume that seismic signal characteristics are similar to those we see on the Earth or the Moon, (2) design an instrument with the highest possible sensitivity, and (3) be alert to the possibility of unexpected seismic sources. It is quite plausible that seismic signals carrying important information about the interior of Mars may come from such sources. In short, we must be prepared for the unexpected and be ready to capitalize on whatever signals are observed in such an experiment.

Another important consideration in designing a seismic network is the cost of operation. The Apollo network was terminated prematurely because it was too costly to keep operating, even though it was fully operational. With currently available technology, the operational cost of a martian seismic network can be reduced considerably from that of the Apollo network. Since a seismic network on Mars needs to be operational for an extended period of time because of the nature of the signals we aim to acquire, it is important that the routine network operation be made as simple as possible to minimize the cost of continued operation.

THE VIKING SEISMIC EXPERIMENT

The primary emphasis on Viking lander science was on biology, organic chemistry, imaging, and meteorology, with most aspects of surface chemistry, petrology, and geophysics relegated to future missions. The exceptions were the inorganic analysis experiment, the magnet experiment, and the seismometer. However, these studies were limited only to reconnaissance measurements. As a result, the Viking

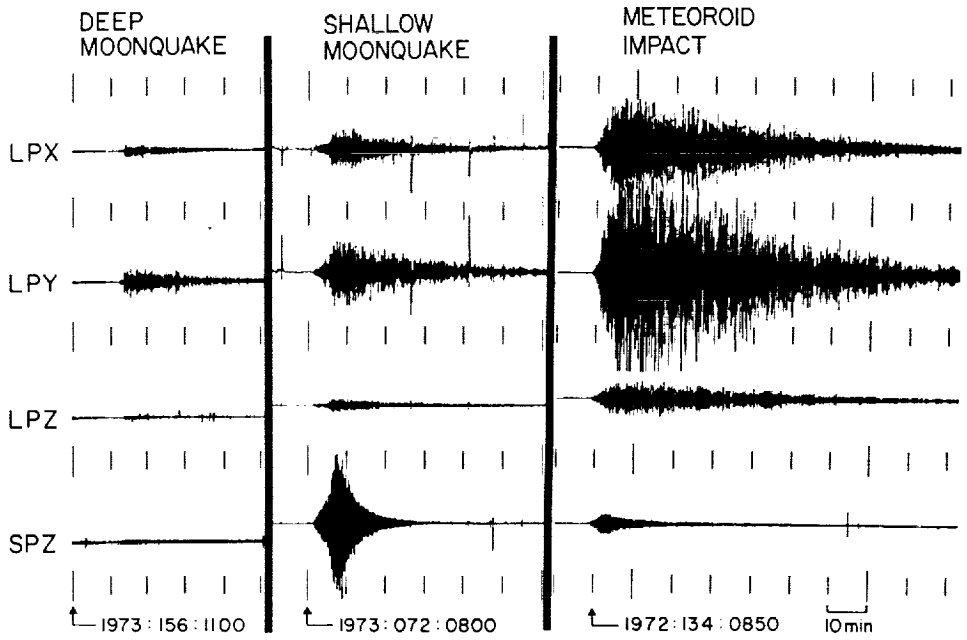

Fig. 2. Representative Apollo lunar seismograms shown at a compressed timescale. From *Nakamura et al.* (1982).

seismic experiment was severely constrained by strict limitations on weight, power, and data rate, and was perturbed by the conflicting demands of the other onboard experiments. The weight constraint precluded an ultrasensitive seismometer of the Apollo class or a broadband seismometer. The original desire to place the seismometer on the surface was sacrificed because of the weight and complexity penalties of such an operation; thus an onboard location was dictated that immediately increased the noise level (by at least three orders of magnitude) because of lander and wind activity. The data-rate constraint required severe data compression using an onboard data processor and thus also imposed weight and power penalties. Overall, the most severe constraints on the Viking seismic experiment were the limited data allocations and the onboard location of the seismometer.

These various constraints and trade-offs led to the design of a short-period three-component seismometer with onboard data compaction and triggering to optimize the data return (*Anderson et al.*, 1972). The objectives were (1) to characterize the seismic noise environment at the landing sites, (2) to detect local events in the vicinity of the lander, and (3) to detect large events at teleseismic distances. Under optimal conditions it would also have been possible to determine the following: (1) the approximate distance of events from the separation of various seismic phases, (2) the direction of events to within a 180° ambiguity in azimuth, (3) the attenuation and scattering properties of the crust to determine if the crust were Moon-like or Earthlike in these characteristics (which are related to the volatile content), and (4) an estimate of crustal thickness if crustal and reflected phases could be identified.

The Viking 1 seismometer failed to uncage, and no useful data were returned. The Viking 2 seismometer, emplaced on the surface of Mars in the Utopia Planitia region, 47.9°N, 225.9°W, successfully uncaged and operated for a period of 19 months (*Anderson et al.*, 1977; *Lazarewicz et al.*, 1981).

The Viking experiment, even though it was highly curtailed by mission priorities and by the inability to uncage the first seismometer, provided valuable information for the planning of future missions to Mars; see also Appendix A. First, it established that the seismic background noise on Mars due to winds and atmospheric pressure fluctuations is very low. The Viking seismometer, mounted on a relatively compliant spacecraft with a large surface area exposed to winds, could still operate at maximum sensitivity at least half the time with no indication of noise visible on the records, a situation that indicated that seismometers with much greater sensitivities can be operated on the planet. Emplaced by penetrators or deployed as small packages, seismometers more sensitive than the Viking instrument by a factor of at least 10^4 can operate on the planet without being affected by typical martian winds.

The indications from Viking are that Mars is probably less seismically active than the Earth (*Anderson et al.*, 1977; *Goins and Lazarewicz*, 1979). Greater sensitivity is a must for any future seismic instruments on the planet. At the same time, a much broader frequency response is desirable than was used for the Viking seismometer, opening up the possibility of detecting normal modes, surface waves, tidal loading, and Chandler wobble.

Another important consideration is the deployment of a network of instruments. With a well-placed network of

four very sensitive Apollo seismographs it was possible to study the seismicity of the Moon and to determine its internal structure, even though most moonquakes are very small. A similar approach with the deployment of a network of highly sensitive instruments is needed for Mars exploration. Since Mars is a larger planet than the Moon and shows much greater geologic and tectonic diversity, both global and regional seismic networks are needed to understand martian structure and tectonics. If Mars, as expected, is intermediate in seismic activity between the Moon and the Earth, then numerous seismic events of internal origin will be recorded by a martian seismic network. It is certainly not valid to say that the Viking experiment shows that Mars is an inactive planet.

Expected Rates of Seismicity on Mars

The principal natural seismic events expected on Mars are marsquakes and meteoroid impacts. While the rates of occurrence are not well known for either type of event, theoretical considerations and experience from the Moon provide a basis for their estimation. We do not consider explicitly in this report possible man-made seismic sources on Mars, such as the impact of spacecraft onto the martian surface or the mechanical or explosive excitation of seismic waves by a lander or surface rover. The use of such sources would obviously augment an otherwise passive global seismic experiment.

MARSQUAKES

Volcanic and tectonic landforms on the surface of Mars provide evidence that the martian lithosphere has been a source of seismic activity over essentially the entire history of the planet. Images of young volcanic deposits that reveal only a few impact craters at the highest Viking Orbiter imaging resolution (e.g., *Carr et al.*, 1977) suggest that internal activity may persist to the present. Thus, Mars should be a seismically active planet today, albeit at lower levels than in its more active geologic past. In this section we review several different potential sources of marsquake activity and present the results of calculations (see Appendix B) of the predicted rate level of seismic activity as a function of marsquake size.

On a local or regional scale, potential sources of marsquakes include magma motion (including extrusion), landslides, time-varying insolation, and freeze-thaw cycles. Some of these sources will contribute to the seismic background noise. In other cases, characteristics of the seismicity may be diagnostic of the nature of the physical process involved (e.g., marsquake swarms near a volcano might be associated with magma motion). The largest of these events will be reliable seismic sources for studying interior structure.

On a larger scale, marsquakes may result from the brittle failure of the lithosphere in response to stresses induced by such processes as crustal thickening by volcanism and plutonism, vertical motions arising from lithospheric buoyancy changes, and horizontal tractions exerted by convective flow in the mantle. Additional potential seismogenic processes on a large scale are the cooling and thickening of the lithosphere and changes in the principal moments of inertia. The rates of marsquake generation associated with this latter group of processes can be estimated (Appendix B) and provide a lower bound on the expected level of seismic activity.

Differential cooling of the martian lithosphere constitutes an ongoing source of potential seismogenic strain. Such

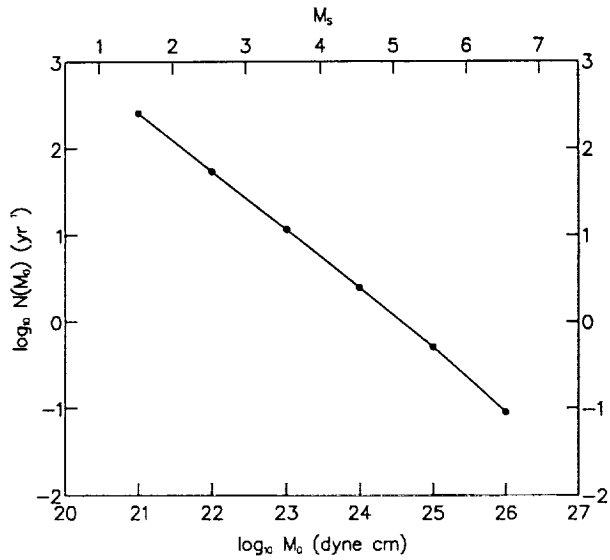

Fig. 3. Expected rate of marsquakes generated by the global cooling of the martian lithosphere. The quantity N (M_o) is the number of marsquakes per Earth year with seismic moment equal to or greater than M_o. The equivalent surface-wave magnitide M_S is also indicated, under the assumption the M_S-M_o relation is similar to that on Earth.

differential cooling is the major contributor to seismicity in young oceanic lithosphere on Earth (*Bratt et al.*, 1985; *Bergman*, 1986) and may be at least partly responsible for the generation of shallow moonquakes (*Nakamura et al.*, 1979). For a simple parameterized convection model of the recent thermal history of Mars the rate of global cooling is equivalent to a mean lithospheric strain rate of 1.0×10^{-19} s^{-1} (Appendix B). If the distribution of marsquakes by moment is similar to that in terrestrial oceanic lithosphere, then this mechanism yields a rate of seismicity as a function of marsquake size as given in Fig. 3. Global lithospheric cooling thus is expected to generate about 12 marsquakes per year with moment in excess of 10^{23} dyn cm and 2.5 events per year with moment in excess of 10^{24} dyn cm. Events with moments in excess of about 10^{23} dyn cm (about m_b 4.6) are routinely located on Earth with body-wave arrival time readings from global seismic networks, and for events with moments in excess of 5×10^{23} to 10^{24} dyn cm (about m_b 5) the source mechanisms are routinely determined (e.g., *Dziewonski et al.*, 1987).

Of course, other mechanisms will contribute to lithospheric strain and will thus add to the expected population of marsquakes over that depicted in Fig. 3. For instance, greater than average rates of cooling beneath the major volcanic provinces in Tharsis and Elysium will lead to

enhanced rates of marsquake activity in those areas. Solar tides and variations in polar cap loading due to changes in the planet's obliquity contribute comparatively high strain rates over half cycles of 1–10^5-yr duration, respectively, and may act to trigger marsquakes where the sense of strain reinforces that associated with longer-term processes (Appendix B). Ongoing strains associated with mantle convection or the motions of any fluids (magma or water) through the planetary interior will also act to raise the level of seismicity above that due solely to global cooling.

We conclude that internal seismic activity will occur on Mars on a rate more than adequate to record, locate, and characterize marsquakes with a global seismic network. Over a 10-year period of observations, an effectively global distribution of activity is expected, although areas of significant topographic relief, large gravity anomalies, and comparatively recent volcanic activity are all favored sites for higher than average rates of seismicity. The records from such a population of marsquakes should be sufficient to address all the principal scientific objectives for a martian global seismic experiment described above.

METEOROID IMPACTS

Impacts of meteoroids in the mass range between 10^2 and 10^6 g detected on the Moon by the Apollo lunar seismic network contributed significantly to our understanding of the deep internal structure of the Moon as well as the characteristics of the population of small objects in Earth-crossing orbits (*Duennebier et al.*, 1975). Similar observations on Mars are expected to be equally useful.

There are several factors that influence the seismic detectability of meteoroid impacts. They include (1) the impact rate on the martian surface of various classes of meteoroids; (2) the effect of the atmosphere in retarding impacts; (3) the efficiency of impacts in generating seismic waves; and (4) the efficiency of seismic wave propagation through the interior of Mars. The combined effect of these factors in relation to the sensitivity of the sensors and the expected levels of ground noise, then, will determine the detectability of seismic signals from impacts. The effect of each of these factors is evaluated in Appendix C.

Meteoroid impact rates depend on the population density of various types of objects in the inner solar system, as well as their approach velocity and the size and mass of the target planet. Available data indicate that we can expect impacts of both cometary meteoroids and asteroidal fragments at rates, per unit area, on Mars similar to those on the Moon. Impact rates of asteroidal objects, however, may be somewhat higher on Mars than on the Moon if there is abundance of meteoroids originating from asteroids with Mars-crossing orbits.

The effect of the martian atmosphere may be significant. Available data on this important effect are rather scarce, but they indicate that most meteoroids of cometary origin are likely to be effectively consumed in the atmosphere, while those of asteroidal origin in the mass range of interest are likely to be only partially affected.

The efficiency of conversion of impact kinetic energy to seismic wave energy depends on the impact velocity, as well as other factors such as the properties of the target. The impact velocities of cometary objects are expected to be only slightly lower on Mars than on the Moon, while those of asteroidal origin are expected to be about 30% lower on Mars than on the Moon, or about half the kinetic energy for a given mass. The difference in physical properties between the martian surface and the lunar surface may be significant for seismic wave generation. However, we do not have reliable data at present to estimate this difference.

There are substantial differences in seismic wave propagation and attenuation between the Moon and the Earth. Available data indicate that the peak amplitude of the scattered seismic wave train observed on the Moon is about an order of magnitude greater than the amplitude of the P wave on Earth for a seismic source of a given energy, while the initial P-wave amplitude on the Moon is about an order of magnitude smaller than that on Earth. What it would be like on Mars is difficult to estimate, but the likely high volatile content of the martian interior suggests that seismic wave propagation in Mars may be similar to that in the Earth. As noted below, however, even if the intrinsic attenuation of seismic waves is similar in Mars and the Earth, the decay of seismic wave amplitudes with angular distance on Mars is less than on Earth because of the smaller planet size.

As noted above, the Viking seismometer was not capable of determining the level of ground noise on Mars. However, it was also noted that when the wind was calm the observed ground noise was below the threshold of detection of the Viking seismometer. Thus, although we expect that wind stress will be the dominant source of noise, and that when the wind speed is high the ground noise will similarly be high, when the wind is calm the ground noise will be quite low. The ground noise at times of calm winds may be significantly below typical background noise on Earth, where seismic noise is dominated by wind-driven ocean waves.

Given the greater surface area of Mars than the Moon, the likely higher seismic attenuation in the martian interior, the effect of the martian atmosphere, and the probable intervals of significant wind-generated ground noise, we expect a somewhat reduced detection level of large impacts and a greatly reduced detection of small cometary impacts on Mars compared with the Moon. An estimate of the rate of seismicity due to large impacts of asteroidal origin is derived in Appendix C and shown in Fig. 4. The rates

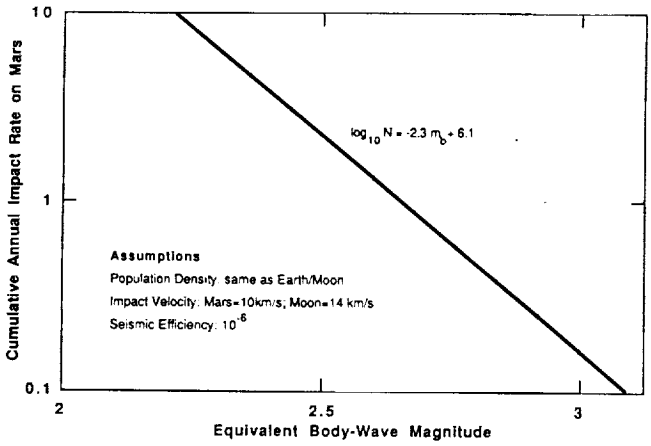

Fig. 4. Expected rate of meteoroid impacts per Earth year expressed in terms of equivalent body-wave magnitude m_b. The underlying assumptions are conservative, and the actual rates may be as much as a factor of 10–100 greater than those shown.

indicated in the figure are conservative by as much as one to two orders of magnitude. Nonetheless, for a given size of seismic events, meteoroid impacts are expected to be less frequent than marsquakes.

Seismic Observations in Relation to Objectives

For each potential model for the internal structure of Mars, including assumed values for the radius and state of the core, the moment of inertia, the nature and location of any mantle discontinuities, and the thickness of the crust, seismic velocity distributions can be derived through the application of equations of state (*Anderson*, 1967, 1972) to a mineralogy satisfying the zero-pressure density. *Okal and Anderson* (1978) investigated both the properties common to all generalized models, as well as those that could resolve key unknowns, within the framework of seismological observations that could be made on the surface of the planet. Figures 5–7 present one example of such an inquiry, showing the computed density and seismic velocity profiles, the travel-time curves of the principal body waves traveling through the interior of the planet, and a sketch of the actual geometry of the direct P waves through the mantle and of PKP waves transiting through the core. In addition, Figs. 8 and 9 show the dispersion of Rayleigh and Love waves, which are dominantly at longer periods than body waves and travel along the surface of the planet. The periods of the various modes of free oscillation of the planet were also computed for a variety of models.

MANTLE STRUCTURE

Because of the smaller size and lower gravitational acceleration of Mars, the effect of pressure on density and elastic constants will be significantly weaker than on Earth, resulting in gentler gradients of seismic velocity. If the planet has a large temperature gradient (e.g., because a layered mantle prevents efficient convection), velocities could be practically constant throughout the mantle. If, on the other hand, efficient convection has left the mantle at relatively cool temperatures, the mantle is olivine-rich, and the core smaller, phase transitions (similar to Earth's 400-km and 650-km discontinuities) could occur in the lower mantle, between 1000 and 2000 km depth. One such transition is shown in the model presented in Fig. 5, resulting in the triplication of P arrivals between distances of 50° and 90° (Figs. 6 and 7).

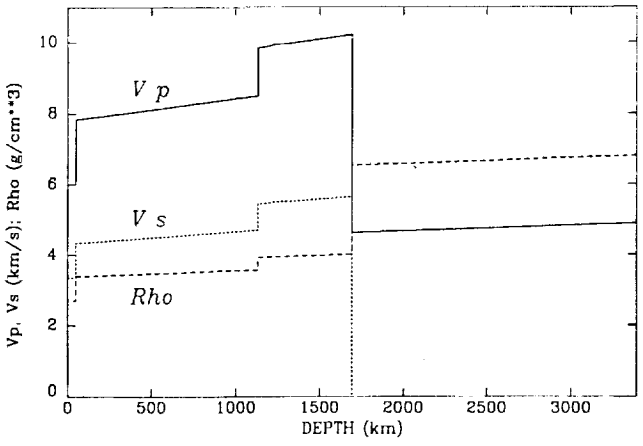

Fig. 5. Density and seismic velocity profiles for internal structure model AR. From *Okal and Anderson* (1978).

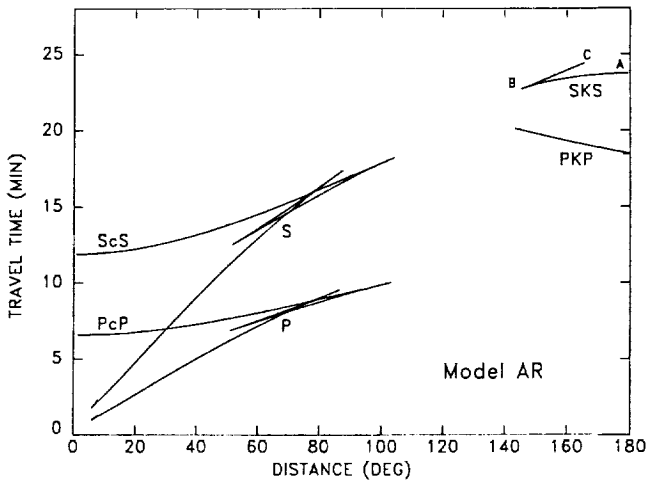

Fig. 6. Travel-time curves for body wave phases P, PcP, PKP, S, ScS, and SKS in model AR. Note that PKP has been folded about the 180° axis. After *Okal and Anderson* (1978).

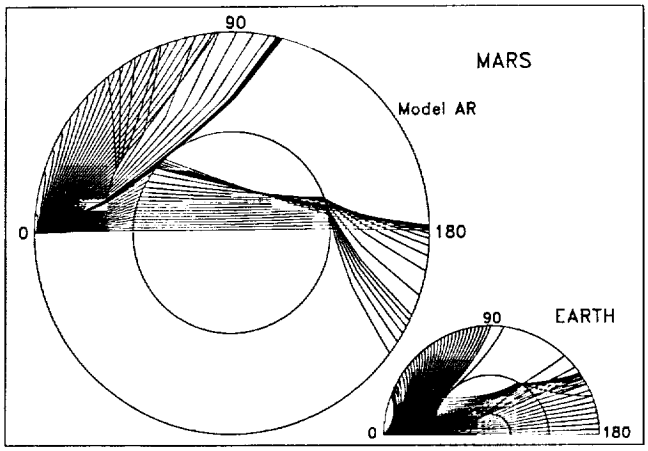

Fig. 7. P and PKP ray paths inside Mars for model AR. A surface-focus event is assumed. The take-off angles vary from 1° to 50° in 1° increments and from 16.5° to 17.5° in 0.1° increments. The smaller diagram, reproduced from *Julian and Anderson* (1968; Fig. 9), is for the Earth. After *Okal and Anderson* (1978).

Mantle velocities may be obtained by inversion of observed travel times vs. distance by the Herglotz-Wiechert method, barring the presence of strongly developed low-velocity layers (see below). The resolution of mantle velocities, and in particular the recognition of possible stepwise increases, will be critical to an understanding of the composition, thermal state, and differentiation history of the planet. It will be important in this respect to have good distance coverage, particularly in the distance range 50°–90°, to allow identification of possible triplications.

SIZE AND STATE OF THE CORE

While all models require that Mars have a core, the size and physical state of the core are poorly constrained: The core could be either liquid or solid, and the possibility of an Earth-like solid inner core cannot be discounted. If the (outer) core is liquid, S waves incident vertically on the core-mantle boundary (CMB) will be totally reflected, leading (as on Earth) to large-amplitude signals for core-reflected S (ScS) waves recorded at short distances (0°–20°) after bouncing on the CMB (Fig. 6). Also, in the case of a liquid core, the relatively low pressures involved lead to very low velocities in the core (4.6 km/s), a significant velocity drop at the CMB, and an extensive shadow zone for P phases between 100° and 140° (see Figs. 5 and 6), as well as for their S counterparts (direct S and SKS).

If the core is solid, the higher P wave velocities in the core would substantially reduce the shadow zone for P and eliminate the one for S. In addition, the amplitude of ScS at short distances would be considerably reduced.

Crucial evidence for the state of the core will therefore be obtained from observations at close ranges (ScS, 0°–20°) and at far distances (100° and beyond). In this respect, it is vital that the seismic network span a wide range of distances on the planet and, in particular, that some stations be located at considerable distances from areas of potentially greater than average rates of seismicity.

If an inner core is present, significant chemical differentiation can be anticipated, with more of any lighter element (e.g., sulfur) in the liquid outer core. The inner core-outer core transition might then be sharper than in the Earth, and the resulting triplication would be detectable in the 90–180° distance range.

Finally, the state of the core profoundly affects the fundamental modes of free oscillation of the planet, with the gravest spheroidal mode ($_0S_2$) having a period of about 2100 ± 200 s if the core is liquid and only about 1350 s if it is solid (*Okal and Anderson*, 1978). Should sufficiently large marsquakes occur to excite these oscillations above ambient noise, their observation would strongly constrain the state of the core.

CRUSTAL STRUCTURE AND VOLATILES

The thickness of the martian crust can, in principle, be resolved by the inversion of first-arrival travel times at very short distances. Such an experiment would, however, require dense coverage along a profile of stations or sources, an unlikely geometry for a passive experiment given our inability to predict locations of activity. An alternative method is the use of surface wave (Rayleigh and Love) dispersion at periods in the range 10–100 s. The method can work both with the record at a single station of surface waves from a source at a known location and origin time (*Landisman et al.*, 1969) or over a small array of three or more stations, where the phase velocity can be measured directly across the array (e.g., *Talandier and Okal*, 1987) independently of the precise epicenter and origin time. In this respect, three-station broadband arrays would not only permit a direct measurement of the crustal structure, but their deployment at various sites could also help to identify lateral heterogeneity.

Similarly, surface wave dispersion will be the key method to identify and resolve any low-velocity zone (LVZ) in the crust or upper mantle. LVZs cannot be formally obtained by the inversion of body wave travel times, so their resolution benefits significantly from the use of surface waves. The decrease in elastic moduli and increase in seismic attenuation evidenced by an LVZ (such as that between 100 and 250 km depth beneath oceanic areas on Earth) has usually been interpreted as due to partial melting, probably induced by

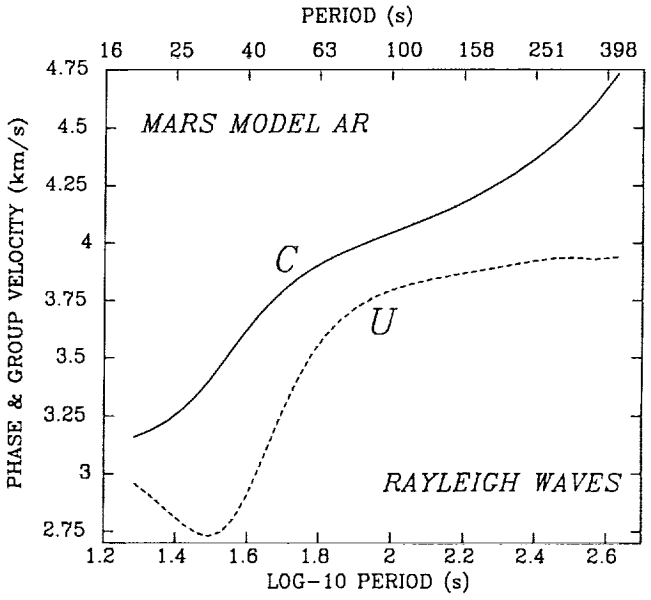

Fig. 8. Rayleigh wave phase and group velocities computed for model AR.

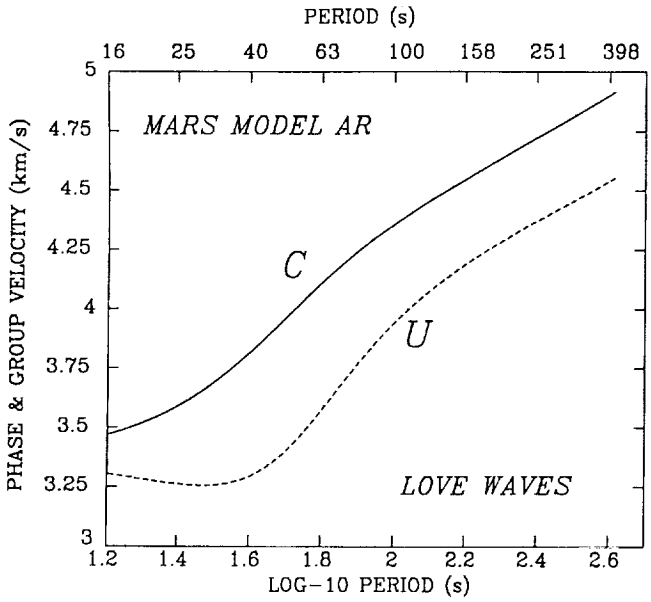

Fig. 9. Love wave phase and group velocities computed for model AR.

the presence of volatiles such as water. The mapping of LVZs, on a global or regional scale on Mars, would give insight into the history of planetary volatiles and could suggest links to magmatism and volcanic activity.

Expected Detection Capabilities

The ability of a seismic station on Mars to detect a signal from a given seismic event depends on several factors independent of the intrinsic sensitivity of the sensors and recording system. These factors include the level of seismic noise, the rate of attenuation of seismic wave energy within Mars, and the decay of seismic amplitudes with recording distance.

SOURCES OF SEISMIC NOISE

Seismic noise levels on Mars are likely to be well below those detected on the Earth. Seismometers to be placed on Mars should therefore be designed to have the highest sensitivity possible to detect the smallest events possible. Some of the factors affecting relative levels of seismic noise on Mars, Earth, and the Moon, and instrument design considerations for reducing noise are given in Table 2. It is quite likely that even the most sensitive instruments and electronics (as are practical) will not be able to detect natural noise levels on Mars above their own intrinsic noise levels for much of the time and over a broad range of frequencies. If noise levels are as low as expected, it could be possible to detect very small marsquakes, possibly as low as m_b 3, from anywhere on the planet. While natural noise sources such as wind stress and changes in diurnal thermal stresses will certainly contribute to the visible seismic noise at times, a major component of the expected noise could result from the presence of the equipment placed on the martian surface.

Important natural noise sources are expected to include thermal cracking events caused by diurnal thermal stress variations in the near-surface rocks and soils, and noise caused by propagation of wind stresses into the martian surface. Thermal cracking events are seldom observed as seismic noise on Earth, mainly because other noise sources dominate and because thermal variations are relatively small (approximately 20 K/day, compared with about 100 K/day on the Moon and Mars). Thermal events were a major source of noise at frequencies above 3 Hz in the Apollo lunar seismic data. On Mars, such events will probably be even more common, as the length of the day is much shorter and stress variations will be more pronounced, although they will not penetrate as far into the surface. Major thermal-stress event swarms were observed on the Moon during eclipses, indicating that even very shallow penetration will cause these events.

The lander and seismic package should be constructed to minimize thermal variations that could cause instrument-generated seismic noise. Insulation from direct sunlight should accomplish this.

The high wind velocities on Mars will almost certainly contribute to the martian seismic noise levels. Wind impacting on the Viking lander was the only known external source of noise observed by the Viking seismometer. Wind-induced noise on Earth makes it necessary to avoid trees and other structures when emplacing seismometers on Earth, and burial in deep boreholes is preferred. While the wind velocities on Mars are often higher than those on Earth, the density of the atmosphere is much lower, and wind stresses will be less. However, motions of the lander and seismic package caused by the wind are still expected to be the largest single noise source. Thus, every effort should be made to minimize their cross sections and streamline their shapes. In addition, a substantial decrease in lander-generated noise can be realized by placing the sensor package at some distance from the station.

TABLE 2. Seismic noise considerations on Mars.

Instrument Design Considerations		
Detached from lander		
Cross section in atmosphere		
Burial		
Thermal insulation		
	Earth Noise (Compared to Mars)	Lunar Noise (Compared to Mars)
Atmosphere		
Density	Higher	NA
Wind speeds	Lower	NA
Surface roughness	Same	NA
Q	Same	Higher
Thermal Variations	Lower	Lower
Volcanic/Seismic Activity	Higher	Lower

SEISMIC ATTENUATION

Seismologists have had the opportunity to measure seismic attenuation on two planetary bodies—the Earth and the Moon. The Earth is a tectonically active planet with an atmosphere and a hydrosphere, in contrast to the inactive, volatile-poor Moon. Attenuation is typically parameterized by the quality factor "Q." High Q corresponds to low attenuation, and vice versa. The crust and upper mantle of the Moon have seismic Q values in the range 4000 to 15,000 for shear waves in the frequency band 3 to 8 Hz (*Nakamura and Koyama,* 1982). For the Earth the corresponding values range from less than 25 to about 2000. At higher frequencies Q values in the Earth have been measured to 3000 and higher. Research on lunar materials indicates that the state of vacuum of the lunar environment is the

primary factor that dramatically increases Q on the Moon relative to the Earth (*Tittmann et al.*, 1975, 1979). In this regard, the existence of an atmosphere and presumed subsurface volatiles on Mars suggests that attenuation on Mars is more similar to the Earth than the Moon.

The principal physical variables that influence Q for materials at depth (i.e., under pressure, with pores and cracks substantially closed) are temperature and pressure. At a constant pressure (depth), moderate temperature variations lead to strong Q variations since attenuation is an exponentially activated process. Thus, on Earth the hotter, tectonically younger provinces have systematically greater attenuation than older, more stable, and cooler regions. For example, a moderate-sized earthquake that might be felt in southern California would, for the same size event, be felt throughout the entire eastern United States if it had occurred there. Thus, higher temperatures and, indirectly, recency of tectonic activity lead to greater attenuation.

To first order, then, the relative thermal environments of Mars and Earth likely dictate the relative attenuation. If radioactive elements are similarly distributed on Earth and Mars, then the thermal environment of Mars is likely to be similar to the stable shield provinces of Earth. The shield provinces on Earth are the low-attenuation, high-Q end members in the range of attenuation over the Earth. Under these assumptions, seismic wave propagation conditions on Mars are likely to be as good as the best conditions on Earth. If mantle heat transport has been sufficiently less efficient on Mars than on Earth so that mantle temperatures are now higher, however, there may be greater attenuation than beneath the Earth's shields.

For the core of Mars, the value of attenuation will depend strongly on its physical state. Liquid metals have nearly infinite Q values. Thus, a solid core on Mars implies a greater attenuation of seismic core phases as well as of free oscillation modes that are sensitive to core properties.

AMPLITUDE-DISTANCE RELATIONS

The rate of decay of amplitude with distance for seismic waves on Mars depends on several factors, including geometrical spreading and intrinsic attenuation; further details are given in Appendix D. Stronger body-wave amplitudes will be recorded on Mars than on Earth at a similar angular distance, Δ, from a seismic source of comparable moment, primarily because of the smaller size of Mars. Geometrical spreading alone accounts for a factor of 3.5; the effect of attenuation will depend significantly on the Q structure of the planet, which is still unknown. At a period of 1 s, if Q in Mars is at least as high as in the Earth, the final amplitude increase is a factor of at least 8.5 (and possibly as much as 15) for P waves and at least 50 (and as much as 3000) for S. The latter figure raises the possibility of a wealth of short-period teleseismic S data, in contrast to the case of the Earth, where large travel times and low Q values effectively eliminate them.

For surface waves, geometrical spreading is independent of the radius of the planet and varies as $1/\sqrt{\sin\Delta}$. Anelastic attenuation depends critically on the Q structure of the planet, but generally the shorter the distance traveled, the less the attenuation. On the other hand, surface-wave excitation is significantly larger on Mars than on Earth for a seismic source of a given moment and depth. As a whole, Rayleigh wave spectral amplitudes should be higher by a factor of about 3 (depending on Q) on Mars than Earth for a similar source. Time-domain amplitudes should be larger by an even greater factor, because of significantly less dispersion on Mars due to lesser gradients of velocity with depth (see above). Love waves should be similarly enhanced on Mars for a given seismic source.

Required Station Characteristics

SURFACE VS. BURIED SENSORS

Technical specifications for the seismic instrument depend on the type of installation. Two installation modes are currently under consideration: surface installation by a rough lander (10–100 g decelerations) and subsurface installation using a penetrator. The pros and cons of these two modes are listed in Table 3. The trade-offs are as follows:

Surface installations will be more susceptible to thermoelastic strains. Given that the diurnal temperature variation is 100 K at the equator, the thermal inertia of the installation will buffer out short-term fluctuations, but long-term variations (e.g., longer than 200 s) will appear as significant noise on a broadband instrument. Because of this effect, surface installations will probably be restricted to short period bands (0.04–20 Hz).

A surface installation will be much more susceptible to wind-induced noise than a penetrator. This problem can be mitigated to some extent by removing the seismometer from the lander and placing it some distance away in a low-drag housing. A detached seismometer package has the added advantage of isolating the sensors from mechanical noise on the lander spacecraft, an option that would be difficult on a penetrator. Seismometer coupling will be much better with a penetrator than with a sensor emplaced on the surface unless some provision is made to attach a surface sensor with a spike or similar device. Burial of the seismometer is an ideal that may be met by penetrator installation, but uncertainties in penetrability, equipment survival, and the technical difficulty in designing a power source (RTG/solar cell) that can withstand penetrator impacts (of order 10,000 g) are serious obstacles at this stage. Unless long-term power supplies tolerant to high g can be developed, or a mechanism of cushioning the power supply impact can be devised, penetrator installation with long-term power must be ruled out.

TABLE 3. Comparison of surface and buried seismic instruments.

Surface Installation	Penetrator Installation
pro: low-g impact (10–100 g)	con: high g (10,000 g possible)
pro: relatively independent of site conditions	con: site dependence critical–boulders, lava flows, alluvium
con: thermoelastic strain	pro: less sensitive to temperature
con: short period only (25 s–20 Hz)	pro: broad-band (DC–20 Hz) OK
pro: long-term power possible	con: long-term power sources surviving impact not possible with current technology

TECHNICAL SPECIFICATIONS FOR A SURFACE SEISMIC STATION

Specifications for an ideal surface seismic station on Mars are those obtainable in a first class observatory on Earth. These specifications are listed in Table 4. Were a penetrator installation feasible, specifications approaching an Earth observatory could be achievable for sites where the penetration was a few meters. If the schedule of station emplacement or limitations on station mass or complexity were overriding constraints, then—as discussed further below—some of the specifications could be relaxed for a subset of the network stations.

On the basis of the discussion of sources of seismic noise given above, it is clear that surface sensors must be placed directly on the martian surface, i.e., off the lander. The greatest single improvement in signal-to-noise ratio is achieved by this action. Further improvements can be obtained by placing the sensors at some distance from the lander (preferably several spacecraft dimensions distant) and by burying the sensors within the soil (to lessen thermal perturbations). The need for distance between seismic sensors and spacecraft is heightened if the lander includes a meteorological boom, which will exacerbate the lander-generated seismic noise.

TABLE 4. Seismic station specifications.

Specification	Ideal Seismic Station	Martian Surface Installation
Number of channels	3	3
A/D sample rate	1000 sps	1000 sps
A/D	24 bit	24 bit
Stored data rate	50 sps	50 sps
Data compression	3:1	3:1
Data rate	100 Mbits/day	100 Mbits/day
Bit error rate	$<10^{-8}$	$<10^{-4}$
Bandwidth	DC - 30 Hz	0.04 - 20 Hz
Sensitivity	10^{-11} g	10^{-10} g
Mass		
Sensors only	3 kg	1.5 kg
Sensors plus housing	10 kg	5 kg
Volume	0.02 m^3	0.01 m^3
Power	2 W	2 W
Onboard RAM	4 Mbytes	4 Mbytes
Calibration	1/day	1/day

DISCUSSION OF SPECIFICATIONS

1. Number of channels. Three channels are required to discriminate longitudinal P-wave motion from transverse S-wave motion and to distinguish polarized surface waves. Teleseismic body waves have small angles of incidence so that teleseismic S is difficult to record well on vertical component records.

2. A/D sample rate. A high sampling rate, 1000 sps, allows recursive anti-alias filtering, or other filters tailored to meet the site conditions, to be applied to the data stream.

3. A/D. A 24-bit A/D provides 140 db of dynamic range, i.e., 10^{-10} g to 10^{-3} g.

4. Stored data rate. 50 sps/channel is typically used to record local earthquakes on Earth.

5. Data transmission rate. This figure is calculated assuming continuous recording at 3 channels $\times$ 24 bits $\times$ 50 sps $\times$ 1 day $= 3.1 \times 10^8$ bits. It is estimated that with data compression this figure can be reduced by a factor of at least 3; see below. However, further compression, e.g,. by event detection, which in principle could reduce the total by a factor of 10 (to 10^7 bits), is much less attractive in that experience shows that array event detection on Earth often ends up with only half the array triggering. If all the data are collected, postacquisition processing can extract the signal from the remaining stations.

6. Bit error rate (BER). Because of the finite bandwidth of the seismic sensor, a greater BER can be tolerated than for many other experiments. Therefore, a larger amount of high error-rate data is preferred to a small amount of error-free data.

7. Bandwidth. The bandwidth depends on the thermal stability of the installation, how well coupled the sensor is to the surface, and how streamlined the superstructure is, in order to minimize wind effects. Critical to the performance of the site will be the lander-generated noise. If the lander includes booms that resonate in the wind at seismic frequencies, such motions will be the chief source of noise. Long-period waves may be difficult to observe at the surface. However, with an interrogable system and a broadband instrument, the bandpass might be altered if conditions (e.g., at night) are favorable.

8. Power. Power is based on the requirement of the Guralp seismometers (low power version, 100 mW/channel) and the Reftek data acquisition package (the IRIS-designed portable digital seismograph) that operates at 1.5 W. Data acquisition systems with lower rates of power consumption (a few hundred mW) can be designed if power is a limitation.

9. RAM. The RAM estimate is based on the assumption that data are transmitted to an orbiter every 8 hours, which for 10^8 bits/day gives a requirement of 4 Mbytes storage.

10. Calibration. Calibration once per day would be used to track seismometer performance.

DATA COMPRESSION

The data compression scheme used by the Global Seismographic Network on Earth utilizes a first-difference encoding. With 24-bit data samples, most of the samples can be compressed to a one-byte first difference. When high-dynamic-range signals are encountered, either two or three bytes are used as necessary. The encoding uses bytes, rather than bits, for speed and convenience when using standard computers. The typical performance of this encoding is about 3 to 1 compression. These data may be further compressed by standard computer file-compression methods such as Huffman or Limpel-Ziv, achieving an additional 33% reduction. Thus, seismic data compression of about a factor of 5 is possible.

In considering compression schemes, the robustness of the methods in the presence of bit errors must be considered. The standard first-difference encoding method used by the terrestrial Global Seismographic Network packages data into 64-byte frames, each of which contains an absolute reference sample. Thus, if there is a bit error, no more than about 60 bytes of data are lost. With alternative coding schemes that do not "packetize" the information, bit errors can introduce substantial data loss in compressed data, and this consideration is important in the final selection of a compression scheme.

STATION COMMANDABILITY

Because we do not know the form that all seismic signals or noise will take on Mars, it will be extremely important to have the capability to send a few simple commands to each seismic station after acquisition and analysis of initial data. Commands can include control of corner frequencies and rolloff rates of bandpass filters, the application of notch filters or other noise suppression algorithms, changes in sampling rates or instrument gain settings, or modifications to data compression parameters. As the flexibility of the instrument is increased and the adaptability to unforeseen seismic signals is maximized, trade offs are possible in the required overall rate of data transfer from each station to an orbiter relay. With sufficient station commandability it is possible that an overall data rate of 10 Mbits/day per station might be sufficient to achieve all the scientific objectives of a global seismic network on Mars.

Station Siting Requirements

THE STATION TRIAD CONCEPT

A station siting plan must strike a compromise among the various scientific objectives. There must be a mix of closely spaced stations to detect and locate nearby seismic events and to serve as arrays for measurements of phase velocity and propagation direction, and more globally dispersed stations to provide planetary coverage and to ensure the recording of core phases and other signals diagnostic of deep structure. While broadband, three-component systems are preferred for all stations, we can envision that, because of different emplacement systems (e.g., penetrator vs. lander), cost constraints, or sequential station emplacement scenarios, there may be strong reasons to consider a simpler and more rugged station with only short-period seismometers. The recommended plan, consistent with overall mission constraints as currently defined, consists of nested triads of stations.

Small triads should consist of stations located approximately 100 km apart in local arrays. If there must be a compromise among station types, then we recommend that each small triad consist of 3 three-component short-period instruments arranged in a triangle around a broadband observatory-class three-component sensor. If broadband three-component sensors can be emplaced at all sites, then the central station in each small triad could be omitted. If this second scenario is followed, in order to provide backup signals in the event of an unexpectedly hard landing or high levels of long-period noise, we recommend that the broadband sensors be augmented at each station with an additional set of more rugged short-period seismometers.

Three of these small triads should be emplaced in a larger triangular pattern, approximately 3500 km on a side. One such large triad should occupy each of the eastern and western hemispheres of Mars. This arrangement gives a total of 12 stations in each hemisphere, or 24 stations in all.

RATIONALE FOR STATION SPACING

The 100-km spacing of instruments in the small triads will permit the detection (by comparison of signal character on several stations) and location (by inversion of local P and S travel times) of seismic events within and near the triangular area, so several of the small triads should be located in regions likely to have above-average rates of seismic activity. For instance, the Viking 2 seismometer was emplaced about 110° from the Tharsis region, possibly the most seismically active region on Mars. It has been estimated that an instrument 20 times more sensitive could have detected at least 120 seismic events per year if it were located closer to Tharsis (*Goins and Lazarewicz*, 1979). The station spacing for the small triads represents a compromise between resolution of source location and areal coverage. A simple rule of thumb in local networks is that the depth of focus of a natural seismic source can be resolved as long as the nearest station is closer to the epicenter than one focal depth. Most earthquakes are located in the upper 20 km, but the lesser thermal gradients expected on Mars than on Earth and the likelihood that thermal stress associated with global cooling will generate marsquakes throughout an elastic lithosphere as much as several hundred kilometers thick suggest that a 100-km spacing will be adequate to locate most of the local events recorded by each small triad.

In addition, a 100-km spacing will permit the triads to serve as quadripartite arrays for measurement of surface-wave phase velocities, which for periods of 15–100 s have wavelengths of 50–450 km (Figs. 8 and 9). The triads will also serve to measure the propagation azimuth and phase velocity of body wave phases. Among the key body wave phases at short distances that will benefit from phase velocity measurements are near-vertical reflections (which arrive at very high phase velocities) from the crust-mantle boundary, from the core, and potentially from any prominent mantle discontinuities, as well as direct and mantle-refracted waves from local events (which tend to arrive at phase velocities closer to the seismic wave speed) that yield information on crustal structure. Azimuth and phase velocity measurements of waves from events distant from all triads will constitute primary information for the location of such sources.

The 3500-km spacing of triads in each hemisphere will permit the siting of a number of triads in distinct regions likely to have greater than average rates of seismicity. The 3500-km distance, about 60° of arc, will ensure that some stations are located at a key distance range to record body wave triplications from mantle discontinuities. In addition, the three triads will ensure a reasonable level of detectability and locatability of seismic sources throughout each hemisphere.

The siting of one large triangle in each hemisphere will give effectively global coverage. Further, such an arrangement will afford the opportunity to observe core phases from seismic sources well located on the basis of travel times to one or more of the triads on the opposite hemisphere.

STRAWMAN STATION LOCATIONS

Our suggested strawman plan for seismic station layout includes two hemispheric arrays—one in the eastern hemisphere and one in the western hemisphere (Fig. 10). All

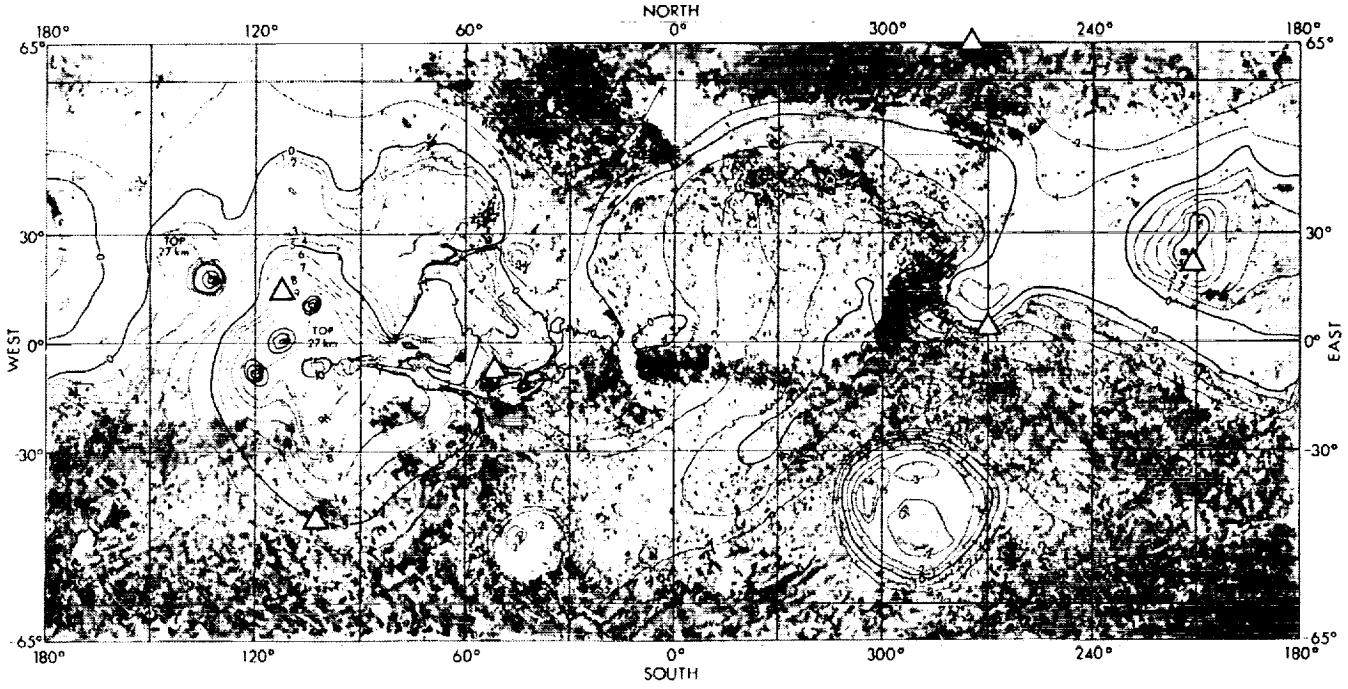

Fig. 10. Possible locations (triangles) for seismic station triads for a martian global seismic network. The background map depicts topography (in kilometers) with respect to a fourth degree and order equipotential.

locations are at altitudes less than 6 km, as required by present mission constraints, and all but one are at absolute latitudes less than 45° to permit the use of solar power. The proposed western array has vertices in Tharsis west of Ascraeus Mons (15°N, 110°W), just north of the eastern portion of Valles Marineris (7.5°S, 52.5°W), and in the southern highlands (45°S, 105°W). The choice of Tharsis is obvious, since it is the region of the planet with arguably the most recent volcanic activity (*Tanaka et al.*, 1988) and consequently highest interior cooling rates. Valles Marineris has high topographic gradients and displays evidence for recent volcanism (*Lucchitta*, 1987) and landslides. A small triad in the southern highlands extends western hemisphere coverage to the south (e.g., activity triggered by time-variable polar loads) and provides a key locale for the determination of regional structure (e.g., crustal thickness) to test models for the origin of the crustal dichotomy.

The proposed eastern array has a vertex in the Elysium province (22°N, 211°W), in the Isidis Basin (5°N, 270°W), and in the northern lowlands (65°N, 275°W). Elysium is a major volcanic province displaying evidence for relatively recent activity (*Plescia*, 1990). Isidis is a mascon basin (*Sjogren*, 1979); shallow moonquakes have shown some tendency to be associated with mascon mare basins on the Moon (*Nakamura et al.*, 1979). The placement of a triad in the northern lowlands should permit the measurement of local crustal structure, making the site complementary to that in the southern highlands for tests of the crustal dichotomy, and will extend coverage to the northern portions of the planet, including the north polar region.

STATION SEQUENCING SCENARIOS

Mission design considerations may dictate that stations in a martian seismic network be emplaced in a sequence spanning several distinct launches and perhaps several years. The most important constraint for system emplacement is that as much of the array as possible must record data simultaneously. This constraint dictates that design lifetimes of individual stations must be considerably greater than the time interval over which the network is established.

If seismic activity on Mars consists of numerous large events, and the first stations emplaced are widely scattered (e.g., several thousand kilometers apart), then observations from a sparse, early network could be used to locate regions on the planet where seismic activity is greatest and where small triads emplaced later in the sequence could be located for optimum results. If, in contrast, seismic activity on Mars occurs mainly as small, well-distributed events poorly recorded at distant stations, then a sparse network of widely spaced stations may be able to locate few, if any, events. This second situation is the more likely and favors the early

emplacement of a small triad of stations in a single area (e.g., Tharsis). Observations from such an early array could yield the location of near events, determine local structure, and assess the size distribution and approximate locations of distant large events. Because we do not know the character of martian seismic signals, it is essential that two or more of the earliest emplaced seismic stations be located near (i.e., within 100 km of) each other so that signals from tectonic and impact events can be recognized and distinguished from wind-generated and thermal noise.

We note one additional advantage to a sequenced station emplacement scenario in which signals from the first stations are received and analyzed in time to affect the operational characteristics of later-emplaced stations. Data rate is likely to be a strong constraint on experiment design, particularly once the full network is operational. While many data compression schemes can be envisioned for seismic data, as discussed above, implementation of the more efficient of such schemes is extremely hazardous in the absence of information about the characteristic durations, bandwidths, and frequency of martian seismic events. We expect that the analysis of signals from the first seismic stations on Mars will permit implementation of data compression algorithms that will considerably reduce the necessary data rate from the final, full network with little or no loss of scientific return.

References

Anderson D. L. (1967) A seismic equation of state. *Geophys. J. R. Astron. Soc., 13*, 9–30.

Anderson D. L. (1972) Internal constitution of Mars. *J. Geophys. Res., 77*, 789–795.

Anderson D. L., Kovach R. L., Latham G., Press F., Toksöz M. N., and Sutton G. H. (1972) Seismic investigations: The Viking Mars lander. *Icarus, 16*, 205–216.

Anderson D. L., Miller W. F., Latham G. V., Nakamura Y., Toksöz M. N., Dainty A. M., Duennebier F. K., Lazarewicz A. R., Kovach R. L., and Knight T. C. D. (1977) Seismology on Mars. *J. Geophys. Res., 82*, 4524–4546.

Bache T. C. (1982) Estimating the yield of underground nuclear explosions. *Bull. Seismol. Soc. Am., 72*, S131–S168.

Banerdt W. B., Phillips R. J., Sleep N. H., and Saunders R. S. (1982) Thick-shell tectonics on one-plate planets: Applications to Mars. *J. Geophys. Res., 87*, 9723–9733.

Becker R. H. and Pepin R. O. (1984) The case for a martian origin of the shergottites: Nitrogen and noble gases in EETA 79001. *Earth Planet. Sci. Lett., 69*, 225–242.

Bergman E. A. (1986) Intraplate earthquakes and the state of stress in oceanic lithosphere. *Tectonophysics, 132*, 1–35.

Bills B. G. (1989a) The moments of inertia of Mars. *Geophys. Res. Lett., 16*, 385–388.

Bills B. G. (1989b) Comment on "More about the moment of inertia of Mars." *Geophys. Res. Lett., 16*, 1337–1338.

Bills B. G. (1990) Geodetic constraints on the composition of Mars. *J. Geophys. Res., 95*, 14131–14136.

Bills B. G. and Ferrari A. J. (1978) Mars topography harmonics and geophysical implications. *J. Geophys. Res., 83*, 3497–3508.

Bogard D. D., Nyquist L. E., and Johnson P. (1984) Noble gas contents of shergottites and implications for the Martian origin of SNC meteorites. *Geochim. Cosmochim. Acta, 48*, 1723–1740.

Bratt S. R., Bergman E. A., and Solomon S. C. (1985) Thermoelastic stress: How important as a cause of earthquakes in young oceanic lithosphere? *J. Geophys. Res., 90*, 10249–10260.

BVSP (Basaltic Volcanism Study Project) (1981) *Basaltic Volcanism on the Terrestrial Planets*. Pergamon, New York. 1286 pp.

Carr M. H. (1987) Water on Mars. *Nature, 326*, 30–35.

Carr M. H., Greeley R., Blasius K. R., Guest J. E., and Murray J. B. (1977) Some martian volcanic features as viewed from the Viking Orbiters. *J. Geophys. Res., 82*, 3985–4015.

Duennebier F. and Sutton G. H. (1974) Thermal moonquakes. *J. Geophys. Res., 79*, 4351–4363.

Duennebier F., Dorman J., Lammlein D., Latham G., and Nakamura Y. (1975) Meteoroid flux from passive seismic experiment data. *Proc. Lunar Sci. Conf. 6th*, pp. 2417–2426.

Dziewonski A. M., Ekström G., Franzen J. E., and Woodhouse J. H. (1987) Global seismicity of 1977: Centroid-moment tensor solutions for 471 earthquakes. *Phys. Earth Planet. Inter., 45*, 11–36.

Finnerty A. A., Phillips R. J., and Banerdt W. B. (1988) Igneous processes and closed system evolution of the Tharsis region of Mars. *J. Geophys. Res., 93*, 10225–10235.

Gault D. E. (1973) Displaced mass, depth, diameter, and effects of oblique trajectories for impact craters formed in dense crystalline rocks. *Moon, 6*, 32–44.

Gault D. E. and Baldwin B. S. (1970) Impact cratering on Mars—Some effects of the atmosphere (abstract). *Eos Trans. AGU, 51*, 343.

Goettel K. A. (1981) Density of the mantle of Mars. *Geophys. Res. Lett., 8*, 497–500.

Goins N. R. (1978) Lunar seismology: The internal structure of the Moon. Ph.D. thesis, Massachusetts Institute of Technology, Cambridge. 666 pp.

Goins N. R. and A. R. Lazarewicz (1979) Martian seismicity. *Geophys. Res. Lett., 6*, 368–370.

Halliday I. (1988) Geminid fireballs and the peculiar asteroid 3200 Paethon. *Icarus, 76*, 279–294.

Hartmann W. K. (1973) Martian cratering, 4, Mariner 9 initial analysis of cratering chronology. *J. Geophys. Res., 78*, 4096–4116.

Hartmann W. K. (1977) Relative crater production rates on planets. *Icarus, 31*, 260–276.

Janle P. (1983) Bouguer gravity profiles across the highland-lowland escarpment on Mars. *Moon Planets, 28*, 55–67.

Julian B. R. and Anderson D. L. (1968) Travel-times, apparent velocities and amplitudes of body waves. *Bull. Seismol. Soc. Amer., 58*, 339–366.

Kanamori H. and Stewart G. S. (1976) Mode of strain release along the Gibbs Fracture Zone, Mid-Atlantic Ridge. *Phys. Earth Planet. Inter., 11*, 312–332.

Kaula W. M. (1979) Moment of inertia of Mars. *Geophys. Res. Lett., 6*, 194–196.

Kaula W. M., Sleep N. H., and Phillips R. J. (1989) More about the moment of inertia of Mars. *Geophys. Res. Lett., 16*, 1333–1336.

Landisman M., Dziewonski A. M., and Satô Y. (1969) Recent improvements in the analysis of surface wave observations. *Geophys. J. R. Astron. Soc., 17*, 369–403.

Latham G., Ewing M., Dorman J., Press F., Toksöz N., Sutton G., Meissner R., Duennebier F., Nakamura Y., Kovach R., and Yates M. (1970) Seismic data from man-made impacts on the Moon. *Science, 170*, 620–626.

Laul J. C., Smith M. R., Wänke H., Jagoutz E., Dreibus G., Palme H., Spettel B., Burghele A., Lipschutz M. E., and Verkouteren R. M. (1986) Chemical systematics of the Shergotty meteorite and the composition of its parent body (Mars). *Geochim. Comochim. Acta, 50*, 909–926.

Lazarewicz A. R., Anderson D. L., Anderson K., Dainty A. M., Duennebier F. K., Goins N. R., Knight T. C. D., Kovach R. L., Latham G. V., Miller W. F., Nakamura Y., Sutton G. H., and Toksöz M. N. (1981) *The Viking Seismometry Final Report*. NASA Contractor Rep. 3408. 54 pp.

Lucchitta B. K. (1987) Recent mafic volcanism on Mars. *Science, 235*, 565–567.

McSween H. Y. Jr. (1984) SNC meteorites: Are they martian rocks? *Geology, 12*, 3–6.

McSween H. Y. Jr. (1985) SNC meteorites: Clues to martian petrologic evolution? *Rev. Geophys., 23*, 391–416.

Nakamura Y. (1983) Seismic velocity structure of the lunar mantle. *J. Geophys. Res., 88*, 677–686.

Nakamura Y. and Koyama J. (1982) Seismic Q of the lunar upper mantle. *J. Geophys. Res., 87*, 4855–4861.

Nakamura Y., Duennebier F. K., Latham G. V., and Dorman H. J. (1976) Structure of the lunar mantle. *J. Geophys. Res., 81*, 4818–4824.

Nakamura Y., Latham G. V., Dorman H. J., Ibrahim A. K., Koyama J., and Horvath P. (1979) Shallow moonquakes: Depth, distribution and implications as to the present state of the lunar interior. *Proc. Lunar Planet. Sci. Conf. 10th*, pp. 2299–2309.

Nakamura Y., Latham G. V., and Dorman H. J. (1982) Apollo lunar seismic experiment—Final summary. *Proc. Lunar Planet. Sci. Conf. 13th*, in *J. Geophys. Res., 87*, A117–A123.

Neukum G. and Hiller K. (1981) Martian ages. *J. Geophys. Res., 86*, 3098–3121.

Neukum G. and Wise D. U. (1976) Mars: A standard crater curve and possible new time scale. *Science, 194*, 1381–1388.

Oberst J. and Nakamura Y. (1987) Distinct meteoroid families identified on the lunar seismograms. *Proc. Lunar Planet. Sci. Conf. 17th*, in *J. Geophys. Res.*, 92, E769–E773.

Oberst J. and Nakamura Y. (1989) Monte Carlo simulation of the diurnal variation in seismic detection rate of sporadic meteoroid impacts on the Moon. *Proc. Lunar Planet. Sci. Conf. 19th*, pp. 615–625.

Oberst J. and Nakamura Y. (1991) A search for clustering among the meteoroid impacts detected by the Apollo lunar seismic network. *Icarus*, in press.

Okal E. A. (1989) A theoretical discussion of time-domain magnitudes: The Prague formula for M_S and the mantle magnitude M_m. *J. Geophys. Res., 94*, 4194–4204.

Okal E. A. and Anderson D. L. (1978) Theoretical models for Mars and their seismic properties. *Icarus, 33*, 514–528.

Okal E. A. and Talandier J. (1989) M_m: A variable period mantle magnitude. *J. Geophys. Res., 94*, 4169–4193.

Phillips R. J. and Saunders R. S. (1975) The isostatic state of Martian topography. *J. Geophys. Res., 80*, 2893–2898.

Phillips R. J., Saunders R. S., and Conel J. E. (1973) Mars: Crustal structure inferred from Bouguer gravity anomalies. *J. Geophys. Res., 78*, 4815–4820.

Phillips R. J., Sleep N. H., and Banerdt W. B. (1990) Permanent uplift in magmatic systems with application to the Tharsis region of Mars. *J. Geophys. Res., 95*, 5089–5100.

Plescia J. B. (1990) Young flood lavas in the Elysium region, Mars (abstract). In *Lunar and Planetary Science XXI*, pp. 969–970. Lunar and Planetary Institute, Houston.

Reasenberg R. D. (1977) The moment of inertia and isostasy of Mars. *J. Geophys. Res., 82*, 369–375.

Richter C. F. (1958) *Elementary Seismology*. Freeman, San Francisco. 768 pp.

Rubincam D. P. (1990) Mars: Change in axial tilt due to climate? *Science, 248*, 720–721.

Schubert G. and Spohn T. (1990) Thermal history of Mars and the sulfur content of its core. *J. Geophys. Res., 95*, 14095–14104.

Schubert G., Bercovici D., and Glatzmaier G. (1990) Mantle dynamics in Mars and Venus: Influence of an immobile lithosphere on three-dimensional convection. *J. Geophys. Res., 95*, 14105–14129.

Schultz P. H. and Gault D. E. (1975) Seismic effects from major basin formations on the Moon and Mercury. *Moon, 12*, 159–177.

Sjogren W. L. (1979) Mars gravity: High resolution results from Viking Orbiter II. *Science, 203*, 1006–1010.

Sjogren W. L. and Wimberly R. N. (1981) Mars: Hellas Planitia gravity analysis. *Icarus, 45*, 331–338.

Sleep N. H. and Phillips R. J. (1979) An isostatic model for the Tharsis province, Mars. *Geophys. Res. Lett., 6*, 803–806.

Sleep N. H. and Phillips R. J. (1985) Gravity and lithospheric stress on the terrestrial planets with reference to the Tharsis region of Mars. *J. Geophys. Res., 90*, 4469–4489.

Stacey F. D. (1977) *Physics of the Earth*, 2nd ed., p. 112. Wiley, New York.

Stevenson D. J., Spohn T., and Schubert G. (1983) Magnetism and thermal evolution of the terrestrial planets. *Icarus, 54*, 466–489.

Talandier J. and Okal E. A. (1987) Crustal structure in the Tuamotu and Society Islands, French Polynesia. *Geophys. J. R. Astron. Soc., 88*, 499–528.

Tanaka K. L., Isbell N. K., Scott D. H., Greeley R., and Guest J. (1988) The resurfacing history of Mars: A synthesis of digitized, Viking-based geology. *Proc. Lunar Planet Sci. Conf. 18th*, pp. 665–678.

Thurber C. H. and Solomon S. C. (1978) An assessment of crustal thickness variations on the lunar nearside: Models, uncertainties, and implications for crustal differentiation. *Proc. Lunar Planet. Sci. Conf. 9th*, pp. 3481–3497.

Tittmann B. R., Curnow J. M., and Housley R. M. (1975) Internal friction quality factor $Q \geq 3100$ achieved in lunar rock 70215,85. *Proc. Lunar Sci. Conf. 6th*, pp. 3217–3226.

Tittmann B. R., Nadler H., Clark V., and Coombe L. (1979) Seismic Q and velocity at depth. *Proc. Lunar Planet. Sci. Conf. 10th*, pp. 2131–2145.

Treiman A. H., Jones J. H., and Drake M. J. (1987) Core formation in the Shergottite parent body and comparison with the Earth. *Proc. Lunar Planet. Sci. Conf. 17th*, in *J. Geophys. Res., 92*, E627–E632.

Veith K. F. and Clawson G. E. (1972) Magnitude from short-period P-wave data. *Bull. Seismol. Soc. Am., 62*, 435–452.

Ward W. R. (1979) Present obliquity oscillations of Mars: Fourth-order accuracy in orbital e and I. *J. Geophys. Res., 84*, 237–241.

Wetherill G. W. (1975) Late heavy bombardment of the Moon and terrestrial planets. *Proc. Lunar Sci. Conf. 6th*, pp. 1539–1561.

Wiens D. A. and Stein S. (1983) Age dependence of oceanic intraplate seismicity and implications for lithospheric evolution. *J. Geophys. Res., 88*, 6455–6468.

Willemann R. J. and Turcotte D. L. (1982) The role of lithospheric stress in the support of the Tharsis rise. *J. Geophys. Res., 87*, 9793–9801.

Wood C. A. and Ashwal L. D. (1981) SNC meteorites: Igneous rocks from Mars? *Proc. Lunar Planet. Sci. 12B*, pp. 1359–1375.

Appendix A

RECOMMENDATIONS FROM THE VIKING SEISMOLOGY TEAM

(from *Lazarewicz et al.*, 1981)

The Viking Seismology Experiment

The purpose of the Viking Seismology Experiment was to determine the seismicity of Mars and define its internal structure by detecting vibrations generated by marsquakes and meteoroid impacts. After obtaining more than 2100 hours (89 days) worth of data during quiet periods at rates of one sample per second or higher, the Viking 2 seismometer was turned off as a consequence of a lander system failure. During the periods when adequate data were obtained, one event of possible seismic or meteoroid impact origin was recognized; however, there is a significant probability that this event was generated by a wind gust. The lessons learned from Viking, however, will ensure that seismic systems on future Mars missions will have a considerably higher probability of obtaining their goals.

The Viking seismometer was a three-component short-period system designed to meet severe constraints of weight, size, power consumption, and data rates necessary for incorporation into the Viking lander (*Anderson et al.*, 1972). Its small size and location on the lander body produced a relatively insensitive and noisy seismic system. The Viking seismometer is about 1/20 the sensitivity of the Apollo seismometers at 3 Hz. Over most of the frequency band of seismological interest, the Apollo seismometers are generally 2 to 3 orders of magnitude more sensitive than the Viking seismometer. Because of lander vibrations in response to martian winds, many of the seismic data are contaminated and thus unsuitable for detection of seismic events. When the winds are quiet (<2 m/s), background noise is below the level detectable by the system. An event of possible seismic origin (SOL 80 event) was recognized at a time when wind data suggest relatively quiet conditions. (One SOL is one martian solar day = 24 hr 39 min 35.25 s.) No wind measurements were made within 20 minutes of the event, so it is possible that a gust could have occurred between wind samples and produced the event (*Anderson et al.*, 1977). If the event is seismic in origin, the high frequency and short duration of this event suggest that it was generated locally.

The detection of one local marsquake (at most) during the equivalent of 89 days of operations allows us to set limits on the probable seismicity of the planet. The probability is greater than 67% that Mars has a lower seismicity than the Earth's intraplate seismicity. If martian seismicity is similar to intraplate seismicity on Earth (there is no evidence of plate tectonics on Mars), then about 2 to 3 events would have been detected (*Goins and Lazarewicz*, 1979).

Requirements for successful seismic experiments on Mars and other planetary objects can be met using present-day technology. These include (1) high sensitivity, dynamic range, and frequency bandwidth to allow detection of small and distant events; (2) seismometer networks to allow location of detected events and inversion of seismic parameters to obtain planetary structure; and (3) flexible data collection and compression methods to allow variation of parameters for optimum retrieval of information.

Much like the Viking seismometer on Mars, the first seismometer on the Moon (Apollo 11) was noisy and told us little about the Moon. A great wealth of information was obtained, however, by later Apollo seismometers, and we are confident that the same will be true when more advanced seismic systems are installed on Mars.

In evaluating the Viking Seismology Experiment, it is important to know the history of the experiment, and thus understand the reasons for the design limitations.

Viking was designed primarily as a biologically oriented mission. The search for extraterrestrial life was the motivating force, and other scientific goals were secondary. The original tentative instrument list did not include a seismometer. While design changes were taking place for the Viking lander, a seismometer was proposed and accepted for the Viking mission. From the outset, the primary constraints for this instrument were weight, power, and cost, in that order. Initial tests, using the Caltech engineering unit and a crude lander model, indicated no significant difference among placing the seismometer on, under, or near the lander for seismic coupling of the instrument to the surface. Any seismometer deployment mechanism would have exceeded the weight allocation for the seismic experiment and would have forced a decision between a lander-mounted seismometer or no seismometer at all. Through testing and compromise, the original design evolved into the instrument that went to Mars as a 2.2-kg, 3.5-W instrument. The weight, power, data allocation, and cost constraints forced a relatively low-sensitivity, narrow-band, survey experiment. Although the "noise" environment of Mars is known to some extent, we do not know the characteristics of internal events or the effect of propagation on these characteristics. The high-Q surface scattering layer in the Moon results in very emergent (signals having a gradual onset) seismic arrivals, long codas that obscure secondary arrivals, and the destruction of coherently dispersed wave trains (*Goins*, 1978).

The lunar seismic signatures have proven to be substantially (and unpredictably) different from the Earth's, leading to the obvious inference that seismic signatures need not be similar from one planetary object to another.

The Apollo seismometer systems collected signals that were so radically different from the Earth's that they were not identified as seismic signals until after the second Apollo (12) mission; even then identification was possible only due to the high data rates (40×10^6 bits/Earth day) and effective real-time interaction between scientists and instruments. A similar case may be made for Mars. The fact that there were no positively identified signatures does not imply that there are no seismic events on Mars. The Viking seismometer, if placed on the Moon instead of the Apollo seismic systems, would have detected lunar seismic activity at a rate of only 0.5 event per year, compared to approximately 20,000 events per year observed with Apollo instrumentation. In other words, the Viking instrument probably wouldn't have detected any seismic activity on the Moon.

Recommendations for Future Seismic Experiments on Mars

The Viking Seismology Experiment was a valuable source of experience in performing extraterrestrial seismology. This was the first seismic experiment on an unmanned, extraterrestrial mission. It was expected that the constraints on mass, power, and data allocation and the physical location on the spacecraft would compromise the scientific results. The amount of compromise and specific problems became well understood only after the landings on Mars. In this sense, one of the major accomplishments of this experiment was an improved ability to design similar future missions. Four specific recommendations were presented by the Viking Seismology Team. All four are technically feasible and will significantly improve future extraterrestrial seismic experimentation.

1. Isolation from noise. We know of three noise sources on Mars: lander activity, thermal noise, and wind noise. A seismic package should be isolated from all three as well as possible.

This is the most important recommendation. A first seismic experiment on a planetary object searches for seismic signals of unknown character. Any detected signal must be thoroughly analyzed to determine its origin and thus classify it as a seismic signal or noise. A landed spacecraft is necessarily noisy, and the analysis and categorization of the noise adds greatly to the effort, time, and money spent for data analysis.

The emplacement of a seismometer on a planetary object is not as straightforward a problem as on Earth. Construction of a seismic vault is presumably impossible; even searching for a good site (if one can get to it) is a difficult process. It is reasonable to assume the existence of a surface layer, probably of unknown or poorly understood properties, separating the surface from bedrock (if any). This surface layer will probably modify, possibly severely, an incident seismic signal (as it did on the Moon), thus making interpretation of seismic signals that much more difficult. Furthermore, the surface layer undergoes diurnal changes of temperature with the associated thermal fluxes and changes in the thermal state of a surface seismometer.

Constructing a seismometer package showing a small cross-sectional area to the wind, and planting it on the surface of Mars, should increase the threshold for wind noise to 300 m/s. The sensitivity of the seismometer could be increased by 4 orders of magnitude and the seismometer would still be free of wind noise (*Anderson et al.*, 1977).

The ultimate goal is total isolation from spacecraft and surface noise sources. In order of importance, a planetary seismometer must have its sensors (a) physically separated from the spacecraft, (b) buried, and (c) attached to bedrock (if any). It may be possible to couple seismometer emplacement with a coring mission. After a core is removed from a hole dug by a lander, the hole could be filled with an instrument package containing seismic and other sensors. An instrument package could also be buried with a corer. Alternatively, a penetrator mission could easily carry a seismometer and bury the instrument at each landing site.

2. Seismometer networks in seismically active areas. The Earth and the Moon have been found to have seismic and aseismic zones. Mars is also expected to be heterogeneous in seismic activity. Most notably, the Tharsis area is expected to be characterized by stresses that should produce seismic activity even if the area is in isostatic balance (*Sleep and Phillips*, 1979), so seismic activity in this area is likely to be higher than elsewhere on the planet. There are no planetary objects where a uniform surface seismicity is expected. The strength of seismic signals received by a seismometer generally decreases with distance; as a result, a strong bias exists for sensing the seismicity of the immediate area. For reasons of spacecraft landing safety, the Viking 2 lander was placed in Utopia Planitia, where substantial seismic activity was not expected. Theoretical considerations of martian seismicity, and the physical limitations of the Viking seismometer, place 80% of the potentially detectable events within 10° (590 km) of the lander. It has been estimated that an event in the Tharsis region would have to have had a magnitude greater than 9 to be detected by the Viking 2 seismic experiment (*Goins and Lazarewicz*, 1979). Obviously, the location of a seismometer on a planetary object is very important.

A single seismometer, especially without detailed knowledge of the nature of seismic signals, is insufficient for determining the location and nature of the seismic source. A network of seismometers offers many advantages over a single

instrument, depending on how the network is deployed. Three useful types of seismic networks are

(a) Subwavelength network: Sensors closely spaced (within a fraction of a seismic wavelength) so that the time of arrival of a signal at the different instruments is nearly simultaneous. The signals may be added, reinforcing the coherent signals through constructive interference, while weakening the incoherent signals (noise). In this fashion, the signal-to-noise ratio is improved as the square root of n, where n is the number of sensors.

(b) Local network: Sensors are widely spaced, relative to a seismic wavelength, so that the arrival time differences are much greater than the measurable time resolution, but the instrument separation is much less than the planetary radius. With proper adjustment of the relative phases of incoming signals, this phased network becomes a "steerable beam" for distant events, where azimuthal direction can be calculated for a given signal, or a preferential azimuth for a particular study can be chosen. Local seismic events can be located directly by triangulation and/or travel-time difference analysis.

(c) Planetary network: The network is spread throughout the entire planetary surface. This network allows for studies of heterogeneity in seismicity and interior structure, as well as focal mechanism studies. This approach has the added feature (and complication) of having instrumentation in different geological provinces.

By far, the best system is a combination of all three types. If practical constraints do not allow for a combined system, some type of network is nevertheless desirable. The simplest network is one seismometer with every landed package, a c-type array (such as Apollo). A penetrator mission could deploy a planet-wide c-type network. A planetary rover could emplace a b-type network, for example, three seismometers separated by 1–10 km. Obviously, the more members in the network, the better the resulting resolution.

3. Flexibility through software control. The ability to control instrumental parameters from Earth greatly increases the flexibility of the whole system and could be used to filter in (or out) particularly desirable or undesirable signals.

The sampling rate of an instrument depends on the frequency band of interest and data constraints. The sampling rate must be more than twice the upper frequency limit to prevent aliasing. The ability to modify the recorded sampling rate could be used to save data space. If data compression is used, similar software modification of the degree of compression could also be used.

4. Event detection, data collection, and compression. An important aspect of seismic data is that more than 90% of the data is relatively uninteresting. Important information comes in bursts at random and unpredictable times. While Apollo could afford to send all its seismic data back to Earth, where relative importance could be determined at the leisure of scientists, Viking did not (and future planetary seismic experiments probably will not) have this luxury. Decisions on information content will have to be made before the data are returned to Earth. It is important to maximize the scientific content in the available data space; however, it will probably not become evident how best to accomplish this goal until after the experiment package is placed on another planetary object.

In order to sample three axes at a sampling rate of 20 Hz, 8 bits per sample over a 24-hour period, a seismometer system requires 41.5×10^6 bits plus overhead (e.g., data management, time codes). Estimating 3% of the data space for overhead, or 1.2×10^6 bits, a total of 42.7×10^6 bits are required. The Viking seismometer was allocated a nominal 1.1×10^6 bits per SOL, in other words, a 39:1 reduction from optimum in data allocation. There are three immediately obvious approaches to this problem: (1) increase the data allocation, (2) devise a data compression technique where only the most important parts of a given seismic event are kept, and (3) devise a priority system of data storage that eliminates unwanted noise and periods of low information when more informative data are encountered.

The total data allocation for a given spacecraft is entirely constrained by the state of the art of data storage and transmission capabilities. This is a spacecraft system constraint and is mostly a problem of engineering and economics. Dividing the total data allocation among the various experiments will, for the foreseeable future, leave any seismology experiment far short of the optimum 42.7×10^6 bits/day. This forces optimization of the *in situ* data collection, processing, compression, and transmission schemes.

This recommendation, although a very important one, has no known straightforward or obvious solution. Many different approaches are possible, and much research must be done well ahead of the next mission so that a system may be developed and ready when the time for hardware development arrives (normally around the time of mission approval). It is important to note that the primary target for this study is *in situ* data management.

Conclusion

The most severe problems encountered in the Viking seismic experiment were, in order of importance: (1) failure of the Lander 1 seismometer; (2) wind noise due to the location of the seismometer on the spacecraft; (3) inadequate data compression techniques; and (4) low sensitivity.

It is a straightforward task to eliminate all four problems for future extraterrestrial seismometry experiments. The

Viking Seismology Team has put forward two sets of recommendations for future work on Mars:

(1) Scientific goals - to determine
   (a) seismicity
   (b) velocity-depth relationships
   (c) nature of the core
   (d) location of partially molten areas
   (e) tectonic state of the Tharsis area

(2) Engineering goals - to achieve
   (a) isolation from noise
   (b) emplacement of seismometer networks
   (c) flexibility in software control
   (d) improvement of in situ data handling

All these recommendations are necessary and technically feasible.

Appendix B

EXPECTED RATES OF MARSQUAKES

Roger J. Phillips

Introduction

In this appendix we review several regional and global-scale processes that are potential sources of martian seismicity, and we present the results of a few simple calculations to predict the level of seismic activity as a function of marsquake moment and magnitude.

Moment Recurrence Relation

The most fundamental measure of marsquake size, and that most readily relatable to physical processes, is the scalar seismic moment M_o given by

$$M_o = \mu A u \tag{1}$$

where μ is the shear modulus in the marsquake source region, A is the fault area that ruptures during a marsquake, and u is the average coseismic fault slip. The distribution of seismic events by moment is generally given by a relation of the form

$$N(M_o) = a M_o^{-b} \tag{2}$$

where N is the number of events of moment greater than M_o, and a and b are empirical constants. We assume that equation (2) holds as well for marsquakes, and we further assume that the value of b (but not that of a) is identical to that for earthquakes in oceanic intraplate regions, a terrestrial tectonic setting possibly analogous to that of the martian lithosphere. From a catalog of oceanic intraplate earthquakes of known moment over the inclusive years 1977–1988 (E. A. Bergman, personal communication, 1991), the b value is 0.67, and we adopt this figure for Mars.

From equation (2), the number of events falling in the interval M_o to $\Delta M_o + M_o$ is given by

$$N(M_o, M_o + \Delta M_o) = a [M_o^{-b} - (M_o + \Delta M_o)^{-b}] \tag{3}$$

The sum of the seismic moments of all events occurring over a time interval t can be expressed as

$$\Sigma M_o = \int M_o \, dN = \int_0^{M_o^{max}} M_o [a \, b \, M_o^{-(b+1)}] \, dM_o = \frac{ab}{1-b} (M_o^{max})^{1-b} \tag{4}$$

where M_o^{max} is the largest seismic moment for Mars. For a given mechanism of lithospheric strain, the characteristic rate of shear strain $\dot{\epsilon}$ can be related to the sum of the seismic moments over the time interval t through the relation (*Bratt et al.*, 1985)

$$\dot{\epsilon} V = \Sigma M_o / \mu t \tag{5}$$

where V is the seismogenic volume. Thus

$$\frac{a}{t} \equiv \dot{a} = \frac{1-b}{b} (M_o^{max})^{b-1} \dot{\epsilon} \mu V \tag{6}$$

and the frequency of occurrence of marsquakes in a given interval of moment is given by the relationship

$$\dot{N}(M_o, M_o + \Delta M_o) = \dot{a} [M_o^{-b} - (M_o + \Delta M_o)^{-b}] \tag{7}$$

With an assumed value of μ, an estimation of strain rate and seismogenic volume yields a prediction of the frequency-moment distribution of marsquakes. This can be converted into a magnitude recurrence rule using a moment-magnitude relation (Appendix D).

Thermoelastic Mechanisms

We first consider global cooling of a planetary lithosphere as a source of strain rate. If R_o is planetary radius and L_s is the thickness of the seismogenic lithosphere, then

$$\dot{\epsilon} \approx \frac{\dot{R}}{R_o} \approx \frac{\alpha \dot{T}}{R^2_{L_s/2} L_s} \int_{R_L}^{R_o} r^2 \, dr \tag{8}$$

where $\dot{R}$ is the rate of change of R_o, α is the volumentric coefficient of thermal expansion, $\dot{T}$ is the characteristic rate of cooling of the lithosphere, and $R_{L_s/2}$ is the radius at mid-depth in the seismic lithosphere.

A parameterized convection calculation has been used to predict the change in the martian lithospheric temperature profile during the last 100 Ma. This model includes the effect of the decay of radiogenic heat sources in the crust as well as a decrease with time in heat flux from the sublithospheric mantle. On the basis of analogy with the terrestrial oceanic lithosphere, we define the base of the seismogenic lithosphere at the 800°C (1073 K) isotherm (*Wiens and Stein*, 1983; *Bergman*, 1986). In the parameterized convection solution, this isotherm corresponds to a depth at present of approximately 150 km. The average temperature change within the seismogenic lithosphere during the last 100 Ma is about 11 K, and this figure is used to estimate $\dot{T}$.

The principal change in the temperature gradient with time is caused by the thickening of the lithosphere. For values of α and μ of 3×10^{-5} K^{-1} and 7×10^{10} Pa, respectively, the characteristic lithospheric strain rate is -1.0×10^{-19} s^{-1}. Table B1 shows the predicted number of marsquakes per year as a function of seismic moment interval; a maximum moment of 10^{27} dyn cm is assumed on the basis of the data for terrestrial oceanic intraplate earthquakes. The cumulative number of marsquakes per year is shown in Fig. 3.

TABLE B1. Predicted number of marsquakes per Earth year as a function of moment interval (dyn cm) due to global cooling.

Log_{10} Moment Interval	Number/yr (Predicted)
21–22	200
22–23	42.8
23–24	9.15
24–25	1.96
25–26	0.42
26–27	0.09

Thus, from the thermoelastic cooling of the martian lithosphere alone, a seismic network of 10-year duration could potentially measure about 116 events between moments of 10^{23} and 10^{27} dyn cm. Table B2 expresses this information in terms of surface wave magnitude M_S under the assumption that the M_S-M_o relation is that given for the Earth in Appendix D

$$M_S = \log_{10} M_o - 19.46 \tag{9}$$

where M_o is in dyn cm. From this relation, the maximum moment corresponds to an M_S of about 7. As noted in Appendix D, the surface wave magnitude as measured from time-domain amplitudes may actually be somewhat greater for a given seismic moment on Mars than on Earth, so Table B2 is conservative. For a 10-year network, there are predicted to be about 60 events between M_S 4 and 7 due to global cooling.

TABLE B2. Predicted number of marsquakes per year as function of surface wave magnitude M_S due to global cooling.

Magnitude Interval	Number/yr (Predicted)
1–2	461
2–3	98.5
3–4	21.0
4–5	4.50
5–6	0.96
6–7	0.21

The rate of lithospheric cooling, and thus the volumetric rate of marsquake generation, may be greater in the Tharsis area than for the planet as a whole. We have made a simple estimate of this effect on the supposition that the magmatic source region beneath Tharsis has been cooling for at least several hundred million years. A simple one-dimensional diffusion model is used. The magma source region is presumed to lie beneath a lithosphere of thickness L, which tracks the cooling beneath with a linear temperature gradient. As the source region begins to cool, the lithosphere is anomalously thin; it thickens with time toward its ambient (global average) value. The change in temperature gradient is controlled by the rate of thickening of the lithosphere, which is given by

$$\frac{dL}{dt} = (T_s - T_L)\left(\frac{dT_{amb}}{dz} + \frac{(T_0 - T_L)}{\sqrt{\pi \kappa t}}\right)^{-2} \left[\frac{d}{dt}\left(\frac{dT_{amb}}{dz}\right) - \left(\frac{T_0 - T_L}{2t\sqrt{\pi \kappa t}}\right)\right] \tag{10}$$

where T_L is the temperature at the base of the lithosphere, T_0 is the anomalous temperature $(T_L + \Delta T)$ in the sublithosphere at $t = 0$, T_s is the surface temperature, and κ is thermal diffusivity. The background or ambient temperature gradient is given by dT_{amb}/dz and is time dependent. Equation (10) has been used to evaluate the strain rate at mid-depth in the seismogenic lithosphere beneath Tharsis; the results are shown in Table B3.

TABLE B3. Strain rate and thickness of seismogenic lithosphere due to cooling of a sublithospheric temperature anomaly, ΔT, of 300 K beneath Tharsis.

Time (Ma)	Strain rate (s^{-1})	Seismic Lithosphere Thickness (km)
100	-7.8×10^{-19}	99
200	-3.6×10^{-19}	111
300	-2.4×10^{-19}	116
400	-1.9×10^{-19}	120
500	-1.6×10^{-19}	123
600	-1.5×10^{-19}	125
700	-1.4×10^{-19}	127
800	-1.3×10^{-19}	129
900	-1.2×10^{-19}	130
1000	-1.2×10^{-19}	131
Ambient	-1.0×10^{-19}	154

Thus, for several hundred million years after initial cooling of a 300-K thermal anomaly, the strain rate and thus the volumetric rate of seismicity in the vicinity of Tharsis could be more than twice that due to whole-planet cooling.

Loss of Buoyancy Support

Another process specifically associated with Tharsis involves loss of buoyancy support of the lithosphere. If the region beneath the elastic lithosphere is supporting the

Tharsis load in part by thermal buoyancy, then as this region cools, a load develops, which must adjust isostatically or flexurally. The density change in the source region is given by

$$\Delta\dot{\rho} = -\alpha\, \rho_0\, \dot{T} \tag{11}$$

where ρ_0 is the ambient density. The corresponding strain rate is given by

$$\dot{\epsilon} \approx \frac{\dot{\sigma}}{E} \approx \frac{\Delta\dot{\rho}\, g\, h_s}{E} = \frac{\alpha\, \rho_o\, g\, h_s\, \dot{T}}{E} \tag{12}$$

where h_s is the thickness of the cooling source region and E is Young's modulus. For a source region 400 km thick that has cooled 200 K in 500 Ma (Table B3), the resulting strain rate is about 10^{-20} s^{-1}, a value small compared with the effect of lithospheric thickening.

Change in Principal Moments

The cooling and contraction of the lithosphere in the Tharsis region will also change the difference in the principal moments of inertia, C-A, and this change will lead to membrane strain in the elastic lithosphere.

For a spherical cap of half-angle γ, density ρ, and thickness h, which is displaced downward by χ

$$\Delta(C - A) \approx 4\pi\, R_o^3\, \chi\, \rho\, h \cos\gamma\, (\cos^2\gamma - 1) \tag{13}$$

where R_o is the radius of Mars. The change in planetary flattening is given by

$$\Delta f = \frac{3}{2} \frac{\Delta(C - A)}{M\, R_o^2} \tag{14}$$

where M is the mass of Mars. On the equator

$$\epsilon \approx 0.4\, \Delta f = 0.6\, \frac{4\pi}{M}\, R_o\, \chi\, \rho\, h \cos\gamma\, (\cos^2\gamma - 1) \tag{15}$$

For h = 200 km and ΔT = 10 K, $\chi \approx 20$ m, and with $\gamma = 45°$ and a 100 Ma time interval, $\dot{\epsilon} \approx -5 \times 10^{-23}$ s^{-1}, so this effect appears to be negligible.

Annual Solar Tide

Due to the eccentricity of the martian orbit, the solar tide is time variable with an annual period. The solar tide-raising potential is

$$W \approx \frac{G\, M_s\, R_o^2}{r_s^3} \tag{16}$$

where G is the gravitational constant, M_s is the mass of the Sun, and r_s is the Mars-Sun distance, given by

$$r_s = a\,(1 - e \cos E) \tag{17}$$

where a and e are the semimajor axis and eccentricity of the orbit, respectively. The term E is the eccentric anomaly and can be approximated by

$$E \approx E_0 = M + e \sin M + \frac{e^2}{2} \sin 2M \tag{18}$$

with

$$M = \frac{2\pi}{P}\,(t - T) \tag{19}$$

where P is the period of the orbit and T is the time of perihelion passage of Mars. The radial tidal displacement is given by

$$\delta r = \frac{h\, W}{g_o} \tag{20}$$

where g_o is the martian gravitational acceleration, and h is the tidal Love number. The strain rate in Mars associated with this process is given by

$$\dot{\epsilon} = \frac{-3\, G\, h}{g_o\, r_s^4}\, M_s\, R_o\, \frac{dr_s}{dt} \tag{21}$$

and dr_s/dt is obtained from equations (17–19). The resulting strain rates, of order 10^{-17} s^{-1}, are high compared with the other processes that have been thus far examined. However, as discussed below, the total strains over one half cycle are small, and solar tidal effects are seen to be generally unimportant.

Obliquity Changes and Polar Cap Loading

The final mechanism examined for global lithospheric strain is that of polar cap loading due to the 10^5-year obliquity cycle (*Ward*, 1979). *Rubincam* (1990) describes "post-glacial rebound" on Mars due to the changing obliquity and the consequent growth and decay of large CO_2 loads on the martian poles. As a result of the polar cap changes, the difference in the principal moments (C – A) periodically changes as well, although there is a phase lag due to the finite viscosity of the mantle. This gives rise to a variation in the second harmonic of gravity, J_2, with a perturbation magnitude given by

$$\Delta J_2 = \frac{M_{cap}}{M_0} \cos\Psi \tag{22}$$

where M_{cap} is the mass of the CO_2 load and Ψ is the half-angle of the cap deposits. The strain resulting from this process is given by

$$\epsilon \approx 0.4\ \Delta f = 0.4\ \frac{3}{2}\ \Delta J_2 \tag{23}$$

and the strain rate is given by

$$\dot{\epsilon} \approx \epsilon\ \frac{2\pi}{T} \tag{24}$$

where T is the period of the obliquity variation. *Rubincam* (1990) estimates a total load of $M_{cap} = 10^{17}$ kg with a half-angle Ψ of 10°. With the 120,000-year obliquity variation, this gives a strain rate of about $1.5 \times 10^{-19}\ s^{-1}$.

Conclusions

Several geophysical processes leading to a wide distribution of strain rates have been examined. Those processes associated with thickening of the martian lithosphere can yield significant levels of seismic activity over a decade-long observing period. Other processes, such as periodic loading by obliquity variations, lead to comparable or higher strain rates. However, the total strain should also be considered before concluding which processes might contribute most to seismic activity. If we consider the strength of the lithosphere to lie between 10 and 100 MPa, then with a Young's modulus of E of 10^{11} Pa, a total strain of 10^{-3} to 10^{-4} is required for marsquakes. The strain rates for the various mechanisms considered can each be multiplied by a characteristic duration of the process to estimate the total strain that might accumulate. These results are given in Table B4, and it is seen that only those processes associated with lithospheric cooling can, in and of themselves, lead to sufficient strain levels for marsquake generation. Several of the processes with higher strain rates (e.g., solar tides) may nonetheless act to trigger marsquakes if strain levels due to other processes are favorable. Overall, the mechanisms considered here suggest that a martian global seismic experiment is quite feasible and that the expected level of marsquake activity is sufficient to achieve the principal scientific objectives of the experiment.

TABLE B4. Summary of strain rates, durations, and total strains for the various mechanisms considered for marsquake generation.

Process	Strain Rate (s^{-1})	Duration of Process (Earth yr)	Total Strain
Thermoelastic stress: Whole-planet cooling	1×10^{-19}	1×10^{9}	3.2×10^{-3}
Tharsis: Cooling ($\Delta T = 300$ K, $t = 400$ Ma)	2×10^{-19}	4×10^{8}	2.5×10^{-3}
Tharsis: Loss of buoyancy support due to cooling	1×10^{-20}	4×10^{8}	1.3×10^{-4}
Tharsis: Change in principal moments	5×10^{-23}	1×10^{9}	1.6×10^{-6}
Annual solar tide effect	1×10^{-17}	1×10^{0}	3.2×10^{-10}
Obliquity variation: Polar cap loading	2×10^{-19}	5×10^{4}	3.2×10^{-7}

Appendix C

SEISMIC DETECTION OF METEOROID IMPACTS ON MARS

Yosio Nakamura

Meteoroids, those numerous small bodies in interplanetary space too small to be detectable by astronomical observations, collide with planets and satellites that happen to be on their orbital paths. They range in mass from less than 10^{-6} g, called micrometeoroids or interplanetary dust, to more than 10^{15} g, thus approaching the size of asteroids. Those in the middle of this mass range, generally 10^2 to 10^6 g, are of particular interest to seismologists. Smaller ones, though detectable by a seismometer if they fall close to the instrument, do not generate sufficiently large seismic waves to be useful in studies of regional to global scale, while larger ones are too rare to be expected within a reasonable time of observation (*Duennebier et al.*, 1975).

Impact signals of meteoroids are useful in two different ways. First, as these seismic signals propagate though the deep interior of a planet, they provide important information on the structure of a planetary interior (e.g., *Nakamura*, 1983). Second, the spatial and temporal distribution of impacts on a planetary surface provides information on the orbital distributions of these interplanetary objects (e.g., *Oberst and Nakamura*, 1987).

For these impacts to be useful in seismic studies on Mars, we must detect a significant number of impact seismic signals during the operation of the seismic stations. Can we reasonably expect to do so? To answer this question, we need to examine several factors, all of which influence the seismic detectability of meteoroid impacts. They include (1) the impact rate, or the rate of encounter with Mars, of various classes of meteoroids; (2) the effect of the atmosphere in retarding impacts; (3) the seismic efficiency, or the efficiency of conversion of impact kinetic energy to seismic waves; and (4) the efficiency of seismic wave propagation through the martian interior. The combined effect of these factors, then, must be compared with the sensitivity of the seismic instruments and the expected level of ground noise.

There is a large quantity of information relevant to an assessment of these factors. They include (1) terrestrial observations of meteors and meteorite falls; (2) astronomical observations of comets and asteroids; (3) the Apollo lunar seismic observations, which provided data on impact rates, temporal and spatial distribution of impacts, seismic efficiency, and seismic wave propagation for the Moon; (4) lunar and planetary crater statistics; (5) lunar chronology, which assigns absolute ages to various lunar terrains of known crater density; and (6) theoretical results on the orbital dynamics of interplanetary objects.

In the following we examine, from available information, these factors influencing the seismic detection of meteoroid impacts on Mars. Particular emphasis is placed on a comparison with the Moon, for which extensive information on the seismic effect of impacts is available.

Impact Rate

To estimate the rate of meteoroid impacts on Mars, we need to know what families of objects presently exist in orbits crossing that of Mars. A generally accepted, but not completely understood, scenario is that most meteoroids in the inner solar system are derived from collisional breakup and perturbation through encounters with planets of two principal types of objects, namely comets and asteroids. What proportion of these objects is cometary is difficult to determine from currently available observational data because all observational methods are strongly selective in detecting different kinds of objects. Because of this difficulty, impact rate estimates based on one type of observations, e.g., terrestrial fireball observations, may not be directly applicable to the estimation of impact rates relevant to seismic effects.

Probably the most closely relevant set of data for our purposes comes from the Apollo lunar seismic network. During the 8 years of network operation, 1743 seismic events clearly identified as meteoroid impacts were detected by the long-period instruments (*Nakamura et al.*, 1982). [The short-period instruments detected several times more impact events (*Duennebier and Sutton*, 1974), but these events have not been fully analyzed.] A recent study by *Oberst and Nakamura* (1991) shows that many of the relatively less energetic impacts, too weak to be detected by multiple stations and believed to be of cometary origin, fall in streams, while more energetic impacts, believed to be either asteroidal or possibly derived from short-period comets, are mostly sporadic, with a few important exceptions occurring in streams or swarms, indicating relatively recent breakup from their parent bodies. Of these 1743 impacts, only 18 were large enough to be useful for investigation of the internal structure of the Moon by conventional methods (*Nakamura*, 1983).

To estimate the impact rate on Mars by inference from the lunar data, we need to know how these objects are distributed in the inner solar system. A Monte Carlo calculation of the fate of objects from a wide class of starting orbits by *Wetherill* (1975) shows that they evolve to pro-

duce a similar impact flux on all the terrestrial planets. This is in agreement with the observation that the cratering records on the Moon, Mercury, and Mars are similar. The actual impact flux, however, depends on the orbits of the source objects. Those in original Mars-crossing orbits, for example, produce about 10 times more impacts on Mars than on the Moon (*Wetherill*, 1975). Thus, it is difficult to make a precise estimate of the ratio of impact fluxes on Mars and the Moon without knowing the sources of these meteoroids. On the other hand, observations of actual impact rates on both the Moon and Mars will give us clues as to the origin of these objects.

Crater statistics on the Moon and terrestrial planets (e.g., *Hartmann*, 1973, 1977; *Neukum and Wise*, 1976; *Neukum and Hiller*, 1981: *BVSP*, 1981) provide a vast quantity of data that may be relevant to this problem. Unfortunately, only for the Moon do we have an absolute chronology of impact terrain through radioisotope dating of samples. Thus, the crater statistics by themselves do not provide an independent means of estimating the impact rate on Mars.

For a given population density, n_p, and approach velocity, v_∞, of a class of meteoroids, the impact rate, F_p, depends on the size of the planet on which the impacts occur

$$F_p = n_p\, v_\infty\, S^2/4R^2$$

where R is the geometric radius of the planet, S is the effective radius given by

$$S^2 = R^2[1 + (8\pi G R^2 \rho / 3 v_\infty{}^2)]$$

and ρ is the mean density of the planet.

The approach velocity v_∞ depends on the orbits of the planet and the impacting object. Table C1 lists estimated values of some relevant quantities for the Earth, Moon, and Mars as adopted from those given by *Hartmann* (1977) for typical asteroidal and cometary objects. Also listed are the corresponding impact velocities, v_i, given by

$$v_i{}^2 = v_\infty{}^2 + v_{esc}{}^2$$

where v_{esc} is the escape velocity.

TABLE C1. Estimated values of approach velocity, effective planetary cross section, and impact velocity for the Earth, Moon, and Mars.

	Asteroids*			Comets†		
	v_∞ (km/s)	$S^2/4R^2$	v_i (km/s)	v_∞ (km/s)	$S^2/4R^2$	v_i (km/s)
Earth	14	0.42	18	38	0.27	40
Moon	14	0.26	14	38	0.25	38
Mars	8.6	0.33	10	31	0.26	31

* Includes short-period comets; assumes $v_\infty = 0.4\, v_{orb}$.
† Long-period comets; assumes $v_\infty = 1.3\, v_{orb}$.

Atmospheric Effects

The martian atmosphere, even though tenuous compared with that of the Earth, is sufficient to cause significant ablation and deceleration to meteoroids entering it. *Gault and Baldwin* (1970) have estimated that for a typical entry speed of 10 to 15 km/s, appropriate for asteroidal objects, those with masses less than about 10^3 g are decelerated and consumed in the upper atmosphere, and only those with masses greater than about 10^7 g are relatively unaffected. They estimate that the latter objects would produce craters larger than approximately 50 m in diameter. As mentioned above, most of the objects detected by the Apollo lunar seismic network are in the mass range from 10^2 to 10^6 g. Thus, most of them would be expected to be strongly affected by the atmosphere of Mars.

Since ablation increases significantly with increasing speed, objects coming from highly eccentric cometary orbits will be more effectively consumed by the atmosphere. Cometary objects are also likely to be more friable and thus more easily disintegrated in the atmosphere. The relatively low density of cometary material also contributes to higher ablation through the atmosphere because of the larger surface area for a given mass. Although exact calculations are not available, we expect that among those in long-period cometary orbits only rare, massive fragments and some higher-density objects sometimes found in cometary showers (*Halliday*, 1988) have any chance of being detected by a martian seismic network.

Seismic Efficiency

Only a very small fraction of the kinetic energy carried by the impacting object is converted to seismic energy, with most of the energy spent in excavating an impact crater and heating the target material. For example, the impact of spent spacecraft on the lunar surface during the Apollo missions produced an estimated total radiated seismic energy about 10^{-6} of their preimpact kinetic energy (*Latham et al.*, 1970). The efficiency of the energy conversion depends upon many factors such as mass, speed, and density of the impacting object, angle of impact, and physical properties of the target material (e.g., *Schultz and Gault*, 1975).

The diameter, D, of impact craters generally follows a power-law scaling with respect to the kinetic energy, E_i, of the object

$$D = C\, E_i{}^{\lambda}$$

where the exponent λ is about 1/3. [An experimental value by *Gault* (1973) gives $\lambda = 0.370$]. If we assume that the

amplitudes of seismic waves scale similarly, then the 20% to 30% reduction in the expected impact speed from the Moon to Mars (Table C1) translates to about a 15% to 20% reduction in seismic amplitude, probably insignificant relative to other uncertainties.

The density of the impacting object does not appear to affect the seismic efficiency greatly for the Moon. This is evidenced by the fact that both low-density cometary and high-density asteroidal objects are well detected by the lunar seismic network (*Oberst and Nakamura*, 1989). An empirical relationship by *Gault* (1973) also shows only a very weak dependence of crater diameter on the density of the impactor with an exponent in a power-law scaling of 1/6. As stated above, the martian atmosphere is expected to have a much more profound effect on low-density objects than this slight variation in seismic efficiency.

The physical property of the target material may play a significant role in determining the seismic efficiency of impacts. However, we do not presently have reliable data to estimate the difference in physical properties between the Moon and Mars.

Seismic Wave Propagation and Attenuation

Whether an impact of a given kinetic energy is seismically detectable at a given distance from an impact site on a planetary surface also depends strongly on how seismic waves propagate through the interior of the planet. There is a significant difference in the mode of seismic wave propagation between the Earth and the Moon. On the Earth, generally distinct P and S body-wave arrivals are followed by often dispersive surface-wave trains. On the Moon, in contrast, a relatively weak initial body-wave arrival is followed by a long train of scattered waves of much larger amplitude and little coherency. This unusual behavior of seismic wave propagation in the Moon is attributed to the existence of a highly heterogeneous near-surface zone of very low seismic attenuation.

The observed amplitude decay with distance for P waves on the Earth and that of scattered body waves on the Moon, however, are remarkably similar. This probably reflects the fact that both the Earth and the Moon have a distinct low-velocity crust overlying higher-velocity mantle, thus producing similar geometrical spreading of seismic waves on both bodies. The amplitude generally decays rapidly with distance for the first 20° to 30° of distance, and then decays only slightly from 30° to 90°, beyond which more rapid decay follows (*Veith and Clawson*, 1972; *Nakamura et al.*, 1976).

An empirical surface-focus amplitude-distance curve based on large explosions (*Veith and Clawson*, 1972) gives an average value for log(A/T) on Earth of about 1.5 for distances between 30° and 90°, where A is the P-wave amplitude in nanometers normalized to a source of body-wave magnitude $m_b = 5$, and T is the wave period in seconds. $m_b = 5$ corresponds to about a 100-kT yield (*Bache*, 1982), or 4.2×10^{14} J of released energy. In contrast, the impacts of spent S-IVB rockets, each of which had a preimpact kinetic energy of about 4.6×10^{10} J, produced peak ground vibration on the Moon of about 10 nm at 0.5 Hz at distances beyond 30°. Thus, normalizing for the same energy level as above, we obtain $\log(A/T) = 2.7$ for peak amplitudes expected for impacts on the Moon. This means that the peak amplitudes of scattered wave trains on the Moon are about an order of magnitude greater than those of P-wave arrivals from surface explosions on Earth. The initial P-wave arrivals on the Moon, however, are about two orders of magnitude smaller than the maximum amplitudes of scattered wave trains. Therefore, they are about an order of magnitude smaller than those on Earth.

The amplitude-distance relations for Mars are difficult to estimate without knowing the scattering and attenuation characteristics of the martian interior. If Mars is like the Earth, i.e., relatively low in scattering and low in Q, then amplitude decay should be similar to that on Earth. If Mars is like the Moon, i.e., intensive scattering and extremely high Q, then we may expect an amplitude decay similar to that on the Moon. However, if we have intensive scattering, which might be expected because of the past impact history, and lower Q, which might be expected because of a significant volatile content of the interior, then the decay of amplitudes with distance may be more drastic on Mars than on either the Earth or the Moon.

Ground Noise

For lunar seismic observations we were in a sense very fortunate that we had a combination of extremely high-sensitivity seismometers and extremely low ground noise, except for short intervals just after sunrise and sunset. (The Apollo seismographs had a peak sensitivity of better than 0.1 nm in ground displacement at 0.45 Hz.) As a consequence, we detected literally hundreds of impact events every year. Whether we will see a similar result on Mars is not certain.

The results of the Viking seismic experiment showed that when the wind speed was high, the seismic noise level was also high. However, the Viking seismometer was mounted on the lander, not on the ground, and its sensitivity was about two orders of magnitude lower than that of the Apollo lunar instruments. Therefore, there are no experimental data on how low the ground noise may be when the local atmosphere is calm. It may be possible, however, to estimate this quantity from available data.

Expected Rate of Seismicity from Impacts

From the above discussion, it is apparent that most of the impact signals large enough to be useful for seismic investigation of the martian interior will come from sporadic impacts of relatively large meteoroids of asteroidal origin. The frequency of occurrence of such impacts can be estimated from lunar data.

The latest estimate of the flux of large sporadic impacts on the Moon (J. Oberst and Y. Nakamura, personal communication, 1990) gives an annual rate N of impacts of preimpact kinetic energy greater than E (in J) over the entire lunar surface of

$$\log_{10}N = -0.99 \log_{10}E + 11.4$$

for $2 \times 10^{11} < E < 2 \times 10^{12}$ J (mass range from 2×10^6 to 2×10^7 g using an impact velocity on the Moon of 14 km/s, Table C1). If we assume that the population density of large meteoroids in Mars-crossing orbits is the same as those in Earth-crossing orbits, the impact rate on the martian surface, after adjustment for the differences in impact velocities and effective radii as given in Table C1 and in the surface areas of the Moon and Mars, will be given by

$$\log_{10}N = -0.99 \log_{10}E + 11.6$$

If we assume an efficiency of seismic energy conversion of 10^{-6} as observed for the impacts of spent spacecraft on the lunar surface (*Latham et al.*, 1970) and the relationship $\log_{10}E = 2.3\ m_b - 0.5$ between energy and body-wave magnitude m_b (*Stacey*, 1977), we obtain an estimate of the rate of impacts in terms of equivalent magnitude as

$$\log_{10}N = -2.3\ m_b + 6.1$$

This relation is shown in Fig. 4. This estimate is likely to be conservative. Seismic efficiency observed for missile impacts at White Sands, New Mexico (R. Eggleton, as quoted by *Latham et al.*, 1970) was an order of magnitude larger than that observed for the Moon. Furthermore, the population density of large meteoroids in Mars-crossing orbits may be significantly higher than assumed here. Thus, the rate of seismogenic impacts may be significantly higher (by a factor of as much as 10 to 100) than shown in this diagram.

Conclusions

Although definitive data are still lacking, given the greater surface area of Mars than the Moon, but also the likely higher seismic attenuation in the interior, the effect of the martian atmosphere, and the probable intervals of significant wind-generated ground noise, we expect a somewhat reduced detection of large impacts, mainly of asteroidal origin, and a greatly reduced detection of small, cometary impacts on Mars compared with the Moon.

Appendix D

EXCITATION OF SEISMIC WAVES ON MARS

Emile A. Okal

Despite the fact that the internal structure of Mars is not known, several general conclusions regarding the excitation of body and surface waves by seismic sources can be drawn from what is known and from terrestrial experience. As a basis for simple calculations we use model AR of *Okal and Anderson* (1978) for the internal structure of Mars, and we assume that seismic sources consist primarily of double couples (i.e., marsquakes).

BODY WAVES

We refer to *Kanamori and Stewart* (1976) for the following expression of the amplitude of a body wave recorded at teleseismic distance Δ from a source

$$u = M_o \frac{1}{4\pi\rho v^3} G(\Delta) C R A(t, Q) \qquad (1)$$

We will define and discuss each of these factors separately.

M_o is the seismic moment, scaling the seismic source. Since the purpose of this computation is to assess the response of the planet to a unit moment source, we assume that the range of seismic moments is common to both planets.

The next factor, $\frac{1}{4\pi\rho v^3}$, where ρ is the density and v the seismic velocity (either P or S) at the source, characterizes the efficiency of the source material at generating body waves. This term should not be significantly different in Earth and Mars.

The next factor represents the geometrical spreading of the body wave in a radially inhomogeneous, spherical planet as a function of angular distance Δ. For surficial sources G can be written (*Kanamori and Stewart*, 1976)

$$G(\Delta) = \frac{1}{a}\sqrt{\frac{\sin i}{\sin\Delta}\frac{1}{\cos i}\left|\frac{di}{d\Delta}\right|} = \sqrt{\frac{v}{a^3}\frac{\sin i}{\sin\Delta}\frac{1}{\cos^2 i}\left|\frac{d^2T}{d\Delta^2}\right|} \qquad (2)$$

where a is the planetary radius, and i is the take-off (and emergence) angle of the ray at the surface: $i = \sin^{-1} pv/a$ with $p = dT/d\Delta$, where T is the travel time.

The prominent difference between the two planets comes from the smaller size of Mars, through the $a^{-3/2}$ factor in equation (2). The relative behavior of the other terms in equation (2) is more difficult to assess. Mars is probably a less heterogeneous planet than Earth (because of the reduced compression of the mantle), and crustal velocities can be assumed to be comparable. Thus, at the same angular distance, Δ, the rays are less strongly bent, i.e., sample a shallower fraction of the planet's radius than in the Earth, resulting in stronger values of the incidence angle i, and therefore of $\sin i/\cos^2 i$. On the other hand, because of the lesser refraction and of the shorter travel times, the second derivative $d^2T/d\Delta^2$ is less than in Earth (by about a factor of 1.5). Given this complexity, we computed numerically $G(\Delta)$ in the case of P waves, both for model AR in Mars and for the Jeffreys-Bullen model in the Earth, and found that at typical mantle distances (25° to 95°), the martian value of G is about 3.5 times larger than the terrestrial one. Because neither planet is expected to feature drastic variations in Poisson's ratio throughout its mantle, the ray paths for P and S waves will be nearly identical and the same result would be expected for S waves.

The next two factors in equation (1) are C, which is the surface response to the incident wave, expected to be equivalent in Mars and the Earth, and R, the radiation coefficient characterizing the geometry of the double couple with respect to the surface and the azimuth of the station, also expected to be equivalent to existing geometries on Earth.

The last factor in equation (1) characterizes the anelastic attenuation along the path of the body wave

$$A(t, Q) = \exp\left[-\frac{\omega T}{2Q}\right] = \exp\left[-\omega \int_{ray} \frac{ds}{2\,v(r)\,Q(r)}\right] \qquad (3)$$

where ω is the angular frequency, v(r) and Q(r) are the velocity and quality factor as functions of radius, and the integration is conducted along the wave path. Obviously, the values of A in Mars will depend critically on the Q structure of the planet, especially for high-frequency waves. Even if Mars had the same Q as Earth, the shorter travel times T in equation (3) would boost A significantly, since the average mantle P wave on Mars travels about 420 s, as opposed to 600 s on Earth. Using an average Q_P of 600 for P waves at 1-s period, A would jump from about 0.043 on Earth to 0.11 on Mars, a factor of 2.5. In the case

Appendix D

EXCITATION OF SEISMIC WAVES ON MARS

Emile A. Okal

Despite the fact that the internal structure of Mars is not known, several general conclusions regarding the excitation of body and surface waves by seismic sources can be drawn from what is known and from terrestrial experience. As a basis for simple calculations we use model AR of *Okal and Anderson* (1978) for the internal structure of Mars, and we assume that seismic sources consist primarily of double couples (i.e., marsquakes).

BODY WAVES

We refer to *Kanamori and Stewart* (1976) for the following expression of the amplitude of a body wave recorded at teleseismic distance Δ from a source

$$u = M_o \frac{1}{4\pi\rho v^3} G(\Delta) C R A(t, Q) \qquad (1)$$

We will define and discuss each of these factors separately.

M_o is the seismic moment, scaling the seismic source. Since the purpose of this computation is to assess the response of the planet to a unit moment source, we assume that the range of seismic moments is common to both planets.

The next factor, $\frac{1}{4\pi\rho v^3}$, where ρ is the density and v the seismic velocity (either P or S) at the source, characterizes the efficiency of the source material at generating body waves. This term should not be significantly different in Earth and Mars.

The next factor represents the geometrical spreading of the body wave in a radially inhomogeneous, spherical planet as a function of angular distance Δ. For surficial sources G can be written (*Kanamori and Stewart*, 1976)

$$G(\Delta) = \frac{1}{a}\sqrt{\frac{\sin i}{\sin\Delta}\frac{1}{\cos i}\left|\frac{di}{d\Delta}\right|} = \sqrt{\frac{v}{a^3}\frac{\sin i}{\sin\Delta}\frac{1}{\cos^2 i}\left|\frac{d^2T}{d\Delta^2}\right|} \qquad (2)$$

where a is the planetary radius, and i is the take-off (and emergence) angle of the ray at the surface: $i = \sin^{-1} pv/a$ with $p = dT/d\Delta$, where T is the travel time.

The prominent difference between the two planets comes from the smaller size of Mars, through the $a^{-3/2}$ factor in equation (2). The relative behavior of the other terms in equation (2) is more difficult to assess. Mars is probably a less heterogeneous planet than Earth (because of the reduced compression of the mantle), and crustal velocities can be assumed to be comparable. Thus, at the same angular distance, Δ, the rays are less strongly bent, i.e., sample a shallower fraction of the planet's radius than in the Earth, resulting in stronger values of the incidence angle i, and therefore of $\sin i/\cos^2 i$. On the other hand, because of the lesser refraction and of the shorter travel times, the second derivative $d^2T/d\Delta^2$ is less than in Earth (by about a factor of 1.5). Given this complexity, we computed numerically $G(\Delta)$ in the case of P waves, both for model AR in Mars and for the Jeffreys-Bullen model in the Earth, and found that at typical mantle distances (25° to 95°), the martian value of G is about 3.5 times larger than the terrestrial one. Because neither planet is expected to feature drastic variations in Poisson's ratio throughout its mantle, the ray paths for P and S waves will be nearly identical and the same result would be expected for S waves.

The next two factors in equation (1) are C, which is the surface response to the incident wave, expected to be equivalent in Mars and the Earth, and R, the radiation coefficient characterizing the geometry of the double couple with respect to the surface and the azimuth of the station, also expected to be equivalent to existing geometries on Earth.

The last factor in equation (1) characterizes the anelastic attenuation along the path of the body wave

$$A(t, Q) = \exp\left[-\frac{\omega T}{2Q}\right] = \exp\left[-\omega \int_{ray} \frac{ds}{2\,v(r)\,Q(r)}\right] \qquad (3)$$

where ω is the angular frequency, v(r) and Q(r) are the velocity and quality factor as functions of radius, and the integration is conducted along the wave path. Obviously, the values of A in Mars will depend critically on the Q structure of the planet, especially for high-frequency waves. Even if Mars had the same Q as Earth, the shorter travel times T in equation (3) would boost A significantly, since the average mantle P wave on Mars travels about 420 s, as opposed to 600 s on Earth. Using an average Q_P of 600 for P waves at 1-s period, A would jump from about 0.043 on Earth to 0.11 on Mars, a factor of 2.5. In the case

Appendix E: Workshop Agenda

WORKSHOP ON A MARS GLOBAL SEISMIC NETWORK
May 7-9, 1990
Morro Bay, California

Introduction and Workshop Overview	*S. C. Solomon*
Overview of Mars Exploration Initiatives	*M. H. Carr*
Mars Global Network Mission Concepts	*W. B. Banerdt*
Mission Scenarios	
Lander Technologies	
Engineering Constraints	
Schedules	
Lessons from the Viking Seismology Experiment	*D. L. Anderson*
Lessons from the Apollo Seismic Experiment	*Y. Nakamura*
Other Efforts in Planetary Seismology	*P. M. Davis and Y. Nakamura*
Global Seismic Models (V_p, V_s, ρ)	*E. A. Okal*
Key Measurements	
Implications for Bandwidth, Data Rates, Station Siting	
Expected Seismicity: Geophysical Context for Marsquake Activity	*R. J. Phillips*
Expected Seismicity: Meteoroid Impacts	*Y. Nakamura*
Expected Q Structure	*R. G. Butler*
Effect of Temperature, Volatiles	
Influence on Amplitude-Distance Relations	
Expected Seismic Noise on Mars	*F. K. Duennebier*
Important Technical Issues	
Buried vs. Surface Sensors	*F. K. Duennebier*
Accuracy of Surface Station Location and Timing	*R. J. Phillips*
Data Compression Schemes	*R. G. Butler*
Recent Experiment Prototypes	*P. M. Davis*
Discussion of Scientific Objectives and Technical Requirements	*S. C. Solomon*
Writing Assignments	

Appendix F: Workshop Participants

Prof. Don L. Anderson
Seismological Laboratory
California Institute of Technology
Pasadena CA 91125

Dr. W. Bruce Banerdt
Jet Propulsion Laboratory
Mail Stop 183-501
4800 Oak Grove Drive
Pasadena CA 91109

Dr. Rhett G. Butler
Program Manager
IRIS Global Seismographic Network
1616 N. Fort Myer Drive, Suite 1440
Arlington VA 22209

Dr. Michael H. Carr
U.S. Geological Survey
345 Middlefield Road
Menlo Park CA 94025

Prof. Paul M. Davis
Department of Earth and Space Sciences
University of California, Los Angeles
Los Angeles CA 90024

Dr. Frederick K. Duennebier
Hawaii Institute of Geophysics
University of Hawaii
2525 Correa Road
Honolulu HI 96822

Dr. Yosio Nakamura
Institute for Geophysics
The University of Texas at Austin
8701 North Mopac Boulevard
Austin TX 78759-8345

Prof. Emile A. Okal
Department of Geological Sciences
Northwestern University
Evanston IL 60201

Prof. Roger J. Phillips
Department of Geological Sciences
Southern Methodist University
Dallas TX 75275

Prof. Sean C. Solomon
Department of Earth, Atmospheric, and Planetary Sciences.
Building 54-522
Massachusetts Institute of Technology
Cambridge MA 02139

Early Mars (P12)

N94-24997

Room 102 Mon PM

Presiding, H. Frey

NASA/Goddard Space Flight Center

J. R. Zimbelman

Smithsonian Inst.

S1-91
ABS. ONLY
19831
P-1

P12-02 1344H INVITED

The Geophysical Signal of the Martian Global Dichotomy

Roger J. Phillips (Department of Geological Sciences, SMU, Dallas, TX 75275)

A first-order tectonic question for Mars is the origin and nature of the global dichotomy (GD) separating approximately the northern and southern hemispheres of the planet. It is appropriate to focus on hypotheses for the origin of the GD as well as on geophysical models of related internal structure that are constrained by present-day observations.

There are basic planetary scale observations that relate to the GD: (i) The dichotomy boundary separates two fundamentally different elevations on the planet, as the terrain to the north is lower by an average of about 3 km. (ii) The boundary separates terrain of regionally distinct crater ages, heavily cratered (older) in the south and sparsely cratered (younger) in the north. (iii) The amount of ancient crust apparently removed from north of the dichotomy boundary cannot be accounted for by simple surface erosion and deposition in the south, and the constraint becomes particularly severe if isostatic adjustment is presumed to have accompanied this process. This last point leads to the supposition that some type of interior process must have been responsible for the creation of the GD.

An obvious way to create the observed elevation difference between the two hemispheres is with a thinner crust in the north, although a denser crust would also work. Hypotheses for producing a thinner northern crust include preferential sub-crustal erosion, a giant impact, and simply invoking the crustal thickness difference as a primordial feature of the planet.

If the GD represents a fundamental change in the crustal thickness of Mars, then there should be geophysical evidence of this. The center-of-figure to center-of-mass offset of the planet may be related to the GD, but the Tharsis topography must certainly also contribute. If the Tharsis and GD effects can be separated, then a crustal thickness model can be tested, though the results will not be unique.

The gravity field provides another geophysical constraint on GD models. A simple change in thickness of an isostatically compensated crust should show a characteristic gravity signal across the dichotomy boundary. There *is* a gravity anomaly that is clearly associated with the boundary in regions where the gravity signal is not cluttered by contributions from other features such as Tharsis and Elysium. The gravity signal has a complex spatial relationship with the boundary, and efforts are presently underway to model this anomaly.

JOURNAL OF GEOPHYSICAL RESEARCH, VOL. 95, NO. B4, PAGES 5089–5100, APRIL 10, 1990

Permanent Uplift in Magmatic Systems With Application to the Tharsis Region of Mars

ROGER J. PHILLIPS

Department of Geological Sciences, Southern Methodist University, Dallas, Texas

NORMAN H. SLEEP

Departments of Geology and Geophysics, Stanford University, Stanford, California

W. BRUCE BANERDT

Jet Propulsion Laboratory, California Institute of Technology, Pasadena

There has been considerable debate as to the importance of permanent structural uplift in attaining the immense topographic relief of the Tharsis rise on Mars. The presence of ancient terrain high on the rise suggests uplift took place, and this idea is supported by the presence of graben and fractures in the Claritas Fossae region that are orthogonal to extensional stress directions predicted by flexural uplift models of Tharsis. We derive expressions for total elevation and crustal displacement resulting from the partial melting associated with an upper mantle magmatic system. The effect of lateral mass loss is included in the derivation, as is the difference between mass balance and isostatic balance. This "isostatic effect" is due mainly to membrane stress support. The total elevation requirement for Tharsis is rather easy to meet by the choice of source region vertical dimension, but significant upward displacement of the crust requires a special condition. While most of the buoyancy for uplift is provided by a low density residuum, the crustal extrusive load will strongly counteract this effect unless it is only a small fraction of the melt products. A lower bound estimate of the fraction of intrusives necessary for any uplift at all is about 85% of the total magmatic products at Tharsis. Thus we propose that most of the magmas associated with Tharsis evolution ended up as intrusive bodies in the crust and upper mantle.

INTRODUCTION

The nature of the origin and evolution of the Tharsis and Elysium provinces of Mars, in terms of their great elevation and areal extent, volcanic activity, and tectonic style, has sparked intense debate over the last fifteen years. Central to these discussions are the relative roles of structural uplift and volcanic construction in the creation of immense topographic relief. *Phillips et al.* [1973] and *Plescia and Saunders* [1980] have argued that the presence of very old and cratered terrain high on the Tharsis rise, in the vicinity of Claritas Fossae, points to structural uplift of an ancient crust. *Solomon and Head* [1982] have pointed out, however, that there is no reason that this terrain could not be of volcanic origin and thus part of the constructional mechanism.

Any explanation for Tharsis that calls for structural uplift must carry a scheme to make this uplift more or less geologically permanent, as the requirements for thermal expansion are far too severe in terms of the strength and longevity of the temperature anomaly [e.g., *Sleep and Phillips*, 1979; *Solomon and Head*, 1982].

The purpose of this paper is to develop a model to predict both crustal displacement (leading to permanent uplift) and topographic elevation in regional, large-scale magmatic systems associated with partial melting of peridotitic mantle rocks and to apply this model directly to the Tharsis region of Mars to test the uplift versus construction question. In contrast to the well-known transient effects associated with thermal isostasy [e.g., *Crough*, 1978, 1979; *Crough and Jarrad*, 1981], we are here interested in the phenomena associated with compositional volume increase due to partial melting, lateral transport of volcanic products, and the resulting "permanent" uplift [e.g., *McKenzie*, 1984]. The mechanisms for this uplift are buoyancy forces resulting from the low density of both intrusive melt products and a Mg-rich residuum.

In another paper, *Finnerty et al.* [1988] focus on the petrological aspects of plateau generation by "closed system" partial melting, approximating isostasy by mass balance. In the present paper, we concentrate on differences between isostasy as defined by mechanical equilibrium, and simple mass balance. The more general "open system" environment is also considered.

We use the concept of open and closed systems as applied to lateral mass movement. A closed system is defined as one in which there is no lateral loss of original mass from the vertical boundaries, extended to the surface, of a mantle source region for magmatic materials. Topographic elevation is gained by constructional and intrusive (with resulting uplift) processes in a closed system. In either an open or closed system, conversion of high density mantle mineralogy to lower density by partial melting to produce garnet-free gabbroic melt products can lead to an elevation increase by: (1) the increased volume (relative to original mantle material) of the solidified melt products and (2) the lower density of the solid Mg-rich residuum in the mantle.

Open system models allow movement of some fraction of

Paper number 89JB03477.
0148-0227/90/89JB-03477$05.00

igneous material laterally across the vertical boundaries of the source volume and there is attendant isostatic adjustment. Such a process is also mass-conservative, but some of the original mass is replaced by material flowing into the column from beneath. This is entirely analogous to isostatic rebound following erosion. The amount of structural uplift of the crust, in either an open or closed system, will be the result of buoyant support of positive relief by both a low density magmatic residuum and the melt products that remain in the interior (intrusive into the crust and upper mantle). Lateral mass loss in the open system will affect this uplift, depending on the fraction of intrusive melt product and on the distribution of loss between intrusive and extrusive material.

In either the open or closed state, the isostatic state will depend on, at least, the mechanical state of the lithosphere, radial variation in planetary gravity, and membrane stresses. In particular, a magmatic column that transfers material to the surface will be subject to downward isostatic adjustment because of the last two effects. These processes do not conserve mass; in the presence of radial gravity variations alone, for example, it is weight that is conserved. However, it is important to note that in the model to be developed below there is "petrological mass conservation." This means that the mass of all elements of a partial melting process (residuum, melt products, lateral mass loss) is equivalent to the mass of the original source region that undergoes partial melting. This is a constraint that has heretofore not been applied to Tharsis models, with the exception of *Finnerty et al.* [1988]. Our work here continues the work of *Sleep and Phillips* [1985] on isostatic and flexural models by searching for models that will satisfy the dual constraints of petrological mass conservation and mechanical equilibrium. Additionally, we seek model results that satisfy the topographic elevation requirement for Tharsis as well as provide non-negative crustal displacement. Finding such models is the major goal of this paper.

Structural uplift may be resisted by flexure of an elastic lithosphere. We use the term "flexural uplift" in this paper to mean that bending stresses are important during the uplift process. Flexural strains that occur in an elastic lithosphere during this type of uplift may not be accommodated, and flexural failure may result. By "isostatic uplift" we specifically mean that bending stresses are not important doing the uplift process. This might occur, for example, during buoyant uplift when flexural strains in an overlying elastic lithosphere are accommodated by movement on pre-existing flexural fault zones. That is, large flexural stresses cannot build up, and the stress distribution is largely isostatic. We use the term "uplift" in a general sense, when we do not wish to distinguish between the isostatic and flexural mechanisms.

The models discussed in this paper can be inherently linked to hot spot volcanism and the pressure release partial melting associated with the buoyant rise of hot low-density material in a convecting system. We wish, of course, to isolate the "permanent" or lasting effects of the plume from transient effects associated, for example, with dynamically or thermally maintained topography. The models discussed here are consistent with the plume environment if the plume simply provides a heat flux into the uppermost parts of the mantle. In this circumstance, the plume provides the heat source for partial melting of in situ mantle material. Alternatively, the plume material itself could undergo pressure release partial melting and ultimately supply a net mass flux to the lithosphere. In this case, mass would not be conserved petrologically, as in the model to be developed below. We defer discussion of this situation until the end of the paper, but note now that the general conclusion of this work, that most of the magmas at Tharsis ended up as intrusive, is not negated if there is a net mass flux into Tharsis.

The Tharsis system may have been stable against convective disruption during its magmatic history because its magmatic residuum was less dense than normal mantle. This is analogous to the continental tectosphere or chemical boundary layer proposed for the Earth by *Jordan* [1975, 1981]. We will show that this residuum appears to be providing the majority of isostatic support for broad-scale Tharsis topography. In effect, the system was stabilized, through isostasy, by the strength of the upper lithosphere, although there was probably some lateral spreading of the entire configuration. To first order, this does not affect the lateral mass loss of the open system model.

Below we develop the general theory for permanent uplift in open magmatic systems. Subsequently, we apply these results to Tharsis in the context of its stress history, which we first review to motivate the theoretical development.

REVIEW OF THARSIS STRESS STATES

Introduction

We present a brief summary of the stress states that appear to have existed during the evolution of Tharsis. They suggest that while Tharsis was isostatic over much of its history, mechanisms must be found to provide both flexural uplift and flexural loading.

Stress States: Uplift Resisted by Flexure

Mechanical models for Tharsis that involve flexural stresses in the lithosphere resulting from uplift (known as "flexural uplift models") have been rejected by *Banerdt et al.* [1982], *Solomon and Head* [1982], and *Willemann and Turcotte* [1982] on the basis that the tectonic pattern from the resulting stress pattern is not observed. Conversely, *Hall et al.* [1986] find tectonic evidence for flexural uplift stresses in the Elysium Province and speculate that the same process must have occurred for Tharsis, but that the scale was very small or the evidence has been obliterated by subsequent volcanism and faulting.

If flexural uplift was an early phase in the evolution of Tharsis, tectonic evidence for it might be found in the oldest geological units in the region, for example, those associated with Claritas Fossae. Flexural uplift would produce faults or graben circumferential to Tharsis, which in the vicinity of Claritas Fossae would strike approximately ENE-WSW. There is, in fact, a strong set of fractures and graben in the Claritas Fossae region that match fairly well the prediction for flexural uplift. Figure 1 is a map showing this area and the stratigraphic units mapped by *Masursky et al.* [1978]. Also shown are just those extensional features we have mapped in the ENE-WSW set. They are confined to the two oldest units, "cratered plateau material" and "old fractured plains material." (Both of these units are now classified as Noachian in age in the Claritas Fossae region.) Also shown in Figure 1 are the stress predictions from a flexural uplift

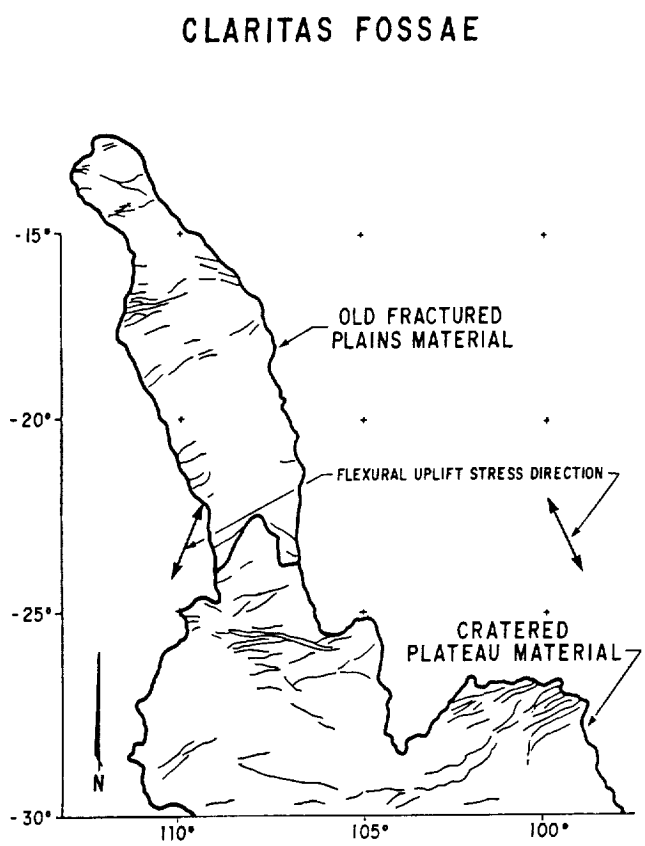

Fig. 1. Sketch map of the Claritas Fossae region of Mars modified from *Masursky et al.* [1978] and other sources. Graben and fractures circumferential to Tharsis are shown. Extensional stress directions predicted by flexural uplift model of Tharsis are also plotted [from *Banerdt et al.*, 1990].

model [from *Banerdt et al.*, 1990]. The maximum extensional stress is horizontal and the maximum compressional stress is vertical; thus normal faults and graben are predicted. The calculated stress directions are approximately orthogonal to the mapped features in Figure 1. We, of course, do not know the state of gravity and topography at the time of uplift. Figure 1 merely suggests that flexural uplift in the Tharsis region could have produced the tectonic features shown.

Claritas Fossae was first cited [*Phillips et al.*, 1973] as evidence for structural uplift of Tharsis because of its great age and elevation, reaching an altitude of 9 km. It is also clear now that Claritas Fossae also shows clear tectonic signs of flexural uplift. Based on this same tectonic evidence, *Tanaka and Davis* [1988] have reached a similar conclusion, proposing that flexural uplift is the earliest tectonic event (Early Noachian time) in the Syria Planum region of Tharsis, and by inference elsewhere in Tharsis.

It should be emphasized that these inferred flexural uplift stresses were probably confined to the outermost parts of the lithosphere, i.e., to the crust. Much of the underlying lithosphere, which we will subsequently argue was subject to massive intrusion during the major period of Tharsis formation, may have been weak enough to support only creep stress.

We would like to conclude that uplift, flexural or isostatic (see below), played an important role in the early history of Tharsis, but this interpretation is not unique. It is also possible that uplift was minor and followed a major episode of elevation gain by volcanic construction. This places much of the volcanic construction of Tharsis prior to the Early Noachian Claritas Fossae tectonic event. Such a scenario cannot be ruled out at present. However, such a large volcanic pile would have led to quasi-radial to radial normal faults in the immediate Tharsis region, or on the periphery of Tharsis, if this load was supported isostatically, or flexurally, respectively [e.g., *Sleep and Phillips*, 1985]. But there is no evidence for such early tectonic features in Claritas Fossae or anyplace else. The oldest radial fault systems are Late Noachian in age [e.g., *Tanaka and Davis*, 1988].

Stress States: Flexural Loading

For loading of a spherical elastic shell, consideration of a finite flexural rigidity leads to a significantly different stress distribution than the isostatic loading case to be discussed below. *Banerdt et al.* [1982], *Willemann and Turcotte* [1982], and *Sleep and Phillips* [1985] pointed out that the radial graben and fractures on the periphery of Tharsis (or "outer radial fractures") are quite consistent with loading models that lead to flexural stresses.

Stress States: Isostatic Uplift and Loading

Most of the fractures and graben in the immediate area of the Tharsis rise are consistent with an isostatic stress model [*Banerdt et al.*, 1982; *Sleep and Phillips*, 1985]. Such a model can be described by the long-wavelength loading of a thin elastic shell with zero flexural rigidity. Membrane forces control the stress distribution, which produces radial faults. We attribute these inferred stresses to loading by igneous materials and to continued uplift but with flexural strains in the crust accommodated on previously existing faults. Under simple isostasy, the maximum stress difference occurs at the surface and is given by approximately ρgh, where ρ is topographic density, g is gravitational acceleration and h is a harmonic coefficient of topographic height. Isostatic failure takes place when an incremental addition of igneous load or an incremental amount of additional uplift causes the stress difference to exceed the finite strength of the upper crust. (Thus isostatic models cannot distinguish loading from uplift.) The finite strength of the lithosphere may be only a few tens of MPa at shallow depths [e.g., *Brace and Kohlstedt*, 1980]. Stratigraphic units in the Tharsis region that are cut by tectonic features related to isostatic stresses are intermediate to old in age. For example, the youngest unit disturbed by this stress mode in the Phoenicis Lacus Quadrangle [*Masursky et al.*, 1978] is "old fractured plains material," assigned to the last stage of "Elysium volcanism," but preceding "Tharsis volcanism." *Tanaka and Davis* [1988] map these isostatic features as Late Noachian to Early Hesperian in age, younger than the "flexural uplift" set of grabens and faults, as mentioned. The graben and faults lying along the strike of Claritas Fossae are predicted by isostatic stresses [*Sleep and Phillips*, 1985], and this feature may be a horst [*Masursky et al.*, 1978] resulting from this stress system.

The age relationship of the "flexural loading" set of graben and faults to the "isostatic" set remains unresolved.

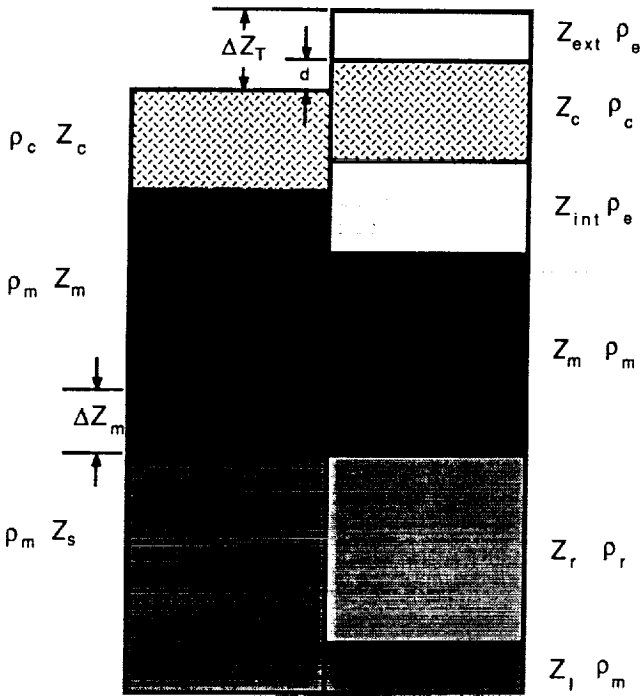

Fig. 2. Elements of the model. Pristine column is composed of crust, Z_c, and pristine mantle that will (Z_s) and will not (Z_m) undergo partial melting. Following partial melting there are intrusive (Z_{int}) and extrusive (Z_{ext}) gabbro/basalt units, and a residuum region (Z_r). Additionally, there has been uplift of the crust, d, and adjustment (ΔZ_m) of the zone of partial melting. The net topographic relief is ΔZ_T and there has been isostatic adjustment at the base of the column (Z_l).

Open System Model

Introduction

We now examine a mechanism to provide uplift of the Tharsis region. Isostatic formulas are used because of their simplicity and for the physical insight that can be gained. The neglect of flexure leads to an upper bound on the amount of isostatic adjustment to loading. In what follows, we assume unit cross sectional area, A, and use column height, Z, instead of Volume, V. To derive this model (Figure 2), it is assumed that the pre-magmatic state is composed of a crustal unit (of density ρ_c, height Z_c, and mass M_c) and a mantle unit divided into a volume that will become a source region for partial melts (ρ_m, Z_s, M_s) and a volume that will remain pristine (ρ_m, Z_m, M_m). As a result of partial melting of the source region, there are six units in the "final" state: (1) an extrusive unit (ρ_e, Z_{ext}, M_{ext}); (2) the crustal unit; (3) an intrusive unit (ρ_e, Z_{int}, M_{int}); (4) undepleted mantle; (5) a Mg-rich residuum (ρ_r, Z_r, M_r); and (6) a region of undepleted mantle beneath the residuum (ρ_m, Z_l, M_l). The formulas to be derived below for elevation and crustal displacement are, to a high degree, independent of the distribution of intrusive material between the upper mantle and crust because the combined mass of Z_c and Z_{int} will remain constant regardless of the distribution of Z_{int} between crust and mantle. For simplicity of presentation, it is assumed that the material resides in the upper mantle (Figure 2).

We specify that a mass fraction f is removed from the original source region by partial melting and that a portion of this fraction, $C(f)$, is lost laterally. The mass of partial melt product in the column is thus:

$$\rho_e[Z_{ext} + Z_{int}] = [f - C(f)]\rho_m Z_s \tag{1}$$

and the mass of the residuum is

$$\rho_r Z_r = [1 - f]\rho_m Z_s \tag{2}$$

Additionally, we stipulate that the fraction of melt products that are emplaced as intrusives is f_i, so that

$$\rho_e Z_{ext} = (1 - f_i)[f - C(f)]\rho_m Z_s \tag{3a}$$

$$\rho_e Z_{int} = f_i[f - C(f)]\rho_m Z_s \tag{3b}$$

Isostasy Versus Mass Balance

In order to proceed, we must consider the difference between isostatic balance and mass balance. In general, less than an equivalent mass at the surface is required to isostatically balance a mass deficiency at depth. This is because: (1) planetary gravity is greater at the surface than at depth, and it is force (or weight) balance that is required for isostasy; and (2) membrane stresses cause strain, which creates subsidence in areas of uplift. For example, a density deficiency at depth gives rise to horizontal tensional forces in the lithosphere which induce changes in surface curvature. The relationship of the topography required for isostasy, $h_i(l)$, to the topography required for mass balance, $h_m(l)$, is given by *Sleep and Phillips* [1985, equation (2)]

$$h_i(l) = f_\varphi(l)h_m(l) \tag{4}$$

where $f_\varphi(l)$ is defined as the "isostatic factor" and is given by

$$f_\varphi(l) = 1 - \left(\frac{R_0 - R_\varphi}{R_0}\right)\left[f_m(l) + \frac{R_0}{g_0}\frac{dg_0}{dr}\right] \tag{5}$$

where l denotes spherical harmonic degree, R_0 is planetary radius, R_φ is the radius of the mean depth of compensation, and g_0 and dg_0/dr are surface gravity and its radial derivative, respectively. Here the isostatic factor $f_\varphi(l)$ represents either Airy compensation, f_a, by gabbroic material at the base of the crust, or Pratt compensation, f_p, due to the low density residuum. The departure of $f_\varphi(l)$ from unity is termed the "isostatic effect." The term $f_m(l)$ is from the membrane stresses associated with isostasy and is found by solving the equations of equilibrium for a thin elastic shell [*Kraus*, 1967] considering only the membrane stresses. The result, generalized from *Sleep and Phillips* [1985, equation (22)] for arbitrary Poisson's ratio ν, is

$$f_m(l) = \frac{\nu}{1 - \nu}\frac{(1 + \nu)l(l + 1)}{l(l + 1) - (1 - \nu)} \tag{6}$$

For $\nu = 0.5$, this expression varies from (18/11) for $l = 2$ to 3/2 for large l. If the density near the surface is ρ_0 and the mean density of the planet is ρ, then [*Sleep and Phillips*, 1985, equation (C9)]:

$$\frac{R_0}{g_0}\frac{dg_0}{dr} = \frac{3\rho_0}{\rho} - 2 \tag{7}$$

Isostatic Column Balance

In terms of equation (4), we turn to Figure 2 to derive a statement for isostatic balance from which to calculate the amount of crustal displacement, d, at the surface. Isostatic balance requires $M_{\text{load}} = f_a M_{\text{comp-Airy}} + f_p M_{\text{comp-Pratt}}$, which upon substitution and reduction gives

$$\rho_e Z_{\text{ext}} + \rho_c d = f_a[(\rho_c - \rho_m)d + (\rho_m - \rho_e)Z_{\text{int}}] + f_p(\rho_m - \rho_r)Z_r \quad (8)$$

A complete derivation for d is given in the Appendix. Here we take advantage of the fact that $f_a \approx 1$, and set f_a to unity to obtain a solution that is easier to interpret. Solving for d and substituting for Z_r, Z_{ext} and Z_{int} yields

$$d = \left[\frac{\rho_m}{\rho_r} - 1\right](1-f)f_p Z_s + \left[\frac{\rho_m}{\rho_e} f_i - 1\right](f - C(f))Z_s \quad (9)$$

The total elevation change is the sum of the displacement, d, and the thickness of the extrusive, Z_{ext}. From equation (9), it follows easily that

$$\Delta Z_T = \left[\frac{\rho_m}{\rho_r} - 1\right](1-f)f_p Z_s + \left[\frac{\rho_m}{\rho_e} - 1\right](f - C(f))Z_s \quad (10)$$

The displacement at the lower boundary of the source region, Z_I, is obtained by differencing column heights before and after partial melting:

$$[Z_I + Z_r + Z_m + Z_{\text{int}} + Z_c + Z_{\text{ext}}] - [Z_s + Z_m + Z_c] = \Delta Z_T \quad (11)$$

from which

$$Z_I = Z_s + \left[\frac{\rho_m}{\rho_r}(1 - f_p) + f_p\right](1-f)Z_s - (f - C(f))Z_s \quad (12)$$

The position of the residuum relative to the base of the pristine (unmelted) layer is given by

$$\Delta Z_m = [Z_I + Z_r] - Z_s \quad (13)$$

Using (2) and (12),

$$\Delta Z_m = \left[\frac{\rho_m}{\rho_r} - 1\right](1-f)f_p Z_s - (f - C(f))Z_s \quad (14)$$

Solution Properties

Once the densities are set (and assuming $C(f)$ is small compared to f, the fraction of partial melting), then the crustal displacement, d, is controlled primarily by the fraction of intrusive f_i. On the other hand, it is seen in equation (10) that the total elevation, ΔZ_T, is independent of f_i. The crustal displacement merely reflects a portion of the total elevation in that $\Delta Z_T = d + Z_{\text{ext}}$, but a change in d, through f_i, is exactly matched by a change in Z_{ext} of opposite sign. That is,

$$\frac{\partial d}{\partial f_i} = \frac{\rho_m}{\rho_e}(f - C(f)) = -\frac{\partial Z_{\text{ext}}}{\partial f_i} \quad (15)$$

The first term in both (9) and (10) represents buoyant support of topography by a low density residuum; it is affected by the isostatic factor, f_p, but always makes a positive contribution to total elevation and crustal displacement.

The second term in (9), which can be either positive or negative, represents the buoyancy effect of melt products near the surface. The effect of lateral mass loss, $C(f)$, either contributes to or detracts from positive crustal displacement, depending on the sign of the term in brackets. In general, a significant amount of uplift is provided by the residuum (first term). This can be enhanced by the buoyancy of intrusive material as long as f_i is greater than ρ_e/ρ_m. This requires f_i to be greater than about 0.9; i.e., a large fraction of intrusive is required. Alternatively, if f_i is less than this value, then there is a net downward adjustment and d can be negative. Again, none of this affects the total elevation, ΔZ_T, because a decrease in d as a function of f_i is exactly made up by an increase in Z_{ext}.

When Does Positive Crustal Displacement Lead to Structural Uplift?

We have stated above that our solutions do not depend on the distribution of intrusive material in the crust. That is, we will arrive at essentially the same answers for d and ΔZ_T, regardless of whether the intrusive material resides totally beneath the crust, is intimately mixed in the crust, or exists as a "lens" near the top of the crust. It may seem paradoxical, however, that igneous products sitting just below the surface could lead to upward displacement, while the same mass placed on the surface will lead to a downward isostatic adjustment.

This is easily understood when we separate the response of an increment of intrusive, δZ_{int}, into two parts (Figure 3). There will be an upward displacement (or structural uplift) of the surface by δZ_{int} and a downward isostatic adjustment $(\rho_e/\rho_m)\delta Z_{\text{int}}$. The net change will be positive

$$\delta d_{\text{int}} \approx \delta Z_{\text{int}} - \frac{\rho_e}{\rho_m}\delta Z_{\text{int}} = \frac{\Delta\rho_{me}}{\rho_m}\delta Z_{\text{int}} \quad (16)$$

where $\Delta\rho_{me} = \rho_m - \rho_e$. This is so because the height increase due to intrusion exceeds the downward isostatic adjustment. In the case of a pure increment of extrusion, δZ_{ext}, there is only downward isostatic adjustment

$$\delta d_{\text{ext}} \approx -\frac{\rho_e}{\rho_m}\delta Z_{\text{ext}} \quad (17)$$

Thus, in both cases there is the same downward isostatic adjustment of the surface, but there is also physical uplift of the surface in the case of intrusion that is greater than the downward adjustment.

In general we might expect to see both the effects of structural uplift and downward isostatic adjustment from a single episode of intrusion, δZ_{int}. The former might lead to flexural uplift stresses in an elastic lithosphere, while the latter might lead to flexural loading stresses. Either mechanism might lead to an isostatic stress distribution, as discussed earlier. The determining factor should be the rate of isostatic adjustment relative to the rate of intrusion. If isostatic adjustment can keep pace with the addition of igneous material into the lithosphere, then the net result should be continuous uplift. On the other hand, if for a given

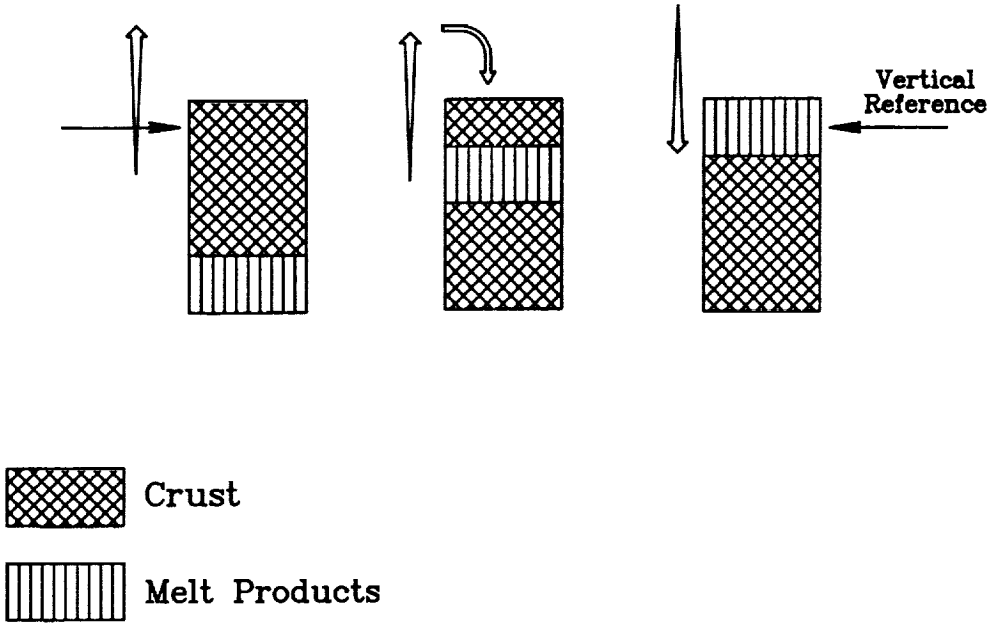

Fig. 3. Cartoons showing three possible configurations of crust and melt products. Elevation is measured relative to "Vertical Reference," which denotes the position of the top of the crust (i.e., land surface) prior to magmatic activity. Subsequent elevation of the surface is the same in all three cases. In the left figure, melt products are added to the base of the crust and "pure" uplift of the crust results. In the right figure, melt products are added to the top of the crust (i.e., extrusive) and there is downward displacement of the crust. In the central figure, melt products are intruded into the upper portion of the crust and crustal movement can be separated into two components: Upward motion due to volume displacement and downward motion due to isostatic adjustment. However, for this cartoon, the net result of these two motions is upward displacement of the crust.

episode of intrusion, the adjustment rate is slower, then uplift followed by downward adjustment might result.

PARAMETERS FOR THARSIS MODELING

Introduction

In this section we set the parameter values for Tharsis modeling. It would be desirable to calculate crustal displacement, d, and total elevation, ΔZ_T, as a function of time. As a time-dependent independent variable, only the mass fraction of partial melting, f, is available and is here considered as an unknown (but undoubtedly nonlinear) function of time. Therefore, we examine solutions as a function of increasing f, which is tantamount to studying their behavior over geological time, albeit the specific time-scale is not known.

Finnerty et al. [1988] point out that the derivation of voluminous tholeiitic basalts in terrestrial ocean basins is consistent with 20% to 30% partial melting of garnet lherzolites. Because we expect that the partial melting episode beneath Tharsis was long-lived, in this paper we adopt a nominal value of $f = 0.3$ for the total amount of Tharsis partial melting. This is done to merely provide a point of discussion for the results, which will be given over the range $f = 0.0$ to 0.5. We will point out subsequently that for f greater than about 0.3, we expect all of the basaltic component to have been extracted from the source region and, additionally, the lower part of the basalt-gabbro column to have entered the eclogite stability field. Both of these effects counteract strongly the increase of total elevation, ΔZ_T, and crustal displacement, d.

Below we specify f-dependent parameters for the problem.

Lateral Mass Loss

Here we wish to establish what might be a plausible value for $C(f)$, since we know of no way to estimate this quantity. We suggest that the most important contribution to lateral mass loss might have been pyroclastic volcanism. *McGetchin and Smyth* [1978] proposed that an early volatile-rich martian mantle would be capable of producing abundant, possibly very mafic, pyroclastic volcanic products. Whether or not a stable eruption cloud could be formed and material carried well away from Tharsis is conjectural because we do not know the atmospheric environment early in martian history. Under present-day atmospheric conditions, magmas with a dissolved water content of 5% or greater can form stable eruption clouds 200 km or more in height [*Mouginis-Mark et al.*, 1982]. A plausible scenario for Tharsis is that early in its evolution there were massive pyroclastic eruptions from a volatile-rich martian mantle. This time-period would coincide with active fluvial processes on the surface. Volatiles on the surface for the most part would not have been recycled to the deep interior, implying a finite lifetime to both major pyroclastic activity and stream flow.

We define C_1 as the ultimate fraction of mass removed laterally from the source region ($\lim_{f \to 1} C(f) = C_1$). We adopt, arbitrarily, a value of $C_1 = 0.03$, so that 10% of the melt products are lost laterally at $f = 0.3$ (if $C(0.3) \approx C_1$; see below). In terms of mass removed by pyroclastic volcanism, we can estimate the average thickness of a global layer of

volcanic deposits by assuming that the Tharsis source occupies a 60° spherical cap on Mars and that the pyroclastic deposit density is 3.0 Mg m^{-3}. This results in an average thickness of 475 m to 950 m as Z_s ranges from 200 km to 400 km. The lower end of this range may not be an unreasonable amount, although we have no means, other than plausibility arguments, to estimate an upper bound on pyroclastic layer thickness. We will show subsequently that the major conclusion of this paper, which is that most of the Tharsis magmas were intrusive, depends only weakly on knowledge of the amount of mass lost laterally from Tharsis.

As discussed above, *McGetchin and Smyth* [1978] envisaged that pyroclastic volcanism was an early phase in the history of Tharsis, and it is suggested here that activity would cease as the interior became devolatilized. Based on this discussion we set

$$C(f) = C_1[1 - e^{(-f/\alpha)}] \tag{18}$$

so that there is a decreasing rate of mass loss with time. Here we set $\alpha = 0.1$, so that mass loss is 95% complete at $f = 0.3$.

Densities

Our understanding of the mantle density of Mars is based on an estimate of the dimensionless moment-of-inertia, $I/M_0R_0^2$, of 0.365 [*Kaula*, 1979] and reasonable assumptions about the plausible range of possible core densities. Here I is the mean moment-of-inertia and M_0 is the mass of Mars. The hypothesis that Kaula put forward to obtain his result is that the nonhydrostatic components of the moments-of-inertia are axially symmetric about Tharsis.

Bills [1989] has recently challenged the deterministic estimate of 0.365 by using the statistical argument that a random distribution of density inhomogeneities would lead to a most probable value of $I/M_0R_0^2$ of 0.345. This yields considerably lower mantle densities. We argue, however, that because of the dominance of Tharsis, a deterministic approach makes the most sense; i.e., there is little reason to adopt a random density distribution to determine the non-hydrostatic principal moments for Mars [see *Kaula et al.*, 1989]. Thus we suggest that the $I/M_0R_0^2$ value for Mars must be close to the 0.365 estimate and the mantle densities, ρ_m, that have been derived from this quantity [e.g., *McGetchin and Smyth*, 1978; *Basaltic Volcanism Study Project*, 1981] are reasonable.

The residuum density, ρ_r, and the erupted and intrusive density, ρ_e, are affected by both the preferential partition of ferrous iron into the melt and the crystallizing of the aluminous phases as basalt at shallow depths rather than as eclogite or garnet peridotite at greater depths. Both effects tend to reduce the density of the residuum because pure fosterite, the end product of gradual extraction of melt, is less dense than primitive mantle, that is, less dense than both the basaltic component as eclogite and the initial iron-rich olivine and orthopyroxene component. Following *Finnerty et al.* [1988], the average density of the residuum is represented as a linear function of the fraction of melt extraction:

$$\rho_r(f) = \rho_m(1 - f) + f\rho_r^* \tag{19}$$

where ρ_r^* is the density of fosterite, 3.224 Mg m^{-3}, and ρ_m is the initial mantle density, assumed to be 3.55 Mg m^{-3} [*McGetchin and Smyth*, 1978]. A feature of the linear relationship between the fraction of melting and the residuum density is that the mantle density anomaly depends only on the fraction of melt generated. According to this relationship, it takes 31% melting, for example, to reduce the residuum density by 0.1 Mg m^{-3}. Thus, a large thickness of extracted basalt is needed to create a large density reduction in the lithospheric mantle.

The effects of ferrous iron and the aluminous phases of the basaltic component of the melt on density and on the net volume change from melting are different. Ferrous iron crystallizes in similar phases at both shallow and great depths (or more precisely, the partial molar volumes of MgO and FeO do not increase rapidly with depth). Hence, upward movement of iron and retention of magnesium at depth do not significantly change the average density or total volume of the column in terms of stable phases alone. In contrast, basalt is about 14% less dense than eclogite of the same composition [e.g., *Yoder*, 1976, page 103], and this can be used as a guide to estimate density behavior. If the total amount of basalt in the pristine mantle is 30%, then the residuum plus basalt density would be 4.2% (= 30% of 14%) less than the original density after the total extraction of basalt ($\Delta Z_T/Z_s \approx 0.042$). We represent the average density of solid basalt and gabbro as a linear function of the fraction of partial melting. The first crystallized melt products of density ${}^i\rho_e$ are iron-rich and relatively dense; the average density, $\rho_e(f)$, decreases as the melting of the source region proceeds:

$$\rho_e(f) = {}^i\rho_e - f\Delta\rho_s \tag{20}$$

where the initial density, ${}^i\rho_e$, of crystallized basalt is taken as 3.40 Mg m^{-3} [*McGetchin and Smyth*, 1978] and $\Delta\rho_s$, the "basalt factor," has units of density. A choice of $\Delta\rho_s = 0.4$ Mg m^{-3} yields $\Delta Z_T/Z_s \approx 0.04$ (or about a 4% density decrease in the column) at 30% melt extraction ($f = 0.3$; see Figure 5).

Once the basaltic fraction of the source region is exhausted, equation (20) does not apply. Additional melting extracts iron from the residuum relative to magnesium. This produces no further net change in density of the column and hence no elevation increase, except for the effects of mass lost laterally. In fact, eruption of dense ultramafic lavas to the surface produces some subsidence because $f_p < 1$. The initial fraction and composition of the basaltic component of the martian mantle is unknown. The fraction might be similar to the terrestrial value (about one-third) as non-volatile elements, aluminum and calcium, are involved. The assertion that the net change in column height is due only to lateral mass loss can be written mathematically as:

$$\frac{\partial}{\partial f}[Z_{\text{int}} + Z_{\text{ext}} + Z_r] = -\frac{\partial C(f)}{\partial f}\frac{\rho_m}{\rho_e}Z_s \tag{21}$$

Substituting from (2) and (3) yields

$$\frac{\partial}{\partial f}\left[\frac{f}{\rho_e(f)} + \frac{1-f}{\rho_r(f)}\right] = 0 \tag{22}$$

If we specify f_{ex} as the value of f for which all the basalt has been extracted from the source region, then the differential equation can be solved to give

$$\rho_e(f) = f\left[\frac{f_{ex}}{\rho_e(f_{ex})} + \frac{1-f_{ex}}{\rho_r(f_{ex})} - \frac{1-f}{\rho_r(f)}\right]^{-1} \tag{23}$$

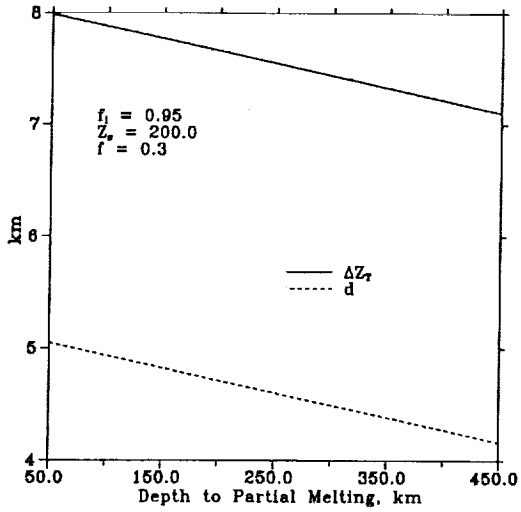

Fig. 4. The effect of the depth to partial melting on the total elevation (ΔZ_T) and the structural uplift (d).

and the value adopted for f_{ex} is 0.33. Equation (23) is used when $f \geq f_{ex}$.

The amount of elevation gain produced by melt extraction is also limited by the stability field of basalt and gabbro in the crust and upper mantle. For the model parameters used in this paper and a temperature gradient of 4 K/km [*Toksöz et al.*, 1978; *Solomon*, 1979], the base of the intrusive gabbro column is just in the eclogite field for $f = 0.31$, corresponding to a depth of approximately 100 km. Then with increasing f, the eclogite portion of the column grows. We have not specifically included eclogite in the model, so that for large values of f, our predictions for d and ΔZ_T are upper bounds.

The densities ρ_m and $^f\rho_e$ used in our calculations are from *McGetchin and Smyth* [1978], with values, as mentioned, of 3.55 Mg m^{-3} and 3.40 Mg m^{-3}, respectively. Additionally, in equation (6), ν is taken as 0.5 and l has a value of 2, the dominant harmonic describing Tharsis [e.g., *Phillips and Saunders*, 1975]. In equation (7), ρ_0 and ρ are set to 3.0 Mg m^{-3} and 4.0 Mg m^{-3}, respectively. The model results given below are insensitive to these last four parameters.

Uplift and Total Elevation: Plausible Models

Introduction

The tectonic studies of Tharsis discussed earlier suggest that there was a phase of true uplift associated with Tharsis, but its magnitude is uncertain. We ask here what ranges of model parameters will predict both the total elevation of Tharsis and a significant amount of upward crustal displacement, which we take to be structural uplift.

Total Elevation

Any total elevation constraint, ΔZ_T, can be achieved by simply specifying a sufficiently large value of the source dimension, Z_s. The broad elevation of Tharsis is about 8 km; a choice of Z_s = 200 km yields ΔZ_T = 7.88 km for a depth to partial melting ($Z_c + Z_m$) of 100 km. Depth to partial melting affects f_p since [equation (5)] $R_0 - R_p = Z_c + Z_m + Z_s/2$. Sensitivity to the depth to partial melting is shown in Figure 4. Over a depth range of 400 km, the effect on both ΔZ_T and d is about a kilometer for $f_i = 0.95$. Other choices of f_i simply shift the d curve up or down. For the remainder of this discussion, the depth to partial melting is fixed at 100 km.

Figure 5 shows the basic results for vertical column quantities for $f_i = 0.95$. For this particular choice of f_i, 5 km of the total elevation of Tharsis is due to uplift. The position of the residuum relative to the original source region is given by ΔZ_m. The adjustment in the base of the column, Z_l, is due almost entirely to isostatic adjustment to lateral mass loss in analogy to the process observed on Earth of isostatic rebound following erosion.

The solution for ΔZ_T is examined in its component contributions [see equation (10)] in Figure 6. Recall that the total elevation is independent of f_i. Here, for $f = 0.3$, melt products and buoyancy of the residuum contribute in approximately equal amounts. Lateral mass loss provides a small negative contribution.

Constraints on Intrusion

The relative contributions of buoyant residuum and buoyant intrusive to the structural uplift, d, are shown in Figure 7 for $f_i = 0.90$ and 0.95. In both cases the dominant contribution is due to the residuum. For $f_i = 0.95$, the effect of intrusion makes a modest contribution to d. For $f_i = 0.90$, however, there is a net downward adjustment caused by the load, Z_{ext}, and the overall uplift is small.

Obviously, the amount of structural uplift of the crust is strongly dependent on the fraction of melt product that ends up intrusive as opposed to extrusive. Figure 8 is an isometric view of uplift, d, as a function of f and f_i. According to the model, a large fraction of intrusion is required to obtain $d > 0$. Over a large range of f, the requirement is that $f_i > 0.85$. We propose that the inference of flexural uplift can be used as a constraint. A reasonably conservative statement might be that d must be greater than zero, which then places a lower bound on the fraction of intrusive beneath Tharsis.

The bound on f_i can be examined in terms of the lateral mass loss at Tharsis. We stated earlier that there is no way to estimate the total amount of this quantity, C_1. We now show that the supposition that most of the Tharsis magmas

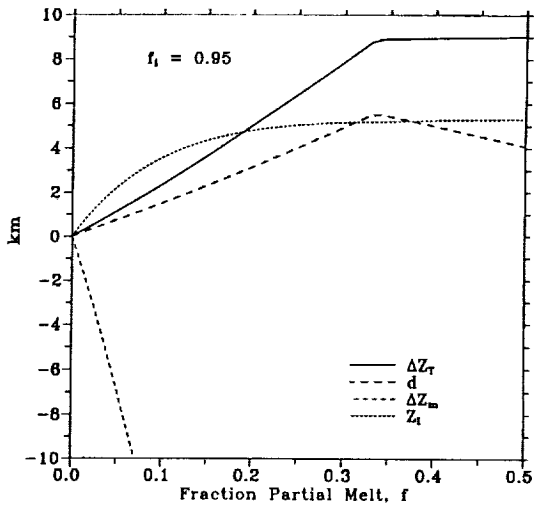

Fig. 5. The four derived quantities, ΔZ_T, d, ΔZ_m, and Z_l, as a function of f for $f_i = 0.95$, Z_s = 200 km, Z_c = 50 km, and a depth to partial melting of 100 km.

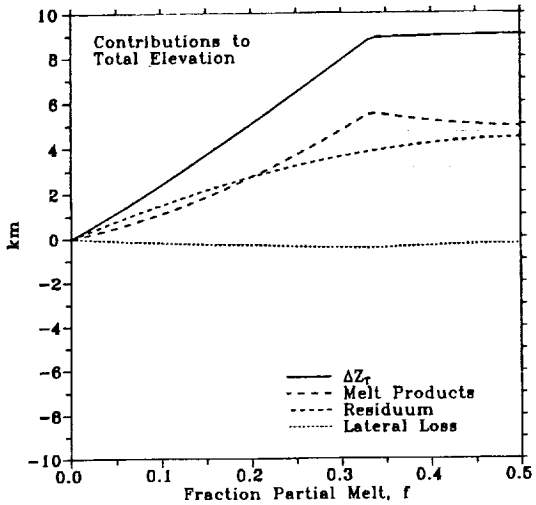

Fig. 6. Total elevation (ΔZ_T) broken down into its component contributions: melt products in the lithosphere, buoyant residuum, and lateral mass loss.

are intrusive is largely unaffected by the lack of knowledge of C_1. Figure 9 plots the lower bound estimate (such that $d = 0$) of f_i as a function of C_1 for $f = 0.3$. The independent variable has been normalized by this value of f, and the x-axis extends to the implausible value of 0.5; i.e., approximately 50% of the total melt product is lost laterally. Over the range of lateral loss from 0% to 50%, the value of f_i decreases only 6%. The decline occurs because there is less mass to be supported at the surface with increasing C_1.

The bound on f_i can be lowered further by partitioning all of the lateral mass loss into the extrusive melt products. Calculations presented to this point have uniformly partitioned the loss between the interior and exterior portions [equation (3)]. Arguments presented above suggest that the most plausible mechanism for lateral mass loss involves processes at the surface. Figure 9 also shows the lower

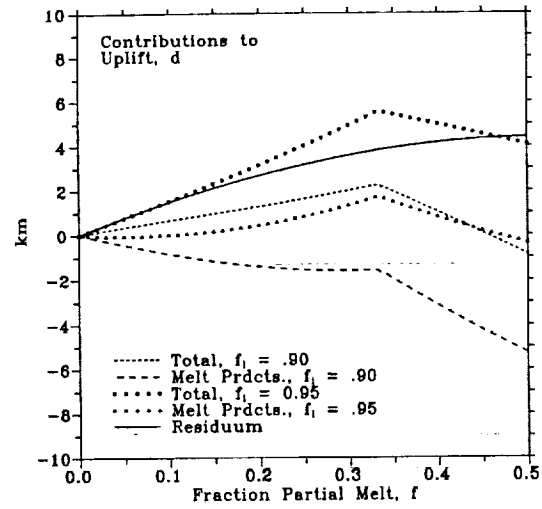

Fig. 7. Structural uplift (d) broken down into its component contributions for 2 values of f_i. The residuum contribution (solid line) is independent of f_i. The lines marked by circles and triangles are the total uplift and melt product contribution, respectively, for f_i = 0.95. The corresponding curves for f_i = 0.90 are the short- and long-dashed lines.

bound on f_i for this situation; i.e., all of the lateral mass loss is taken from the extrusive product. Here, there can be significantly less external mass to support isostatically and the decline now is about 12% over the range of C_1 used. However, we can recalculate the critical intrusive fraction based not on the total amount of partial melt products, but just on that portion remaining at Tharsis (i.e., the locally emplaced intrusive to extrusive ratio). Figure 9 shows that this fraction is almost independent of C_1.

These calculations suggest that our constraint on intrusion is insensitive to the exact amount of material lost laterally from Tharsis. Thus our inability to estimate this quantity does not detract from our conclusion that a high percentage of Tharsis magmas must have ended up as intrusive in the crust and upper mantle.

Discussion

We would argue that intrusion must be an early phase in the history of Tharsis and that the early magmatic history of Tharsis was more likely to have been much more intrusive than extrusive. Presumably magma does not make its way completely to the surface because of some combination of two factors: (i) a high magma density and (ii) a compressive stress state of the lithosphere. We do not consider that the second possibility is important for Tharsis. The dimensionless moment-of-inertia for Mars of 0.365 yields model martian mantles with densities ranging from 3.46 to 3.61 Mg m^{-3} [e.g., *Basaltic Volcanism Study Project*, 1981], which is interpreted in terms of a lower magnesium number for the pristine martian mantle relative to the terrestrial mantle. *Finnerty et al.* [1988] calculated the uncompressed density of the *McGetchin and Smyth* [1978] iron-rich model martian magma to be 3.0 Mg m^{-3}. This density would represent the earliest melts, which would become progressively less dense as partial melting proceeded. Early magmas are then the most likely not to reach the surface and so form intrusive bodies with resulting uplift. Although we do not know the density of the martian crust, we can speculate based on our terrestrial and lunar experience that at least the upper portion of the martian crust might have a density less than that of these postulated iron-rich basaltic magmas. This favors intrusion into the upper mantle as well as intrusion and densification of the lower crust, and disfavors a hypothesis of early massive extrusion.

CONCLUSIONS

In this paper we have explored some complex geological processes with some rather simple relationships: conservation of mass in large-scale partial melting of a mantle source region, lateral loss of partial melt products and the resulting isostatic adjustment, and the difference between mass equilibrium and isostatic equilibrium as it affects the topographic elevation in such a system.

A model for total elevation and crustal displacement in magmatic systems has been derived and applied to the Tharsis region of Mars. While the total elevation requirement is rather easy to meet by the choice of source region dimension, upward crustal displacement requires a special condition. Arguments have been presented suggesting that the ENE-WSW fractures and graben seen at Claritas Fossae are evidence for flexural uplift, and that uplift could account for much of the elevation of Tharsis. While most of the

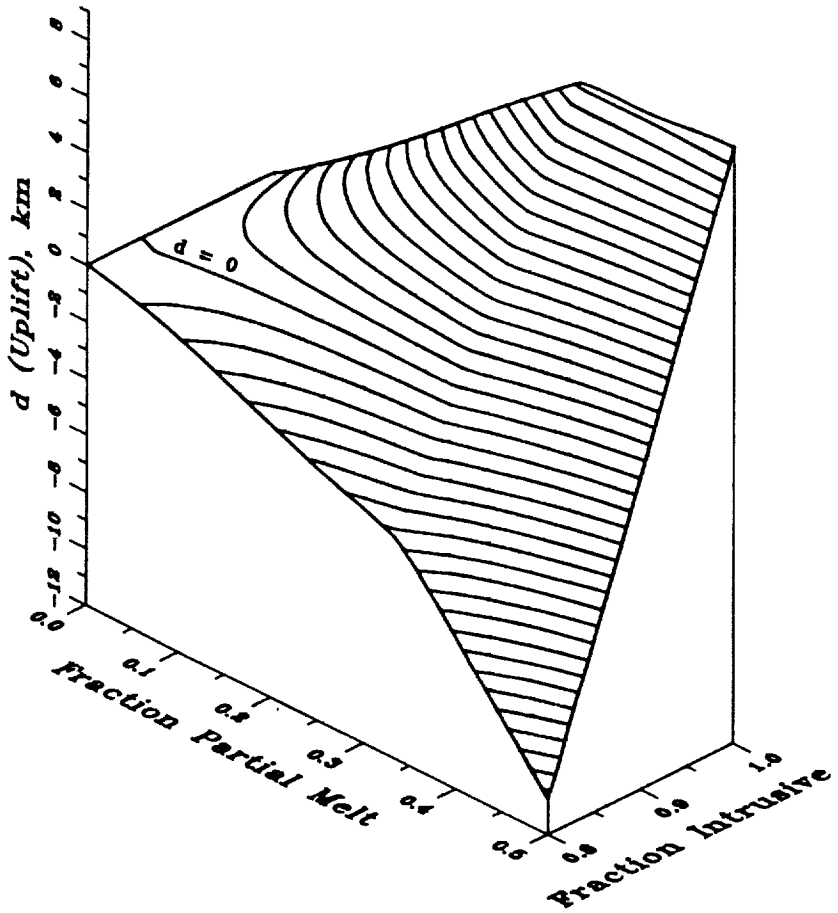

Fig. 8. An isometric view of structural uplift (d) as a function of f and f_i. Contours show constant values of d in kilometers.

buoyancy for uplift is provided by a low density residuum, a crustal extrusive load will strongly counteract this effect unless it is only a small fraction of the total melt product. That is the principal result of this paper: The constraint of non-negative crustal displacement dictates that most of the Tharsis magmas ended up as intrusives in the crust and upper mantle beneath Tharsis.

In the introductory section of this paper, we noted that if a net mass flux is provided to the lithosphere from partial melting associated with upwelling convective flow in the mantle, then mass might not be conserved petrologically in the lithosphere. That is, at least part of the residuum might remain in the mantle flow system and its fate would not be described in the model presented in this paper. Since, as concluded above, most of the buoyancy for uplift appears to be provided by a low density residuum, then the already severe requirements for uplift become exacerbated. If there is no residuum at all, for example, then setting $\rho_m = \rho_r$ in equation (9) yields, for $d = 0, f_i = \rho_e/\rho_m = 0.95$ at $f = 0.1$. That is, at least 95% of the magmas must be intrusive to obtain any uplift.

The model proposed here has similarities to the continental tectosphere proposed by *Jordan* [1975, 1979, 1981]. In that model, the mantles beneath continental cratons are stabilized against convective disruption by chemical gradients. Specifically, these regions, extending to depths of at least a few hundred kilometers, are of lower density than normal mantle because of removal of their basaltic fraction, leaving a Mg-rich residuum. We suggest that the mantle beneath Tharsis is stable and able to support the great topographic elevation for exactly the same reasons. Thus, this portion of the martian mantle may be a good analog to the terrestrial tectosphere.

The mechanism for structural uplift by intrusion was first suggested for Tharsis by *Willemann and Turcotte* [1982]. For the Earth, *McKenzie* [1984] has argued that intrusion of basic magma into the lower portion of the terrestrial continental crust could be locally massive and account for permanent epeirogenic uplift of many features (Colorado Plateau, Western Ghats in India, Lesotho in Southern Africa, surface exposure of high grade metamorphic Archean terrains, etc.). His argument is based on an estimate that basalt generated at oceanic hot spots has locally thickened the crust by about 15 km, and this phenomenon should be more widespread on the continents by the ratio of the average age of the continents to that of the oceanic lithosphere. That this massive amount of volcanism is not seen is attributed to intrusion of magma with density greater than at least that of the upper crust, preventing its extrusion onto the surface [see also *Glazner and Ussler*, 1988]. McKenzie supposes that this material resides in the lower crust as sills or forms a layer between the crust and the mantle.

McKenzie's simple isostatic calculations show that 15 km of intrusion will lead to about 3 km of permanent uplift due

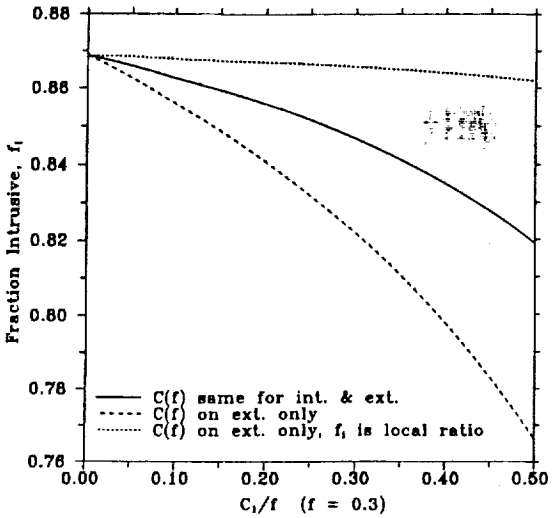

Fig. 9. Lower bound estimates on the fraction of intrusive at Tharsis as a function of ultimate lateral mass loss, C_1, normalized by the fraction of partial melting ($f = 0.3$). The lower bounds are achieved by setting the crustal displacement, d, to zero. The solid curve is the result of lateral mass loss, $C(f)$, uniformly distributed between extrusive and intrusive melt products; the long-dashed curve shows the results when lateral mass loss affects the extrusive products only. The short-dashed curve corrects the latter result to just the mass remaining in the Tharsis column (i.e., not laterally lost), so f_i gives the fraction of local magmatic product that is intrusive.

to the buoyancy of the added material relative to that of the underlying mantle. If McKenzie's argument is correct for the Earth, we think it could have been even more important for the early stages of partial melting of the martian mantle because of the postulated high density of melts. Thus the compelling topography of Tharsis (and Elysium), which we believe could be dominated by uplift, may be the result of an accretion process that gave Mars an iron-rich mantle.

APPENDIX

We derive here a complete expression for structural uplift, d, and attendant vertical quantities Z. Solving for d in equation (8):

$$d = [\rho_c + f_a\Delta\rho_{mc}]^{-1}[f_a\Delta\rho_{me}Z_{\text{int}} - \rho_e Z_{\text{ext}} + f_p\Delta\rho_{mr}Z_r] \quad \text{(A1)}$$

where $\Delta\rho_{mc} = \rho_m - \rho_c$, $\Delta\rho_{me} = \rho_m - \rho_e$, and $\Delta\rho_{mr} = \rho_m - \rho_r$. From the definitions of f, $C(f)$, and f_i it follows that

$$Z_r = (1-f)\frac{\rho_m}{\rho_r}Z_s$$

$$Z_{\text{ext}} = (1-f_i)(f-C(f))\frac{\rho_m}{\rho_e}Z_s \quad \text{(A2)}$$

$$Z_{\text{int}} = f_i(f-C(f))\frac{\rho_m}{\rho_e}Z_s$$

Substituting yields

$$\frac{d}{Z_s} = \rho_m[\rho_c + f_a\Delta\rho_{mc}]^{-1}\left\{\left[\frac{\rho_m}{\rho_r}-1\right](1-f)f_p + \left[\left(\frac{\rho_m}{\rho_e}f_i f_a - 1\right) + (1-f_a)f_i\right](f-C(f))\right\} \quad \text{(A3)}$$

All of the other quantities follow easily from d:

$$\Delta Z_T = (d + Z_{\text{ext}})$$

$$Z_l = \Delta Z_T + \left[1 - (1-f)\frac{\rho_m}{\rho_r} - (f-C(f))\frac{\rho_m}{\rho_e}\right]Z_s \quad \text{(A4)}$$

$$\Delta Z_m = Z_l + \left[(1-f)\frac{\rho_m}{\rho_r} - 1\right]Z_s$$

In the calculations, f_p is a function of unknown solution quantities, most specifically ΔZ_m. Therefore the solution for d must be found by iteration.

Acknowledgments. RJP was supported by the NASA Planetary Geology and Geophysics Program under grant NAGW-459 and by the NASA Mars Data Analysis Program under grant NAGW-1085. WBB was supported by the NASA Planetary Geology and Geophysics Program. We thank Ray Willemann, Sue Smrekar, Matt Golombek, and Bob Grimm for providing extremely helpful criticisms and suggestions. The present version of this paper was initially formulated while the senior author was a Visiting Fellow at the Research School of Earth Sciences, The Australian National University. RJP would like to thank Kurt Lambeck for his hospitality.

REFERENCES

Banerdt, W. B., R. J. Phillips, N. H. Sleep, and R. S. Saunders, Thick shell tectonics on one-plate planets: Applications to Mars, *J. Geophys. Res.*, *87*, 9723–9733, 1982.

Banerdt, W. B., M. P. Golombek, and K. L. Tanaka, Stress and tectonics on Mars, in *Mars*, University of Arizona Press, Tucson, in press, 1990.

Basaltic Volcanism Study Project, *Basaltic Volcanism on the Terrestrial Planets*, 1286 pp., Pergamon, New York, 1981.

Bills, B. G., The moments of inertia of Mars, *Geophys. Res. Lett.*, *16*, 385–388, 1989.

Brace, W. F., and D. L. Kohlstedt, Limits on lithospheric strength imposed by laboratory experiments, *J. Geophys. Res.*, *85*, 6248–6252, 1980.

Crough, S. T., Thermal origin of mid-plate hotspot swells, *Geophys. J. R. Astr. Soc.*, *55*, 451–469, 1978.

Crough, S. T., Hotspot epeirogeny, *Tectonophysics*, *61*, 321–333, 1979.

Crough, S. T., and R. D. Jarrard, The Marquesas-Line swell, *J. Geophys. Res.*, *86*, 11,763–11,777, 1981.

Finnerty, A. A., R. J. Phillips, and W. B. Banerdt, Igneous processes and closed system evolution of the Tharsis region of Mars, *J. Geophys. Res.*, *93*, 10,225–10,235, 1988.

Glasner, A. F., and W. U. Ussler III, Trapping of magma at midcrustal density discontinuities, *Geophys. Res. Lett.*, *15*, 673–675, 1988.

Hall, J. L., S. C. Solomon, and J. W. Head, Elysium region, Mars: Tests of lithospheric loading models for the formation of tectonic features, *J. Geophys. Res.*, *91*, 11,377–11,392, 1986.

Jordan, T. H., The Continental tectosphere, *Rev. Geophys. Space Phys.*, *13*, 1–12, 1975.

Jordan, T. H., Mineralogies, densities and seismic velocities of garnet lherzolites and their geophysical implications, in *The Mantle Sample: Inclusions in Kimberlites and Other Volcanics*, pp. 1–14, edited by H. O. A. Meyer and F. R. Boyd, AGU, Washington, D. C., 1979.

Jordan, T. H., Continents as a chemical boundary layer, *Phil. Trans. R. Soc. Lond., Ser. A.*, *301*, 359–373, 1981.

Kaula, W. M., The moment of inertia of Mars, *Geophys. Res. Lett.*, *6*, 194–196, 1979.

Kaula, W. M., N. H. Sleep, and R. J. Phillips, More about the moment of inertia of Mars, *Geophys. Res. Lett.*, *16*, 1333–1336, 1989.

Kraus, H., *Thin Elastic Shells: An Introduction to the Theoretical Foundations and the Analysis of their Static and Dynamic Behavior*, 476 pp., John Wiley, New York, 1967.

Masursky, H., A. L. Dial, Jr., and M. H. Strobell, Geologic map of the Phoenicis Lacus Quadrangle of Mars, *Atlas of Mars 1: 5,000,000 Geol. Ser.*, map I-896 MC-17, U.S. Geol. Surv., Washington, D. C., 1978.

McGetchin, T. R., and J. R. Smyth, The mantle of Mars: Some possible geological implications of its high density, *Icarus*, *34*, 512–536, 1978.

McKenzie, D., A possible mechanism for epeirogenic uplift, *Nature*, *307*, 616–618, 1984.

Mouginis-Mark, P. J., L. Wilson, and J. W. Head, Explosive volcanism on Hecates Tholus, Mars: Investigation of eruption conditions, *J. Geophys. Res.*, *87*, 9890–9904, 1982.

Phillips, R. J., and R. S. Saunders, The isostatic state of martian topography, *J. Geophys. Res.*, *80*, 2893–2898, 1975.

Phillips, R. J., R. S. Saunders, and J. E. Conel, Mars: Crustal structure inferred from Bouguer gravity anomalies, *J. Geophys. Res.*, *78*, 4815–4820, 1973.

Plescia, J. B., and R. S. Saunders, Estimation of the thickness of the Tharsis lava flows and implications for the nature of the topography of the Tharsis plateau, *Proc. Lunar Planet. Sci. Conf. 11th*, 2423–2436, 1980.

Sleep, N. H., and R. J. Phillips, An isostatic model for the Tharsis province, Mars, *Geophys. Res. Lett.*, *6*, 803–806, 1979.

Sleep, N. H., and R. J. Phillips, Gravity and lithospheric stress on the terrestrial planets with reference to the Tharsis region of Mars, *J. Geophys. Res.*, *90*, 4469–4489, 1985.

Solomon, S. C., Formation, history and energetics of cores in the terrestrial planets, *Phys. Earth Planet. Inter.*, *19*, 168–182, 1979.

Solomon, S. C., and J. W. Head, Evolution of the Tharsis province of Mars: The importance of heterogeneous lithospheric thickness and volcanic construction, *J. Geophys. Res.*, *87*, 9755–9774, 1982.

Tanaka, K. L., and P. A. Davis, Tectonic history of the Syria Planum province of Mars, *J. Geophys. Res.*, *93*, 14,893–14,917, 1988.

Toksöz, M. N., A. Hsui, and D. H. Johnston, Thermal evolution of the terrestrial planets, *Moon Planets*, *18*, 281–320, 1978.

Willemann, R. J., and D. L. Turcotte, The role of lithospheric stress in the support of the Tharsis rise, *J. Geophys. Res.*, *87*, 9793–9801, 1982.

Yoder, H. S., Jr., *Generation of Basaltic Magma*, 265 pp., National Academy of Sciences, Washington, D. C., 1976.

W. B. Banerdt, Jet Propulsion Laboratory, California Institute of Technology, Pasadena, CA 91109.

R. J. Phillips, Department of Geological Sciences, Southern Methodist University, Dallas, TX 75275.

N. H. Sleep, Departments of Geology and Geophysics, Stanford University, Stanford, CA 94305.

(Received August 11, 1986;
revised November 10, 1989;
accepted November 14, 1989.)